-AK81

RU 519
#5182

403
CONTRACT: 03-5-022-67
22 JUNE 1981

TERRA TECH

SPECIAL REPORT

AIR-SEA INTERACTION ALONG THE ALASKAN ARCTIC COAST

PREPARED FOR

OCSEAP

AMSTUTZ

FILE COPY
OCT 22 1981

5182

SPECIAL REPORT

Contract: 03-5-022-67 Task Order #13
Research Unit: 519
Number of Pages: 78

AIR-SEA INTERACTION ALONG THE ALASKAN ARCTIC COAST

PART I

Historical Wind Data Analysis
And Markov Model
To Generate Time Series Of Coastal Winds

Thomas L. Kozo

PART II

Wave Hindcast Statistics
For Lease Areas Under Two
Fetch Conditions Due to Ice Cover

Frank Wu

Tetra Tech, Inc.
Waterways and Harbors Division
630 North Rosemead Blvd.
Pasadena, California 91107

22 June 1981

TABLE OF CONTENTS

SECTION		PAGE
I	GENERAL INTRODUCTION	1
1.0	HISTORICAL WIND DATA ANALYSIS AND MODIFIED MARKOV MODEL TO GENERATE TIME SERIES OF COASTAL WINDS	2
	A. Results	2
	1. Bivariate Distribution Data	2
	2. Probability Density Data	3
	3. Statistical Characteristics of 30 Years of Data from Barter Island	5
	4. Statistically Representative Time Series of Winds for Typical Augusts and Atypical Augusts	5
	REFERENCES	
2.0	WAVE HINDCAST STATISTICS	48
	2.1 Introduction	48
	2.2 Theories	49
	2.2.1 Wave Generation and Propagation	49
	2.2.2 Wave Breaking Criteria	52
	2.2.3 Wave Set-Up	55
	2.2.4 Wave Run-Up	57
	2.2.5 Wave-induced Current	58
	2.3 Results, Discussions, Comparisons, and Conclusions	59
	2.4 Recommendations	61
	REFERENCES	

LIST OF FIGURES

Figure		Page
1	Locations of Atmospheric Pressure Stations (P) (Presently and Previously Existing) and Primary Summer Surface Wind Study Area (A)	10
2	Correlation Percentages For Simultaneously Occurring Surface Wind Directions (Less Than 60° Apart) As a Function of Station Separation For The Alaskan Arctic Coast Taken From Historical Data	11
3	Bivariate Distribution Table of Simultaneously Occurring Surface Winds For August 1969 At Data Stations:	
	Barter (Y Axis) Vs. Lonely (X Axis)	12
4	Barter Vs. Oliktok	12
5	Barter Vs. Deadhorse	13
6	Deadnorse Vs. Lonely	13
7	Oliktok Vs. Lonely	14
8	Deadhorse Vs. Oliktok	14
9	Surface Wind Direction Histogram For Barter Island, Alaska (August 1949)	15
10	(August 1950)	15
11	(August 1951)	16
12	(August 1952)	16
13	(August 1953)	17
14	(August 1954)	17
15	(August 1955)	18
16	(August 1956)	18
17	(August 1957)	19
18	(August 1958)	19
19	(August 1959)	20
20	(August 1960)	20
21	(August 1961)	21
22	(August 1962)	21
23	(August 1963)	22
24	(August 1964)	22
25	(August 1965)	23
26	(August 1966)	23
27	(August 1967)	24
28	(August 1968)	24
29	(August 1969)	25
30	(August 1970)	25
31	(August 1971)	26
32	(August 1972)	26

LIST OF FIGURES

Figure		Page
33	Surface Wind Direction Histogram For Barter Island, Alaska (August 1973)	27
34	(August 1974)	27
35	(August 1975)	28
36	(A.ugust 1976)	28
37	(August 1977)	29
38	(August 1978)	29
39	Surface Wind Direction Histogram For Cottle Island, Alaska (August 1978) - Type I	30
40	Surface Wind Direction Histogram for Cottle Island, Alaska (August 1976) -Type I	30
41	Surface Wind Direction Histogram For Tolaktovut Point, Alaska (Mid August to hid September 1980)	31
42	Surface Wind Direction Histogram for Toloktovut Point Alaska (August 1980) - Type II	31
43	Surface Wind Direction Histogram for Cottle Island, Alaska (August 1977) - Type III	32
44	Lag-One Autocorrelation Coefficients (ρ), Mean (M), and Standard Deviation (SD) For Wind Speed Data From Barter Island For 1949-1978	33
45	Lag-One Autocorrelation Coefficients (ρ), Mean (M), and Standard Deviation (SD) For Wind Direction From Barter Island For 1949-1978	34
46	Amplitude of Fourier Components Compared To a First-Order Markov Continuum (Red Noise) and a White Noise (Random) Continuum For Direction (a) and Speed (b). (August 1949)	35
47	Amplitude of Fourier Components Compared To a First-Order Markov Continuum (Red Noise) and a White Noise (Random) Continuum For Direction (a) and Speed (b). (August 1969)	36
48	Amplitude ofFourier Components Compared To a First-Order Markov Continuum (Red Noise) and a White Noise (Random) Continuum For Direction (a) and Speed (b). (August 1971)	37

LIST OF FIGURES

Figure		Page
49	Amplitude of Fourier Components Compared To a First-Order Markov Continuum (Red Noise) and a White Noise (Random) Continuum For Direction (a) and Speed (b). (August 1975)	38
50	Amplitude of Fourier Components Compared To a First-Order Markov Continuum (Red Noise) and a White Noise (Random) Continuum For Direction (a) and Speed (b). (August 1976)	39
51	Amplitude of Fourier Components Compared To a First-Order Markov Continuum (Red Noise) and a White Noise (Random) Continuum For Direction (a) and Speed (b). (August 1977)	40
52	Amplitude of Fourier Components Compared To a First-Order Markov Continuum (Red Noise) and a W-bite Noise (Random) Continuum For Direction (a) and Speed (b). (August 1978)	41
53	Wind Speed Histogram Generated By The Markov Model for ρ = .25	42
54	Wind Speed Histogram Generated By The Markov Model for ρ = .50	42
55	Wind Speed Histogram Generated By The Markov Model for ρ = .75	43
56	Wind Direction Histogram Generated By The Markov Model To Simulate Actual Historical Data. ρ = .75	43
57	Amplitude of Fourier Components of Model Generated Time Series (Directions) Compared To a First-Order Markov Continuum (Red Noise) and a White Noise Continuum	44
58	Coefficient of Determination Vs. Markov Model Order Number For Real Data From August 1978 (Cottle Island, Typical August)	45

LIST OF FIGURES

Figure		Page
59	Wind Direction Histogram Generated By The Markov Model For ρ = . 5	46
60	Wind Direction Histogram Generated By The Markov Model For ρ = . 25	46
61	Wind Direction Histogram Generated By The Markov Model For P = .75 With A Rectangular Random Number Distribution	47
2.1	Representative Beach Profiles of the Study Area	63
2.2	Wind Speed (August 1977)	64
2.3	Wind Direction (August 1977)	64
2.4	Significant Wave Height (August 1977),	65
2.5	Peak Wave Period (August 1977)	65
2.6	Breaking Wave Height (August 1977)	66
2.7	Breaking Water Depth (August 1977)	66
2.8	Ratio of Deep Water Wave-Induced Current Over Wind Speed (August 1977)	67
2.9	Ratio of Breaking Wave-Induced Current Over Wind Speed (August 1977)	67
2.10	Wind Speed (August 1978)	68
2.11	Wind Direction (August 1978)	68
2.12	Significant Wave Height (August 1978)	69
2.13	Peak Wave Period (August 1978)	69
2.14	Breaking Wave Height (August 1978)	70
2.15	Breaking Water Depth (August 1978)	70

LIST OF FIGURES

Figure		Page
2.16	Ratio of Deep Water Wave-Induced Current OverWind Speed (August 1978)	7.1
2.17	Ratio of Breaking Wave-Induced Current OverWind Speed (August 1978)	71
2.18	Wind Speed (August 1980)	72
2.19	Wind Direction (August 1980)	72
2.20	Significant Wave Height (August 1980)	73
2.21	Peak Wave Period (August 1980)	73
2.22	Breaking Wave Height (August 1980)	74
2.23	Breaking Water Depth (August 1980)	74
2.24	Ratio of Deep Water Wave-Induced. Current OverWind Speed (August 1980)	75
2.25	Ratio of Breaking Wave-Induced Current OverWind Speed (August 1980)	75
2.26	Maximum and Mean Values of H_s, T_p, H_b, and D_b of August 1977	76
2.27	Maximum and Mean Values of H_s, T , H_b, and D_b of August 1978	77
2.28	Maximum and Mean Values of Hs, T , H_b, and D_b of August 1980	78

I. GENERAL INTRODUCTION

The field locations (Figure 1) for OCSEAP meteorological data gathering along the Alaskan Beaufort Sea Coast (since 1976) were mainly concentrated in rectangle A. The P locations were surface pressure data sites. Pt. Barrow, Franklin Bluffs, McClure Islands (Narwhal) and Barter Island are now permanent pressure stations (Kozo, 1981) which offer "continuous" data and calculated geostrophic winds. The April 1981 Beaufort Sea (Sale #71) synthesis meeting outlined several analyses voids which could become serious gaps in the environmental assessment program. These voids were:

(I-a) Comparisons of available historical data to the 5 years of summer field data and degree of applicability.

(I-b) Frequency of "normal and "abnormal" summer wind fields.

For example the summers of 1975 and 1980 were poor operating years for the oil companies since the ice edge was pushed close to the coast by prevailing westerly wind conditions. Also the 1977 (August) data contained a negative storm surge event that dropped the water depth in Simpson Lagoon by 1 meter and produced a direction distribution that showed easterlies dominating over 70% of the month.

(I-c) A development of a statistically representative time series of wind speed and direction to drive the oil spill model being developed by Chris Mungall (O.C.S. investigator) and the wave Hindcast model of Frank Wu (new O.C.S. investigator)

(I-d) Wind-wave data and analyses with zero information on wave induced currents which can reach 1% of the wind speed (Kinsman, 1965) or lead to a 25% error in Mungall's oil spill trajectory model.

1.0 HISTORICAL WIND DATA ANALYSIS AND MODIFIED MARKOV MODEL TO GENERATE TIME SERIES OF COASTAL WINDS.

A. Results

1) Bivariate Distribution Data

It has been shown in previous annual reports (R.U. 519, 1977-1981) that surface winds have been well correlated for OCSEAP data collection locations from Cape Halkett to Brownlow Pt. in the late spring and summer seasons. These data were collected by Meteorology Research, Inc. (MRI) mechanical weather stations with direction accuracy of ± 1% of full scale (360°) and wind SPeed at ± 2% of the measured value. The data are taken in the form of 3 hourly averages.

The historical data analyzed was taken from one Class A-1 weather station (Barter Island) , one airport (Deadhorse) , and two Distant Early Warning Sites (DEW, Lonely and Oliktok) ..The data collected at the DEW sites were instantaneous readings taken every 6 hours at approximately 2 meters above their airplane landing fields. The data collected at the Deadhorse airport were in the form of instantaneous readings several meters above the runway elevation with some years of data collection at hourly intervals but only from 6AM to 8PM. The da-ta from Barter Island was taken hourly but still in the form of instantaneous ("quick-look") readings. The characteristics of the historical data are then, instantaneous readings, variable time periods of collection, directionally coded intervals (21° intervals, ±10.5° error built-in), data elevations less than 10 meters and generally inconsistent methodology . Therefore, Figure 2 is a pleasant surprise. It represents an eight year average (cataloged Deadhorse historical data exists from 1968-1976 with poor summer 1968 data) of total percentages (August) for simultaneously occurring surface winds directions (less than 60° apart) at various station combinations (see Figures 3-8 as examples) taken from bivariate distribution tables. The station

combinations were Lonely-Barter Island (366 km) , Oliktok-Barter Island (232 km), Deadhorse-Barter Island (181 km), Lonely-Deadhorse (190 km), Lonely-Oliktok (130 km) and Oliktok-Prudhoe (66 km). The numbers (percentages)between the two diagonal times (Figure 3-8) designate occurrence of simultaneous wind directions that are within 60° of each other. Totals of the percentages between the lines were used for Figure 2. It can be clearly seen that the correlation increases with decreasing station separation distance in a linear fashion. Extrapolation to O distance (dashed line) indicates that for these data and station combinations 74% is "perfect". The Prudhoe Bay (Deadhorse area) to Oliktok coastal region was the major area of the OCSEAP studies (1976-1980) and Figure 2 shows an avera9e loss of 14% in correlation if Barter Island surface wind data is used to describe all coastal surface winds. It must also be mentioned that all the bivariate distributions (Figures 3-8) exhibit the typical bimodality in east-west directions but no indication of a consistent turning angle difference exists between Oliktok and Barter Island..

2) Probability Density Data

Probability density plots for Barter Island surface wind direction data in August the main open water month can be seen in Figures 9-38 for the years 1949-1978 (in order). Similar plots were generated (not included in this report) for July and September separately as well as combined plots for July 15 through September 15 (typical time period of open water) . There are 3 main types of wind directional fields, all of which show the usual bimodality due to southerly wind (145° - 210°) suppression by the mesoscale coastal thermal contrast (Kozo, 1979) . The first type (Type I) and most predominant (7 of 10 years) show a 60% easterly and 40% westerly directional bias. Cottle Island (Jones Islands) winds from a complete month of August (248 data points) in 1978 (Figure 39) were chosen to represent this Type I condition and are being used by Chris Mungall (OCSEAP investigator) to drive his oil

spill trajectory model (note: compare with histogram from Barter Island Figure 38). The histogram from Barter Island Figure 37 and Figure 40 from Cottle Island for August 1976 represent a "finger-print" of Type I wind directions that led to a banner shipping and operational year for oil companies on the north slope since moderate speed easterly winds were dominant and dept the ice edge away from shore.

It must be noted that calendar months are an artificial break-down of time histories of wind fields. An extreme case (no category like this) wind histogram can be seen in Figure 41 which runs from mid-August 1980 through mid-September 1980. This wind direction distribution (opposite to the Type I case) helped produce what Dome Petroleum of Canada described as the worst ice conditions ever in the Beaufort Sea (Oil and Gas Journal, 1980) .

The second (Type II) and the one damaging to commercial operations on the artic coast is a directional distribution with a mere 50% Easterly - 50% Westerly (or a slight westerly bias) since westerly winds induce shoreward transport in the water column (in less than 6 hours) bringing the sea ice edge closer to shore. Figure 36 from Barter Island (1975) and Figure 42 from Tolaktovut (August 1980) are examples of directional distribution Type II for years were operations were severly hampered due to ice conditions. These conditions appear 2 out of every 10 years and the 1980 (Tolaktovut) data from August 1 through September 24, 1980 has been chosen to drive the OCSEAP oil spill model as representative of the Type II conditions.

The last type of wind distribution (Type III) occurs once every 10 Augusts. It can best be seen in the August 1977 data (-Figure 43) for Cottle Island Figure 38 for Barter Island). This data was influenced by a negative storm surge which contributed persistent synoptic easterly winds for almost a week resulting in a better than 75% easterly wind accumulation for the month. A

large open water area was created between the ice edge and the coast but shipping was hampered by the high winds (up to 40 knots) . It must be noted that wind induced waves and wave induced currents must be fetch dependent. Fetch in-turn is dependent on the prevailing synoptic wind conditions which can bring the ice edge in or out.

3) Statistical Characteristics of 30 Years of Data from Barter Island

Plots of correlation coefficients (P) between adjacent data points in a time series (lag one autocorrelation coefficients), mean (M) , and standard deviation (SD) can be seen in Figure 44 and 45 for speed and direction respectively. (Note: 1979 data had many gaps and was not used). For speed, the typical August had ρ = .75, M = 10 knots (~ 5 m/s) and S.D. = 5 knots (~ 2.5 m/s). For direction, the typical August had ρ = .75, M = .4 (x 360 = 144) and S.D. = .275 (x 360 = 99). Plots of auto correlation coefficients for speed and direction increasing lag (not shown) have a $\frac{1}{e}$ value reached in 3 lags or 9 hours for typical Augusts. This shows that winds are reasonably correlated for a time period greater than the response time of a moving ice floe to the wind.

4) Statistically Representative Time Series of Winds for Typical Augusts and Atypical Augusts

a. Further Component Plots of Barter Island Data for August (1949-1978).

Figures 46 through 52 are examples of Fourier component plots for direction (Part A) and speed (Part B) data in designated years. These individual components are compared with a pure first order Markov continuum (curved line, red noise) generated from lag one (random, straight line) continuum (see Kozo and Tucker, 1974) . The graphs show component wave numbers (abscissa) and variance (ordinate). The wave numbers can be converted to periods by

remembering that the data sample size for one month is 248 (every three hours) , thus wave number 1 has a 744 hour period and wave number 31 has a 24 hour period (diurnal cycle) . Wave numbers less than 16 represent synoptic influences. Statistical significance of component values above the white noise or red noise curves may be obtained (Gilman et al., 1963) by (1) assuming alternate null hypotheses that the data are either all white noise or all red noise (2) calculating the ratio $\frac{F.S.}{N}$ where F ≡ degrees of freedom, S ≡ peak amplitude and N ≡ amplitude of the Markov or white noise continuum at the same harmonic, (3) comparing this to the percentage points of the chi square distribution for the same F value. Individual harmonic amplitudes generated in the respective Fourier analysis have 2 degrees of freedom. Therefore the chi-square distribution table shows that peaks significant at the 5% level must be approximately 3 times larger than their corresponding white or red noise value.

The actual wind speed and direction data (see Figure 52 for example) usually has at least one or two significant non-Markovian components at a synoptic period (less than wave #16) and one significant feature near the diurnal period (wave #31) . The diurnal period is a deterministic function which is imbedded in the time series data with a relatively constant phase angle and amplitude. The significant synoptic periods that occur are not the same from year to year with varying phases and amplitudes. Therefore, trying a Fourier technique to model the typical August open water period has been unproductive.

b. Markov Models

Chow (1964) discussing Markov processes mentions a successful first order Markov chain model that can be used to generate a time series. It can be written:

$$x_t = rx_{t-1} + (1-r)\bar{x} + s_x(1-r^2)^{\frac{1}{2}} \text{ et} \qquad (1)$$

where x_t is the value now, x_{t-1} is the immediately preceding value, r is the Markov chain coefficient (in this case, the lag one autocorrelation coefficient) , $\bar{x}$ and S_x are the mean and standard deviation of the historical data and et is a normally distributed random component with a 0 mean and standard deviation of 1. This is a variation of the Markov chain defining equation:

$$x_t = rx_{t-1} + e_t \qquad (2)$$

where the probability of a system in a given state (x_t) depends on the immediately preceding state (x_{t-1}), the correlation coefficient (r) and a random variable (et) . Equation (1) will generate x_t' s for speed and direction that are normally distributed and preserve the mean, variance and first order correlation coefficient of the historical data (Fiering and Jackson, 1971) .

The" historical wind speed data from Barter Island and the DEW sites (Lonely and Oliktok) show a unimodal distribution (Brewer, et al. 1977) which can be modeled by the generating equation above with a random number "generator" (CDC function-routine) . Figures 53-55 are speed histograms generated by the model for p ≡ r = .25 (Figure 53) , .50 (Figure 54) and .75 (Figure 55) with a constant M ≡ $\bar{x}$ = 10 knots and SD ≡ Sx = 5 knots and random numbers from a normal distribution. Figure 55 gives a wind speed distribution similar to the historical data with the mean standard elevation, and lag-one autocorrelation preserved.

The August historical wind direction data is another problem. It is a bimodal distribution with directions from the SSW to SSE sector suppressed due to the coastal thermal contrast. Equation (1) is again used but when directions are generated in the suppressed sector they are not retained in the synthetic data set but are utilized to generate the next number in the sequence which will be retained when it falls outside the SSE-SSE sector.

In this way the historical defining statistics are minimally disturbed, and retain their original character while preserving the deterministic effect of the coastal thermal contrast.

Figure 56 is an "example of a computer generated wind direction distribution which simulates the modal Augusts (histograms) preserves the statistics, and contains the deterministic effect of the coastal contrast. Figure 57 is a Fourier analysis of the above generated wind direction time series compared to a first order Markov continuum and a white noise continuum (level line). The Wave Number 20 (37 hour period) is a statistically significant peak and the auto correlation function (not shown) hits $\frac{1}{e}$ of its initial value in 9 hours just as the typical historical data.

It must be mentioned that 2nd higher order Markov models were contemplated with above tenth order being computationally excessive. To test the efficiency of equation (1) above, a curve fitting technique for a nth order (up to 100th order) Markov process was used (Fiering and Jackson, 1971) of the form:

$$'_t = b. + b_1X_{t-1} + b_2X_{t-2} + b_3X_{t-3} \; . \; . \; . \; b_mX_{t-m} + et \; S\,(1-R^2)^{\frac{1}{2}} \qquad (3)$$

where b. is analogous to $(1-r)\,\bar{X}$ in equation (1) and b_1 is analogous to r for order 1. et and s are the same as in equation (1) but $5_x\,(1-R^2)^{\frac{1}{2}}$ is the standard error of the estimate with R^2 the coefficient of determination. R^2 signifies a rating of the explanatory power of the successive higher order models. A plot of R^2 Vs. order number can be seen in Figure 58 (data used for fit was Cottle Island 1978, modal year). The criterion is to stop when the R^2 curve levels off at some plateau which is hopefully a higher numerical value than order 1. The 10th order give a value of R^2= .62 and is a significant plateau. However, for order 1 the R^2 is .56, therefore the gain in going to higher orders in the Markov

model is very slight. The real data has a lag one auto correlation of .75 which corresponds, to b_1 in equation (3) or r in equation (1) and the real data also has a mean ($\bar{X}$) of 144° which is contained in b. (equation (3)) and (1-r) $\bar{X}$ of equation (1). The computer generated b. from the curve fitting technique has a value of .7534708 (from 1978 Cottle Island Data, chosen to drive the OCSEAP oil spill model for the typical year) and a b_1 = 35.21342 which yields a $\bar{X}$ = 143. Again this evidence shows that a higher order model from a curve fitting technique will not improve on the numbers generated by equation (l).

The model can be started off with east or west winds using equation (1) and still preserve the historical statistics and probability density functions. The computer generated random numbers from a rectangular distribution are converted to a set of random numbers with a normal distribution having a 0 mean and standard deviation of 1. The same form of histogram is obtained regardless of the set of random numbers provided they have the above characteristics. Figures 59 and 60 are histograms with ρ = .5 and ρ = .25 respectively, showing the sensitivity of the model to the lag one autocorrelation coefficient.

A check on the model output for wind direction in the case of a random number set with a rectangular distribution can be seen in Figure 61. The resultant “fingerprint” is similar to the Type II bad year cases for real data and has the statistics preserved.

RE RE E

Brewer, W.A., H.F. Diaz, A.S. Prechtel, H.W.Searby and J.L. Wise, Climatic Atlas (Vol III) of the Outer Continental Shelf Waters, and Coastal Regions of Alaska, NOAA, NCC. EDS. Asheville, North Carolina, 409 pp., 1977.

Chow, V. T., 1964. Handbook of Applied Hydrology, McGraw-Hill, New York, Section 8-IV. 7 pgs.

Fiering, M.B., and B.B. Jackson, 1971. Synthetic Streamflows, Amer. Geophys. Union, Water Resources Monograph 1, Washington, D.C., 98 pgs.

Gilman, D.L., F.J. Fuglister, and J.M. Mitchell, 1973. On the Power Spectrum of 'Red Noise', J. Atmos. Sci, 20, 182, 1973.

Kinsman, B., 1965. Wind Waves, Prentice Hall, New Jersey, 676 pgs.

Kozo, T.L., 1979. Evidence for Sea Breezes on the Alaskan Beaufort Sea Coast, Geophys. Res. Letters, 6, 849-852.

Kozo, T.L., 1981. Meteorology of the Alaskan Artic Coast P.I., T. Kozo, ocs Contract 03-5-022-67 to 13.

Kozo, T.L., and W.B. Tucker, 1974. Sea Ice Bottomside Features in the Denmark STrait, J. Geophys. Res., 79,4505-4511.

Oil and Gas Journal, 1980.- International Briefs, Penn Well Publishing Co., Tulsa Oklahoma, Oct., p. 54.

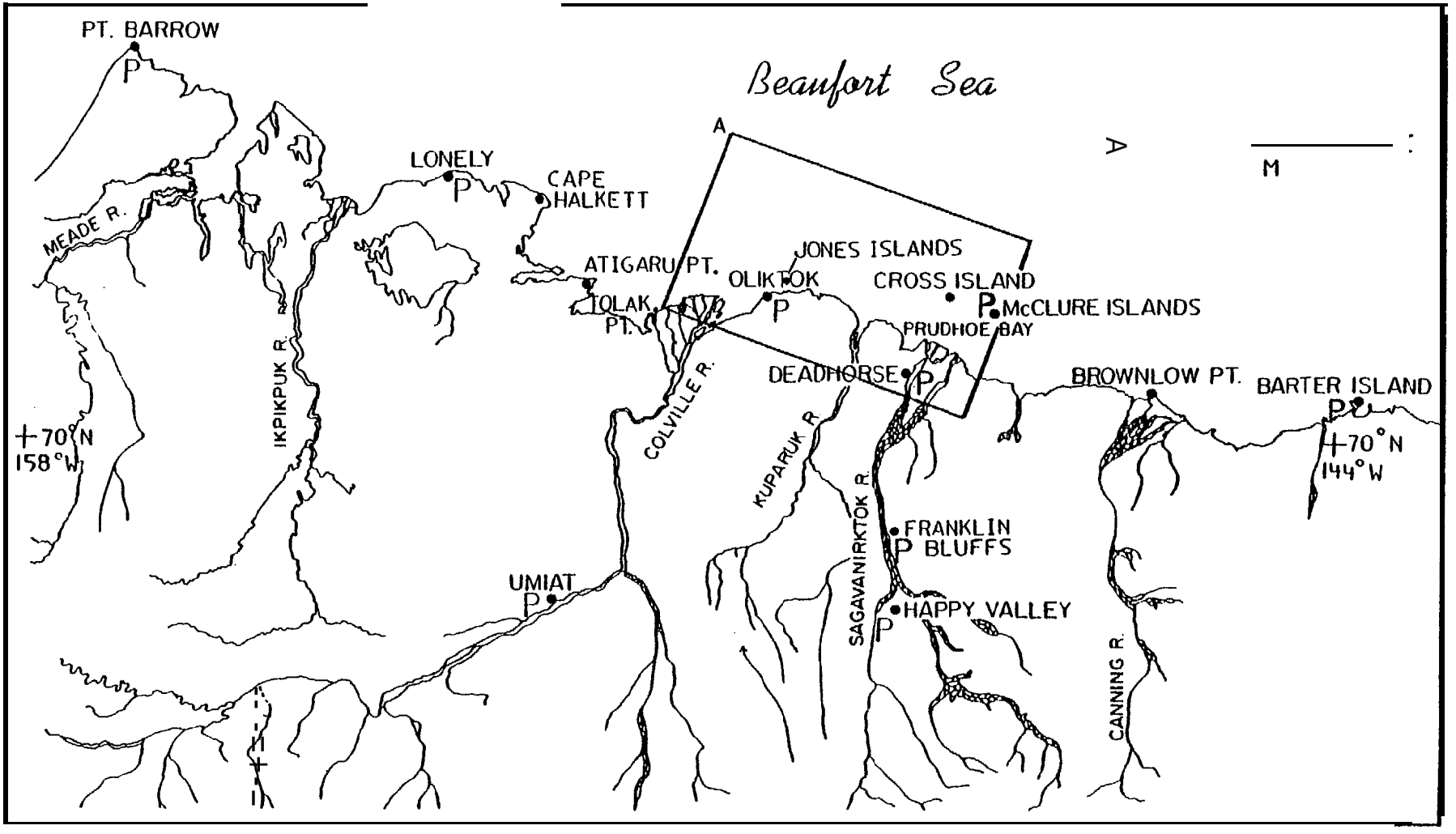

FIGURE 1: LOCATIONS OF ATMOSPHERIC PRESSURE STATIONS (P) (PRESENTLY AND PREVIOUSLY EXISTING) AND PRIMARY SUMMER SURFACE WIND STUDY AREA (A). THE FRANKLIN BLUFFS AND McCLURE ISLANDS STATIONS ARE NOW COUPLED TO PT. BARROW AND BARTER ISLAND FOR " CONTINUOUS" GEOSTROPHIC WIND PREDICTIONS ALONG THE ALASKAN ARCTIC COAST.

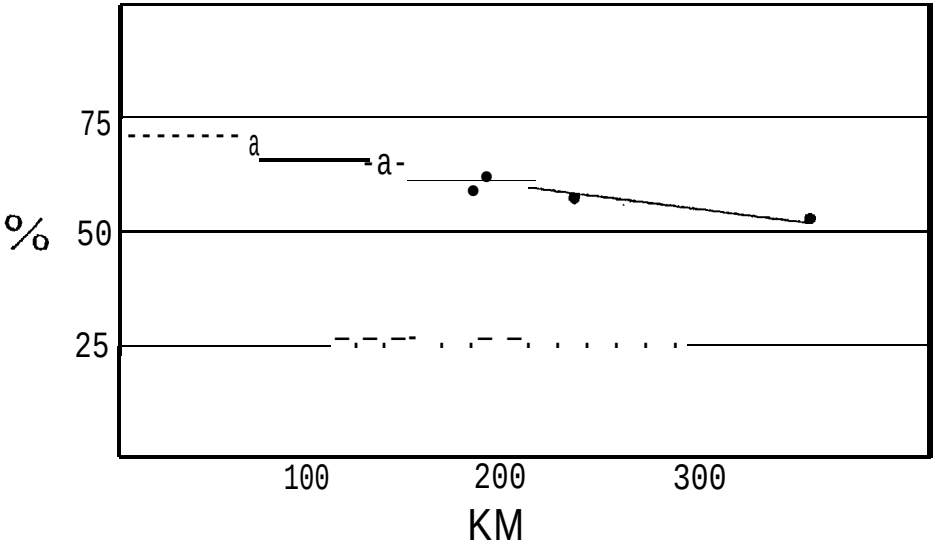

FIGURE 2: CORRELATION PERCENTAGES FOR SIMULTANEOUS OCCURRING SURFACE WIND DIRECTIONS (LESS THAN 60° APART) AS A FUNCTION OF STATION SEPARATION FOR THE ALASKAN ARCTIC COAST TAKEN FROM HISTORICAL DATA.

SURFACE WIND DIR.

WIND DIR.	0- 30	30- 60	60- 90	90-120	120-150	150-180	180-210	210-240	240-270	270-300	300-330	330-360
330-360	0.	0.	0.	0.	0.	0.	.8	.8	0.	0.	0.	0.
300-330	1.6	0.	0.	0.	0.	0.	0.	.8	0.	.8	0.	0.
270-300	2.4	1.6	0.	0.	0.	0.	1.6	1.6	.8	14.6	12.2	4.9
240-270	0.	0.	0.	.8	0.	0.	0.	.8	.8	2.4	0.	.8
210-240	0.	0.	0.	0.	0.	0.	0.	.8	0.	0.	0.	0.
180-210	.8	0.	0.	0.	0.	0.	0.	0.	.8	.0	0.	0.
150-180	0.	0.	0.	0.	0.	0.	0.	0.	0.	0.	0.	0.
120-150	0.	0.	0.	.8	0.	0.	0.	0.	.8	0.	0.	0.
90-120	0.	.8	4.9	14.6	0.	0.	.8	1.6	0.	3.3	0.	0.
60- 90	0.	1.6	.8	1.6	0.	.8	0.	.8	0.	.8	0.	0.
30- 60	.8	0.	0.	0.	0.	0.	0.	0.	.8	0.	0.	0.
0- 30	.8	0.	.8	0.	0.	0.	0.	.8	0.	0.	0.	0.

PER CENT ALONG DIAGONALS= 56.54

FIGURE 3: BIVARIATE DISTRIBUTION TABLE OF SIMULTANEOUSLY OCCURRING SURFACE WINDS FOR AUGUST 1969 AT DATA STATIONS. (BARTER (Y AXIS) VS. LONELY (X AXIS)).

SURFACE WIND DIR.

WIND DIR.	0- 30	30- 60	60- 90	90-120	120-150	150-180	180-210	210-240	240-270	270-300	300-330	330-360
332-360	0.	0.	0.	0.	0.	0.	.8	.8	0.	0.	0.	0.
300-330	1.6	0.	0.	0.	0.	0.	0.	.8	0.	0.	0.	.8
270-300	2.4	0.	.6	0.	0.	0.	1.6	0.	1.6	25.8	5.6	2.4
240-270	0.	0.	0.	.8	0.	0.	0.	0.	0.	4.0	.8	0.
210-240	0.	0.	0.	0.	0.	0.	0.	0.	0.	0.	0.	0.
180-210	0.	0.	0.	0.	0.	0.	.8	0.	.8	0.	.8	0.
150-180	0.	0.	0.	0.	0.	0.	0.	0.	0.	0.	0.	0.
120-150	0.	0.	0.	0.	0.	.8	.8	0.	.8	0.	0.	0.
90-120	0.	2.4	2.4	16.1	.8	.8	.8	1.6	0.	0.	0.	0.
60- 90	.8	0.	2.4	1.6	0.	0.	0.	0.	0.	.8	0.	0.
30- 60	0.	0.	0.	0.	0.	0.	0.	.8	0.	0.	.8	0.
0- 30	.8	0.	0.	.8	0.	0.	0.	0.	.8	0.	0.	0.

PER CENT ALONG DIAGONALS= 63.71

FIGURE 4: BIVARIATE DISTRIBUTION TABLE OF SIMULTANEOUSLY OCCURRING SURFACE WINDS FOR AUGUST 1969 AT DATA STATIONS (BARTER VS. OLIKTOK).

SURFACE WIND DIR.

WIND DIR.	0- 30	30- 60	60 - 90	90-120	120-150	150-180	180-210	210-240	240-270	270-300	300-330	330-360
330360	o.	0.	0.	0.	0.	0.	0.	o*	.4	.4	0.	.4
300-330	1.6	c*	n.	(.	0.	0.	0.	0.	.4	.6	.4	0.
270-300	3.6	.4	.4	.4	0.	0.	'o.	1.6	3.2	21.0	9.3	3.2
240-270	.4	o*	o.	(.	0.	0.	.4	.4	.4	3.2	0.	o,
210-240	0.	0.	0.	0.	1.	0.	0.	.4	0.	0.	0.	0.
180-210	0.	0.	o.	0.	(.	0.	.8	.4	0.	0.	.4	0.
150-180	0.	0.	0.	1.	0.	0.	.4	0.	0.	.4	0.	0.
120-150	0.	0.	17.	0.	0.	.4	.4	.8	0.	0.	0.	c.
90-120	.8	0.	1.2	15.0	1.2	1.2	2.4	.4	1.6	.8	c,	t.
60-90	0.	0.	1.6	106	0.	0.	.4	0.	.4	0.	0.	o.
30- 60	0.	1.2	.8	0.	0.	0.	0.	0.	.4	0.	0.	0.
0- 30	.4	.4/	1.2	0.	c.	o.	0.	● 4	o.	0.	,.	0.

PC RCENTALONG O! AGONALS= 68.95

FIGURE 5: BIVARIATE DISTRIBUTION TABLE OF SIMULTANEOUSLY OCCURRING SURFACE WINDS FOR AUGUST 1969 AT DATA STATIONS. (BARTER VS. DEADHORSE).

SUR FACE WIND DIR.

WIND DIR.	0- 30	30- 60	60- 90	90-120	120-150	150-180	180-210	210-240	240-270	270-300	300-330	330-360
330-360	.*	0.	0.	0.	G.	0.	o.	0.	0.	6.	.8	.8
300-330	c.	.8	0.	0.	0.	c.	o*	o.	0.	4.9	2.4	0.
270-s01	.8	0.	0.	0.	1.	0.	.8	1.6	.8	10.6	7.3	3.3
240-270	0.	0.	o.	r.	0.	0.	0.	3.3	1.6	2.4	0.	0.
21 O-2*O	0.	0.	o.	(*	c.	c.	0.	1.6	1.6	1.6	0.	0.
● IWO DIR. 180-210	.8	0.	.8	1.6	0.	0.	.8	0.	0.	0.	0.	0.
150-180	o.	0.	0.	1.6	0.	0.	0.	0.	0.	c.	0.	0.
120-150	0.	0.	0.	.8	0.	0.	0.	0.	o.	0.	0.	0.
90-120	0.	.6	4.9	11.4	0.	0.	.8	.8	o.	.6	c.	0.
60- 90	.8	1.6	.8	2.4	0.	0.	0.	0.	o.	0.	c.	0.
30- 60	0.	0.	0.	0.	0.	0.	0.	0.	o.	c.	●:	0.
0- 30	3.3	.8	0.	0.	0.	0.	0.	0.	o.”	1.6	.8	1.6

PERCENT ALONG DI AGONALS= 65.24

FIGURE 6: BIVARIATE DISTRIBUTION TABLE OF SIMULTANEOUSLY OCCURRING SURFACE WINDS FOR AUGUST 1969 AT DATA STATIONS. (DEADHORSE VS. LONELY).

SURFACE WIND DIR.

WIND DIR*	0- 30	30- 60	60- 90	90-120	120-150	150-180	180-210	210-240	240-270	270-300	300-330	330-360
330-360	c.	.8	0.	0.	0.	G.	0.	c.	0.	.8	0.	.8
300-330	.8	0.	o*	r.	(.	t.	o.	0.	0.	2.4	2.4	1.6
270-300	.8	0.	0.	r.	(*'	c.	.8	1.6	.8	13.8	8.5	2.4
240-270	0.	0.	0.	0.	t.	c.	o*	.8	2.4	.8	0.	0.
210-240	0.	0.	n.	K.	c.	0.	.8	1.6	.8	.8	o.	0.
180-230	.8	0.	n*	.8	0.	0.	.8	2.4	0.	0.	0.	0.
150-180	n.	o.	0.	.8	0.	0.	0.	0.	0.	t.	o*	o.
120-150	0.	n.	n.	0.	0.	0.	0.	0.	0.	c.	c.	0.
99-120	0.	1.6	4.9	11.4	0.	0.	0.	.8	0.	c.	c*	c.
60- 98	0.	1.6	.8	2.4	0.	0.	0.	0.	o*	.8	0.	0.
SO- 60	0.	0.	.8	1.6	0.	0.	0.	0.	0.	0.	c.	0.
0- 30	3.3	0.	0.	0.	0.	0.	0.	o.	0.	1.6	o*	0.

PERCENT ALONG DIAGONALS= 67.48

FIGURE 7: BIVARIATE DISTRIBUTION TABLE OF SIMULTANEOUSLY OCCURRING SURFACE WINDS FOR AUGUST 1969 AT DATA STATIONS. (OLIKTOK VS. LONELY).

SURFACE WIND DIR.

WIND DIR.	0- 30	30- 60	60- 90	90-120	120-150	150-180	180-210	210-240	240-270	270-300	300-330	330-360
330-360	0.	0.	0.	0.	c.	0.	0.	o*	o.	c*	1.6	.8
300-330	.8	0.	c.	f.	(.	c.	o.	0.	0.	3.2	3.2	.8
270-300	c*	o.	0.	f.	c.	0.	0R	0.	0.	24.2	.8	0.
240-270	0.	0.	0.	t.	0.	0.	.8	2.4	.8	2.4	0.	0.
210-240	0.	0.	0.	0.	c.	0.	.8	.8	3.2	0.	c.	0.
180-210	0.	.8	0.	.8	t.	0.	1.6	.8	0.	0.	0.	0.
150-104	0.	0.	0.	1.6	0.	.8	0.	0.	0.	0.	0.	0.
120-150	0.	0.	o*	.8	0.	0.	0.	0.	0.	0.	o.	0.
90-120	0.8	1.6	1.6	13.7	.8	.8	0.	0.	0.	0.	0.	r.
60- 93	0.	0.	2.4	2.4	0.	0.	0.	0.	0.	0.	0.	0.
37- 60	0.	0.	0.	(.	0.	o.	c.	o.	0.	r.	.8	0.
o- 30	4.0	0.	.8	1.	0.	(.	o.	0.	o*	.8	.8	1.6

FIGURE 8: BIVARIATE DISTRIBUTION TABLE OF SIMULTANEOUSLY OCCURRING SURFACE WINDS FOR AUGUST 1989 AT DATA STATIONS. (DEADHORSE VS. OLIKTOK).

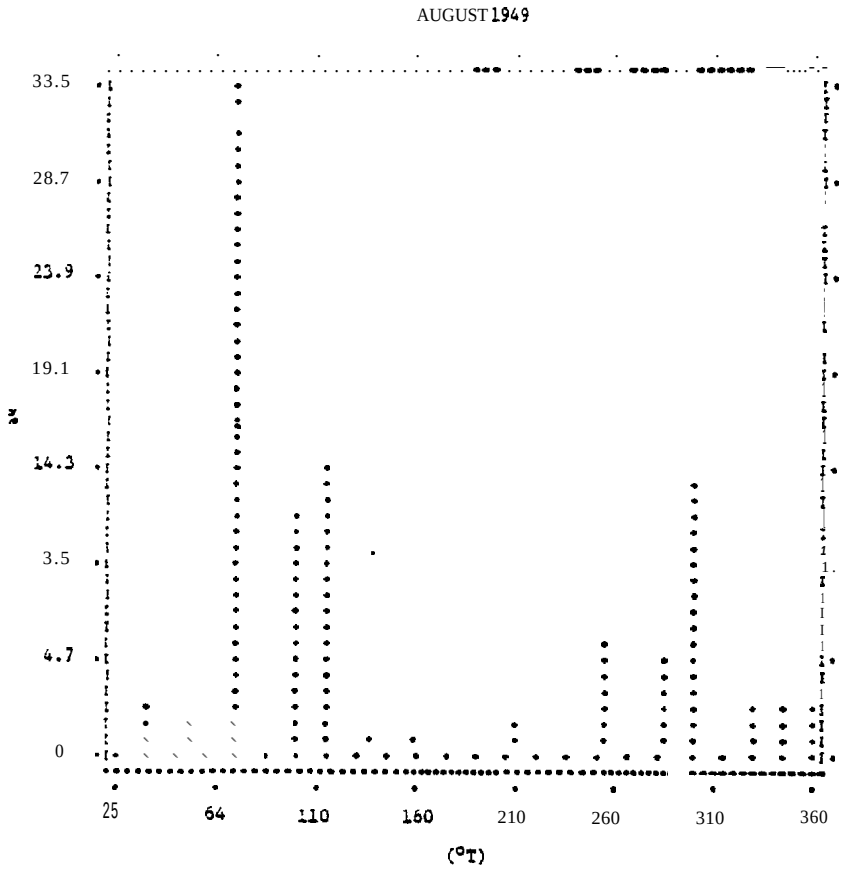

FIGURE 9: SURFACE WIND DIRECTION HISTOGRAM FOR BARTER ISLAND, ALASKA (AUGUST 1949).

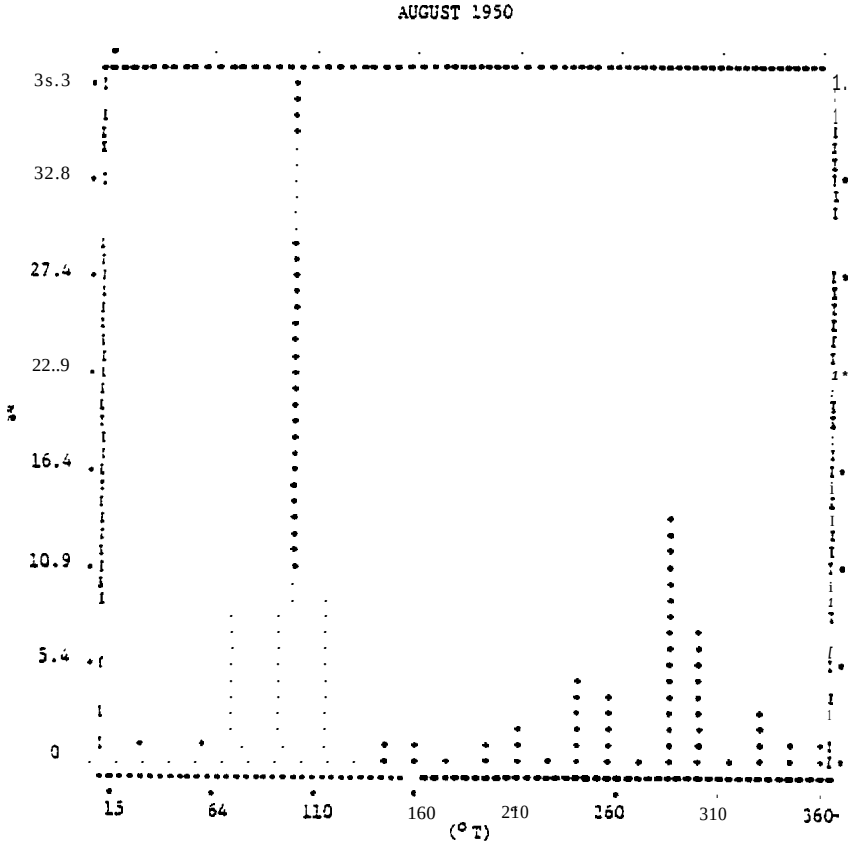

FIGURE 10: SURFACE WIND DIRECTION HISTOGRAM FOR BARTER ISLAND, ALASKA (AUGUST 1950).

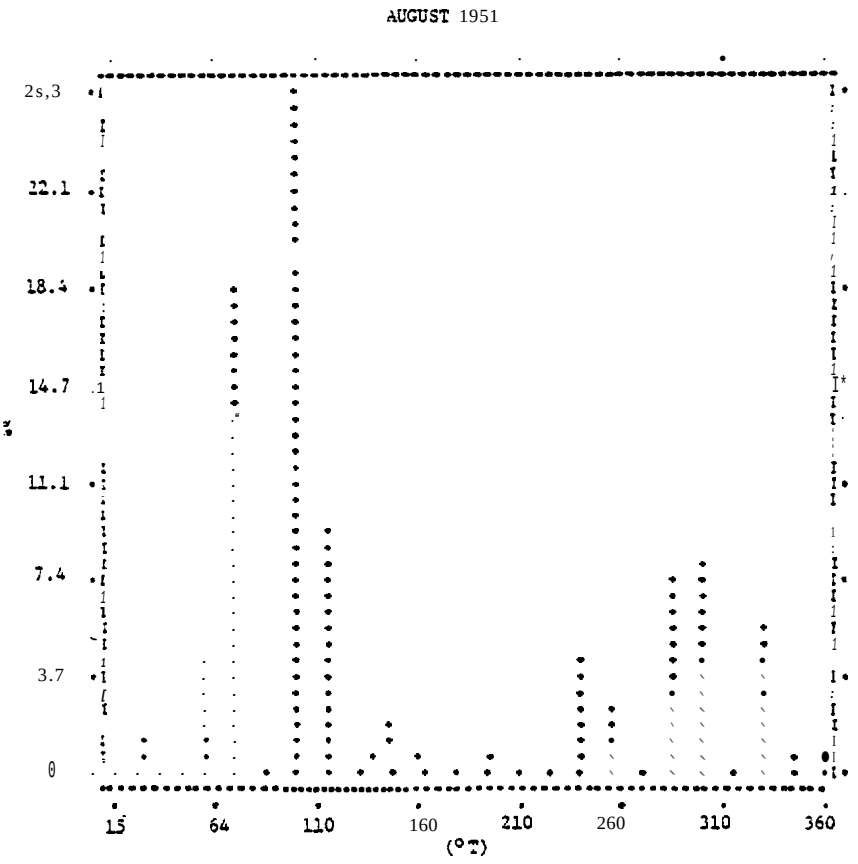

FIGURE 11: SURFACE WIND DIRECTION HISTOGRAM FOR BARTER ISLAND, ALASKA (AUGUST 1951).

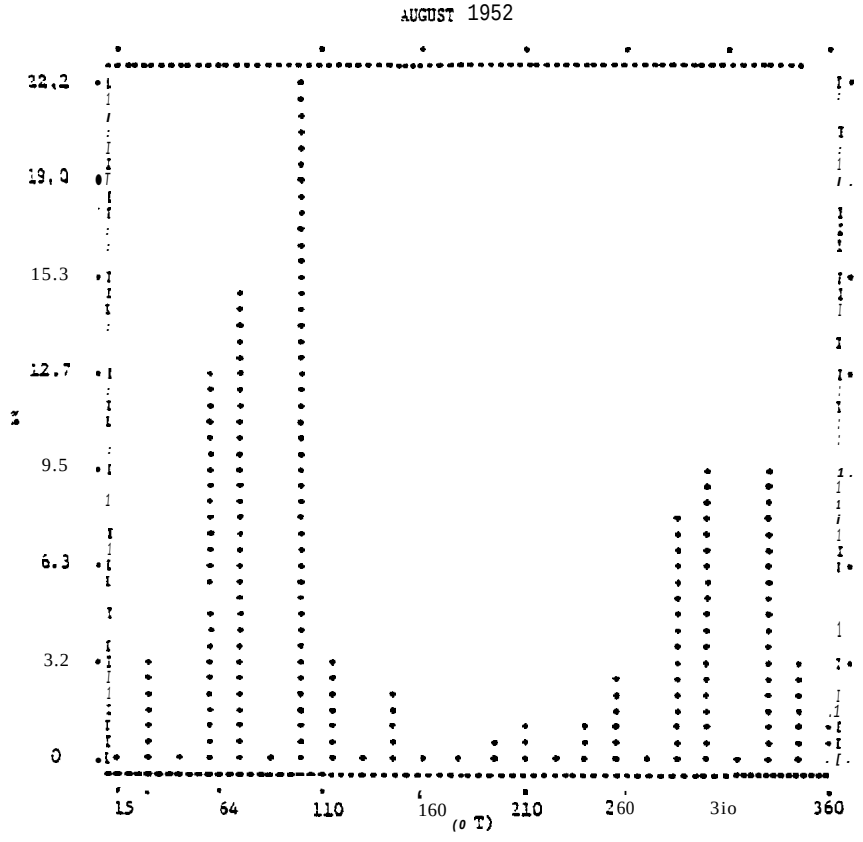

FIGURE 12: SURFACE WIND DIRECTION HISTOGRAM FOR BARTER ISLAND, ALASKA (AUGUST 1952).

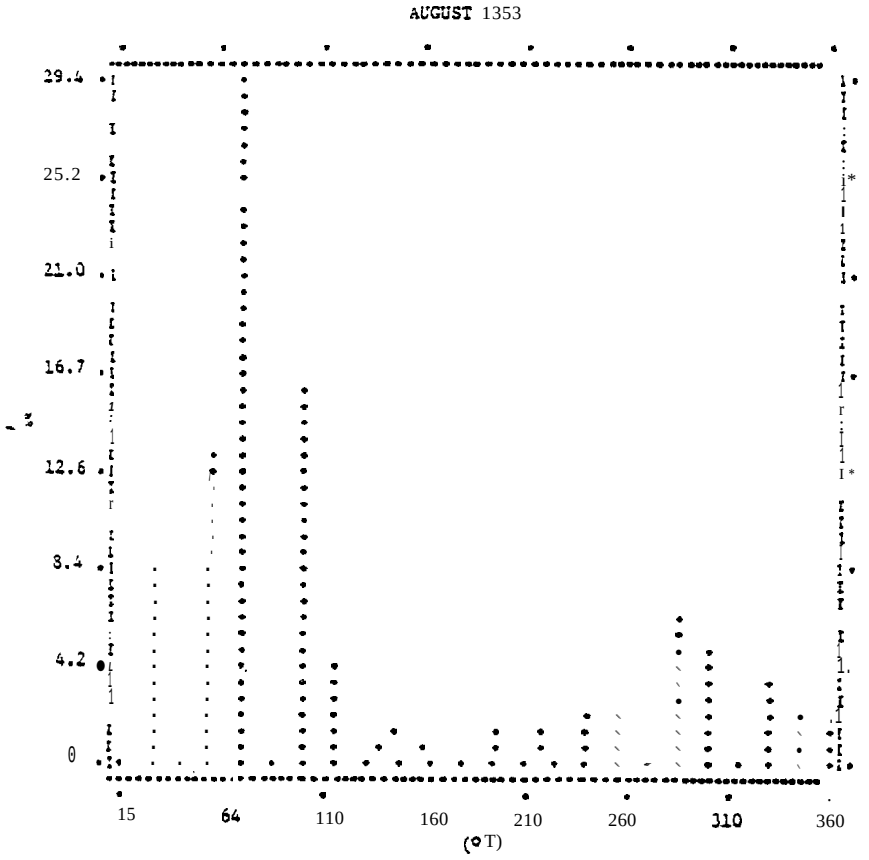

FIGURE 13: SURFACE WIND DIRECTION HISTOGRAM FOR BARTER ISLAND, ALASKA (AUGUST 1953).

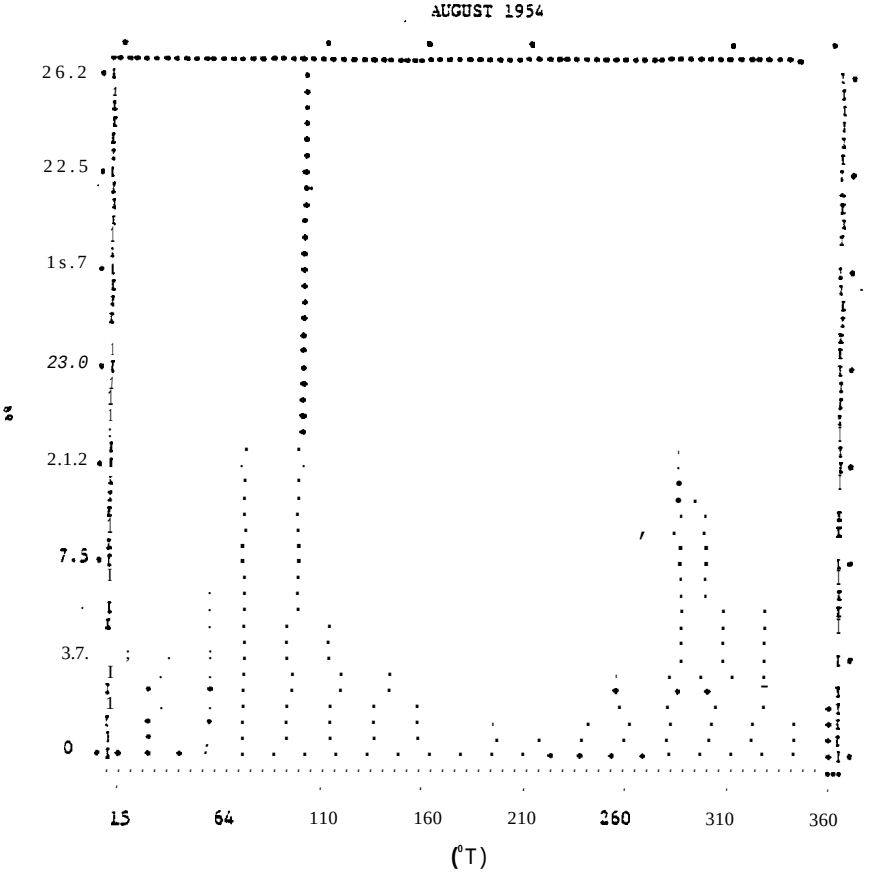

FIGURE 14: SURFACE WIND DIRECTION HISTOGRAM FOR BARTER ISLAND, ALASKA (AUGUST 1954).

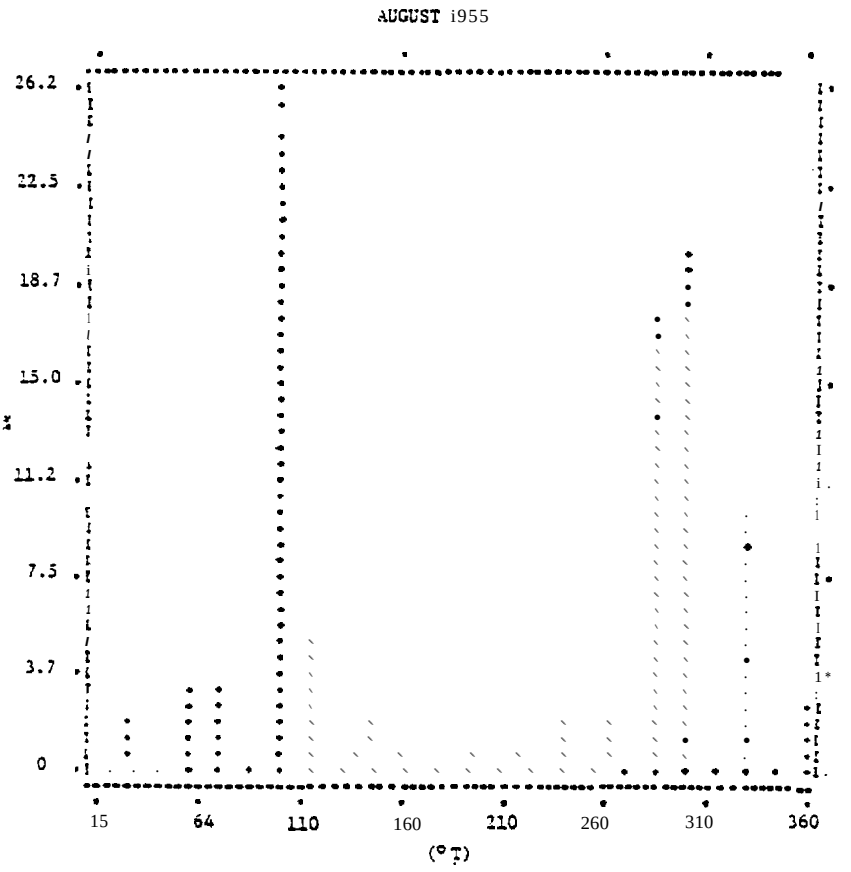

FIGURE 15: SURFACE WIND DIRECTION HISTOGRAM FOR BARTER ISLAND, ALASKA (AUGUST 1955).

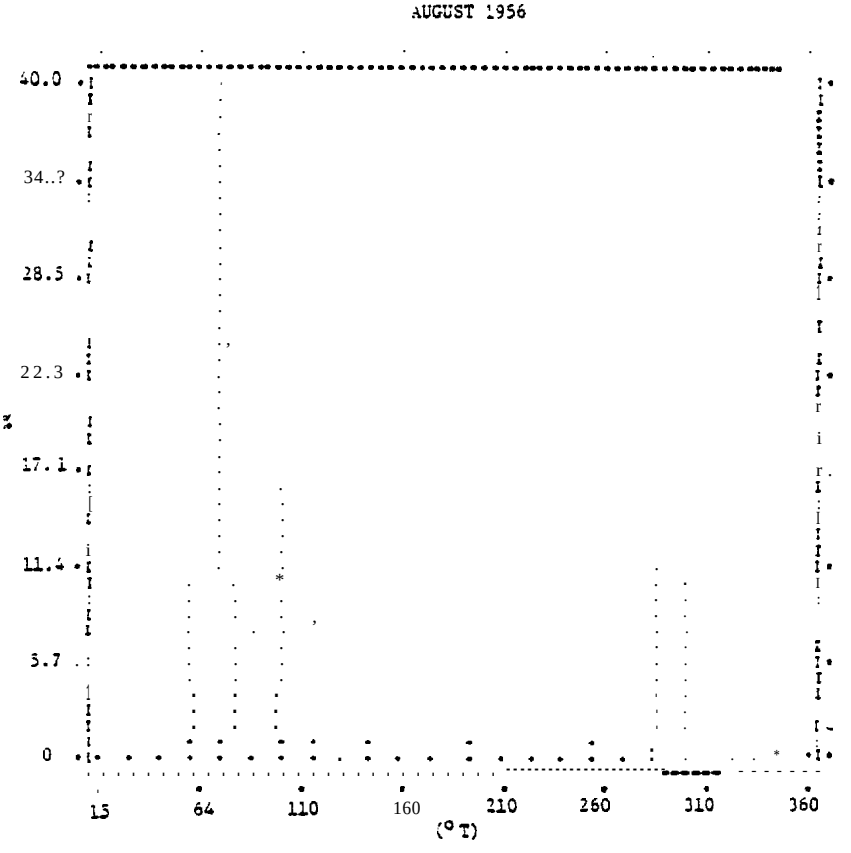

FIGURE 16: SURFACE WIND DIRECTION HISTOGRAM FOR BARTER ISLAND, ALASKA (AUGUST 1956).

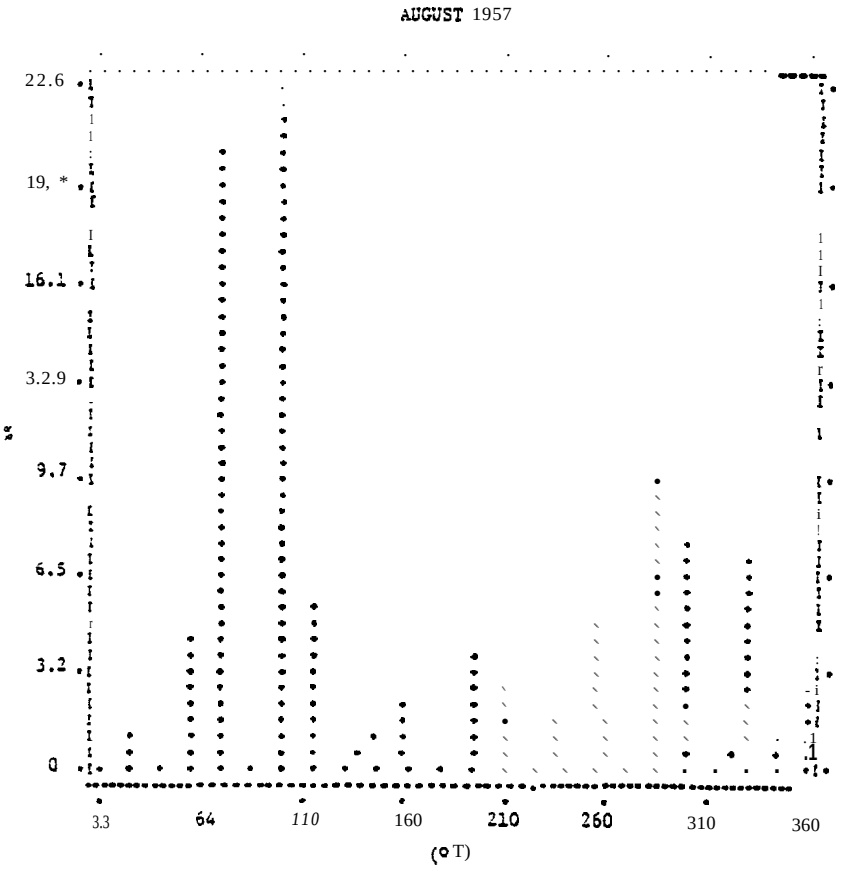

FIGURE 17: SURFACE WIND DIRECTION HISTOGRAM FOR BARTER ISLAND, ALASKA (AUGUST 1957).

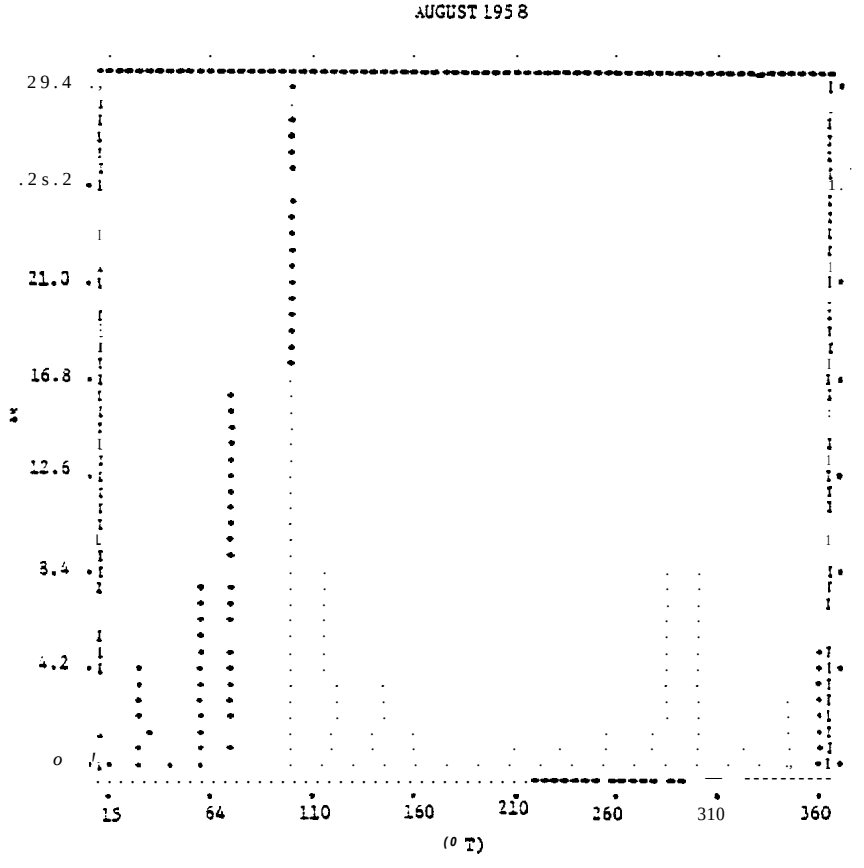

FIGURE 18: SURFACE WIND DIRECTION HISTOGRAM FOR BARTER ISLAND, ALASKA (AUGUST 1958).

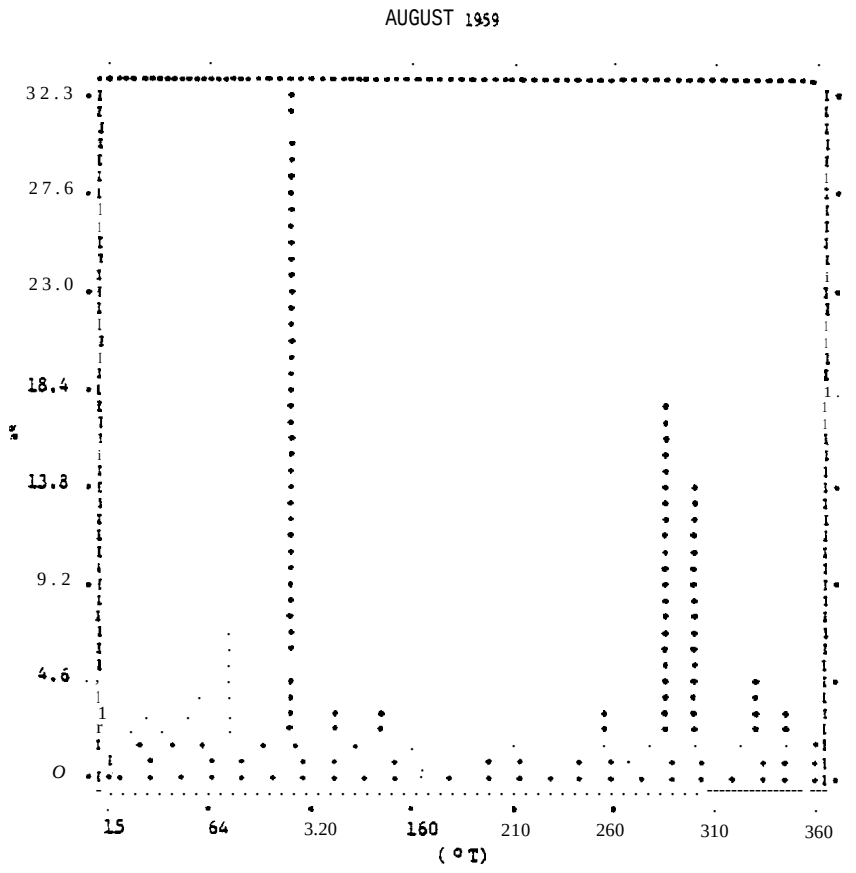

FIGURE 19: SURFACE WIND DIRECTION HISTOGRAM FOR BARTER ISLAND, ALASKA (AUGUST 1969).

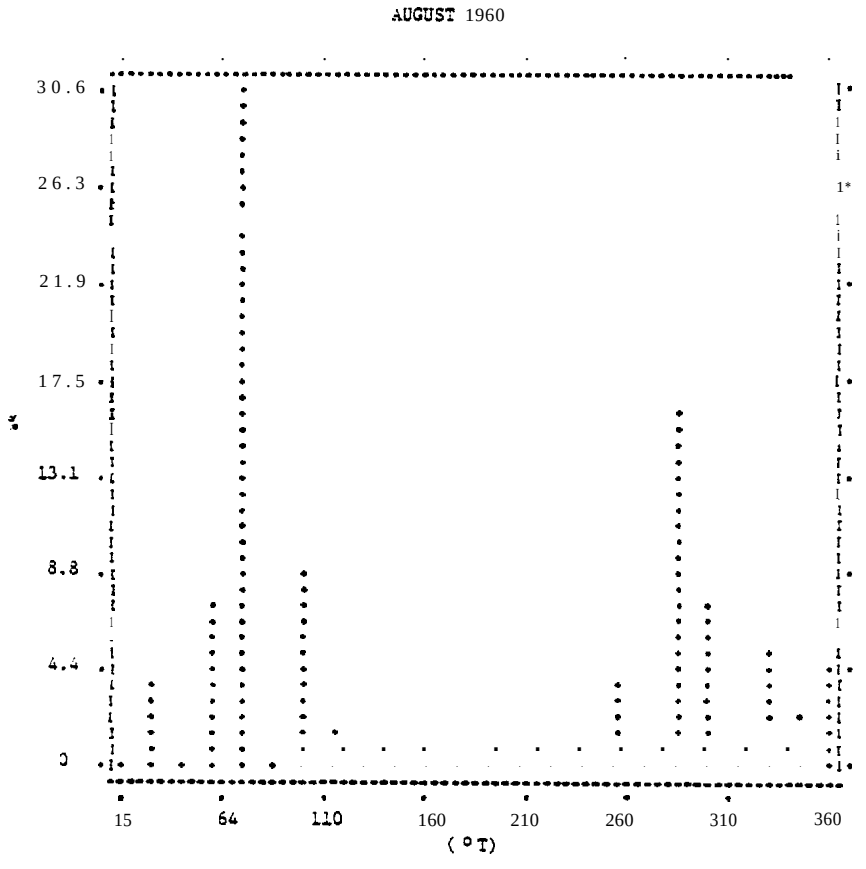

FIGURE 20: SURFACE WIND DIRECTION HISTOGRAM FOR BARTER ISLAND, ALASKA (AUGUST 1960).

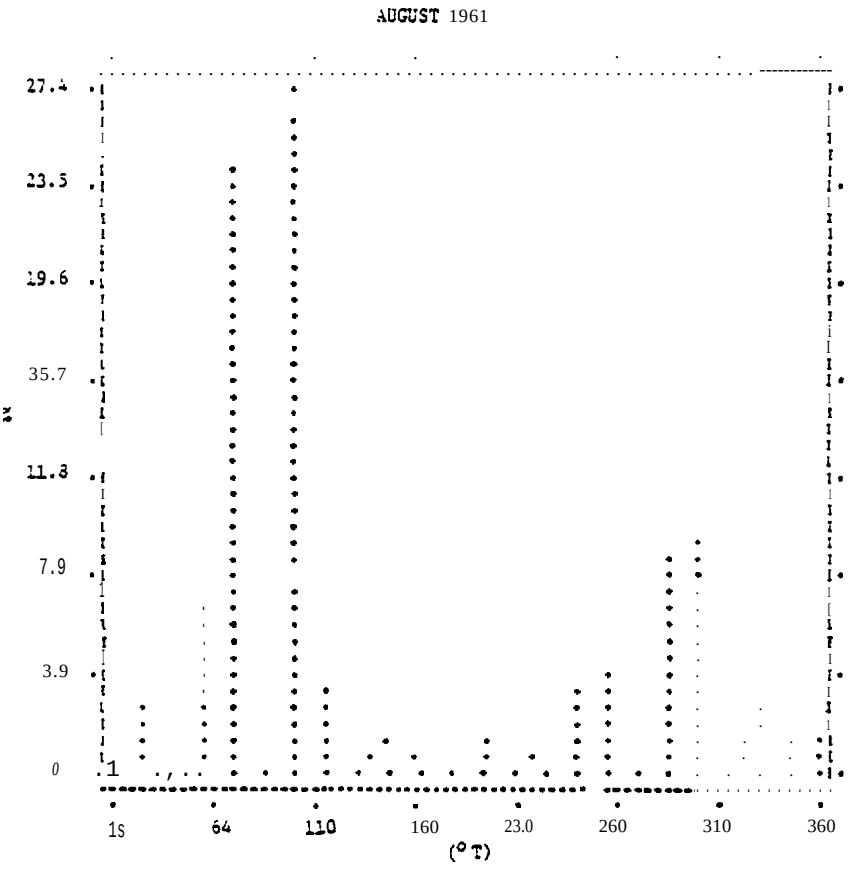

FIGURE 21: SURFACE WIND DIRECTION HISTOGRAM FOR BARTER ISLAND, ALASKA (AUGUST 1961).

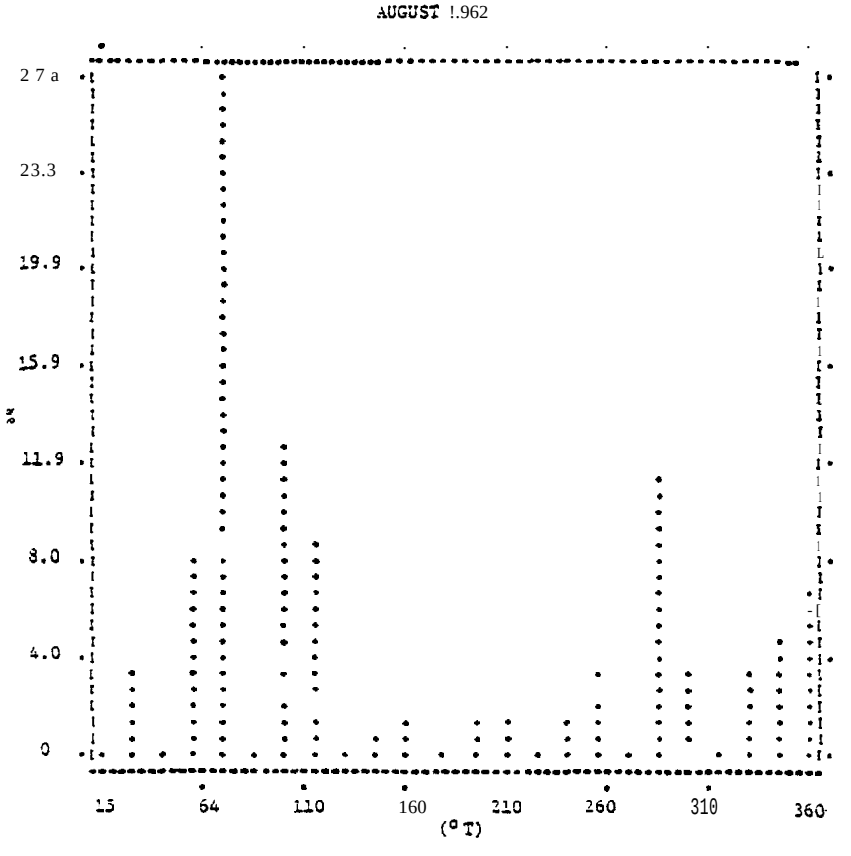

FIGURE 22: SURFACE WIND DIRECTION HISTOGRAM FOR BARTER ISLAND, ALASKA (AUGUST 1962).

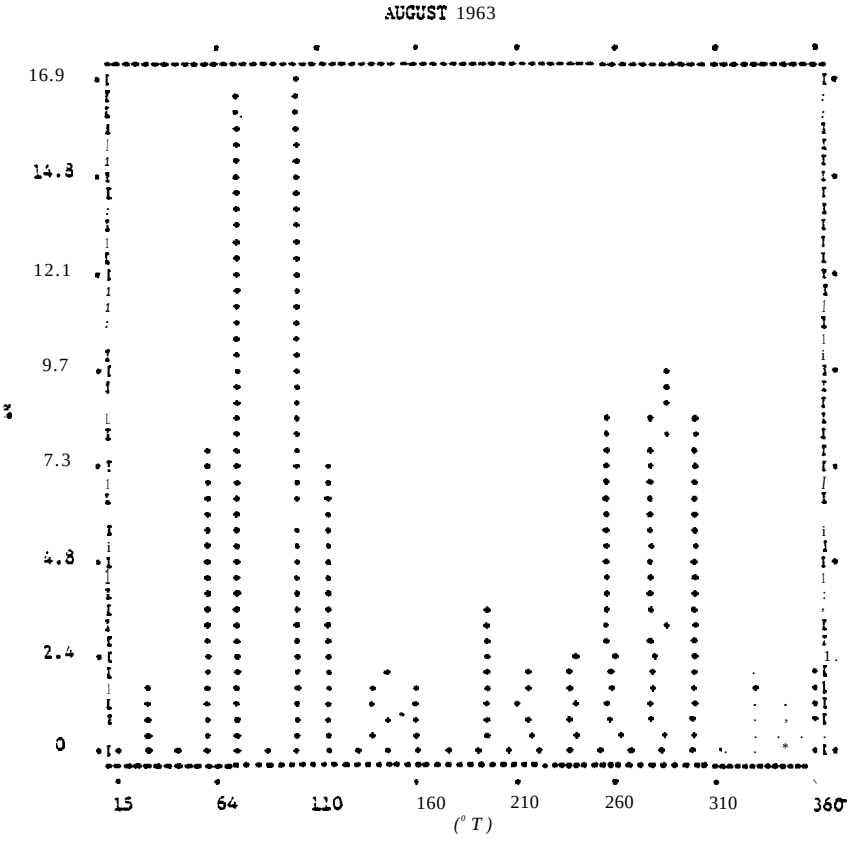

FIGURE 23: SURFACE WIND DIRECTION HISTOGRAM FOR BARTER ISLAND, ALASKA (AUGUST 1963).

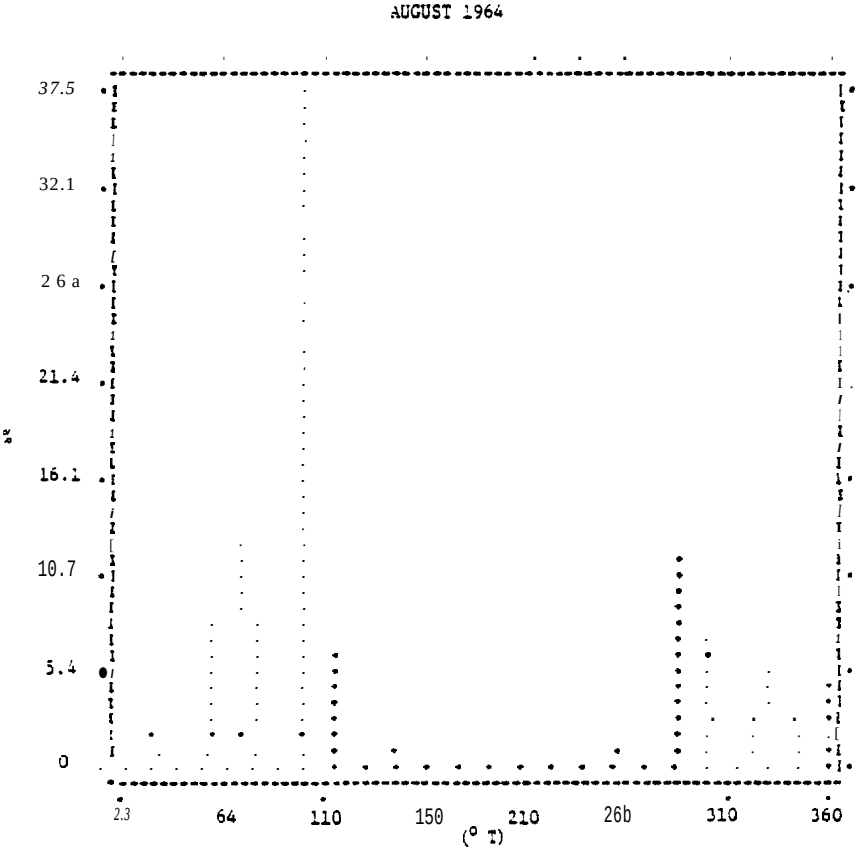

FIGURE 24: SURFACE WIND DIRECTION HISTOGRAM FOR BARTER ISLAND, ALASKA (AUGUST 1964).

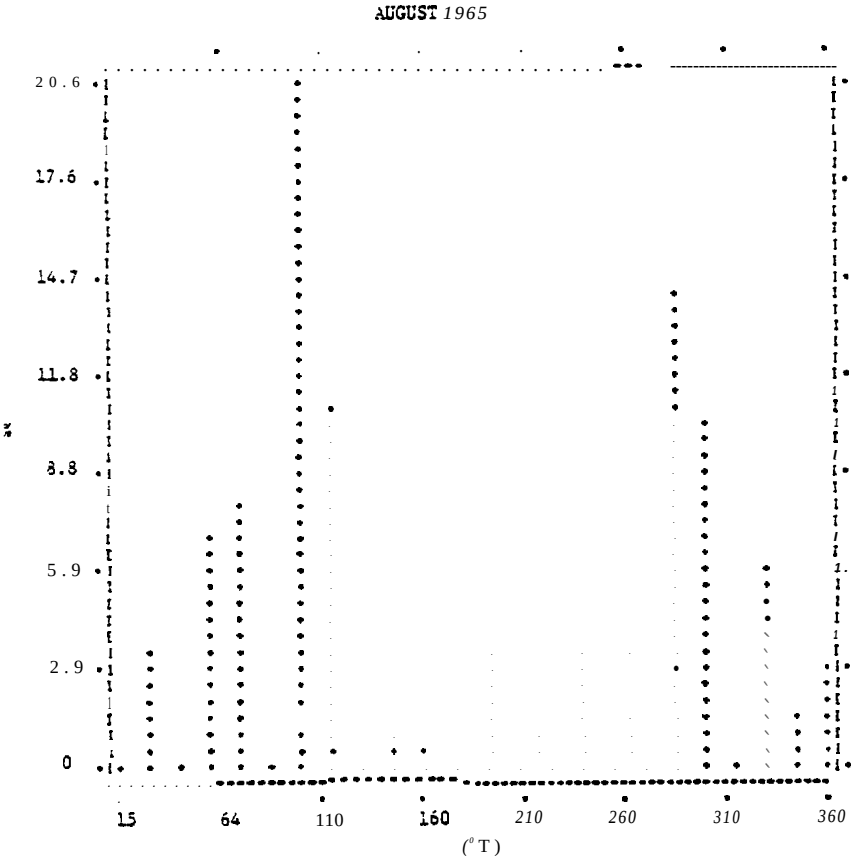

FIGURE 25: SURFACE WIND DIRECTION HISTOGRAM FOR BARTER ISLAND, ALASKA {AUGUST 1965).

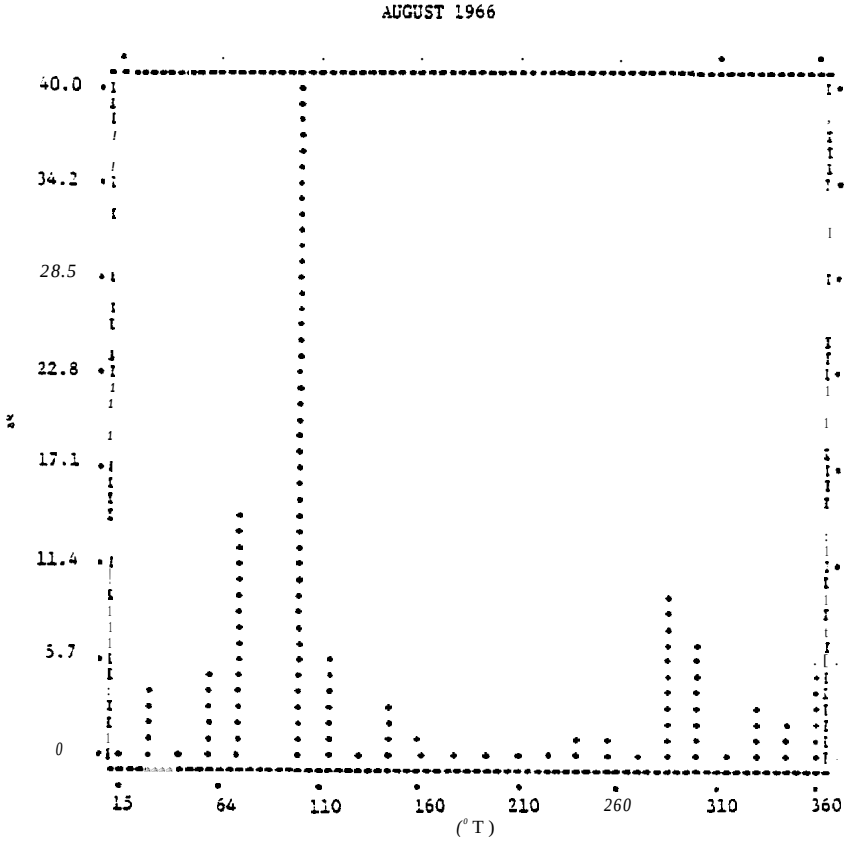

FIGURE 26: SURFACE WIND DIRECTION HISTOGRAM FOR BARTER ISLAND, ALASKA (AUGUST 1966)s

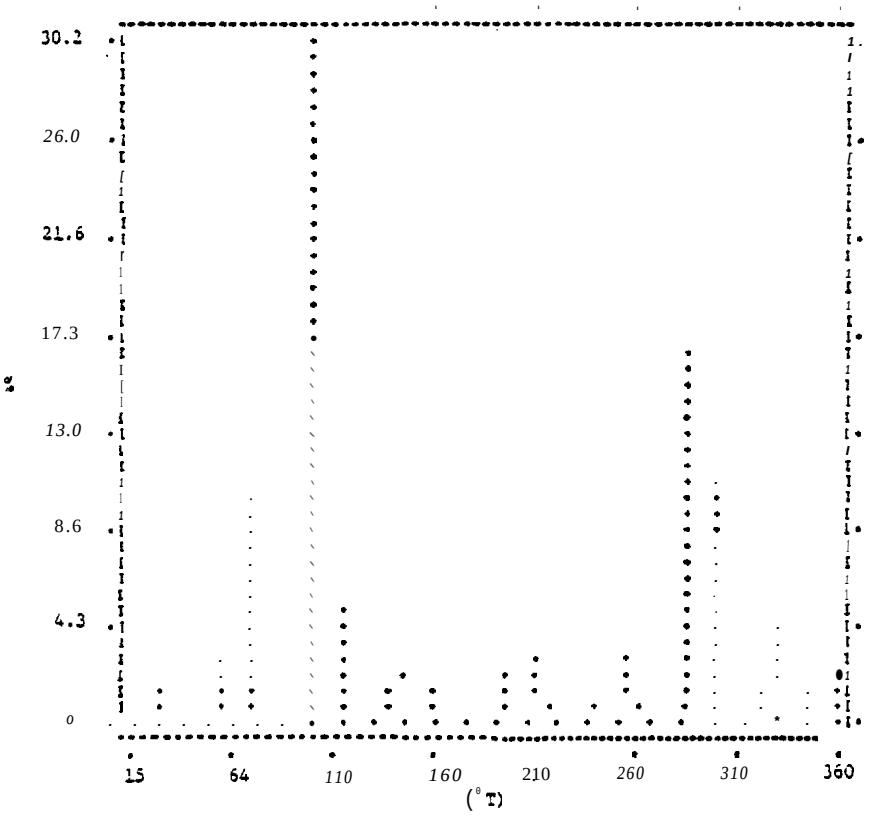

FIGURE 27: SURFACE WIND DIRECTION HISTOGRAM FOR BARTER ISLAND, ALASKA (AUGUST 18'87).

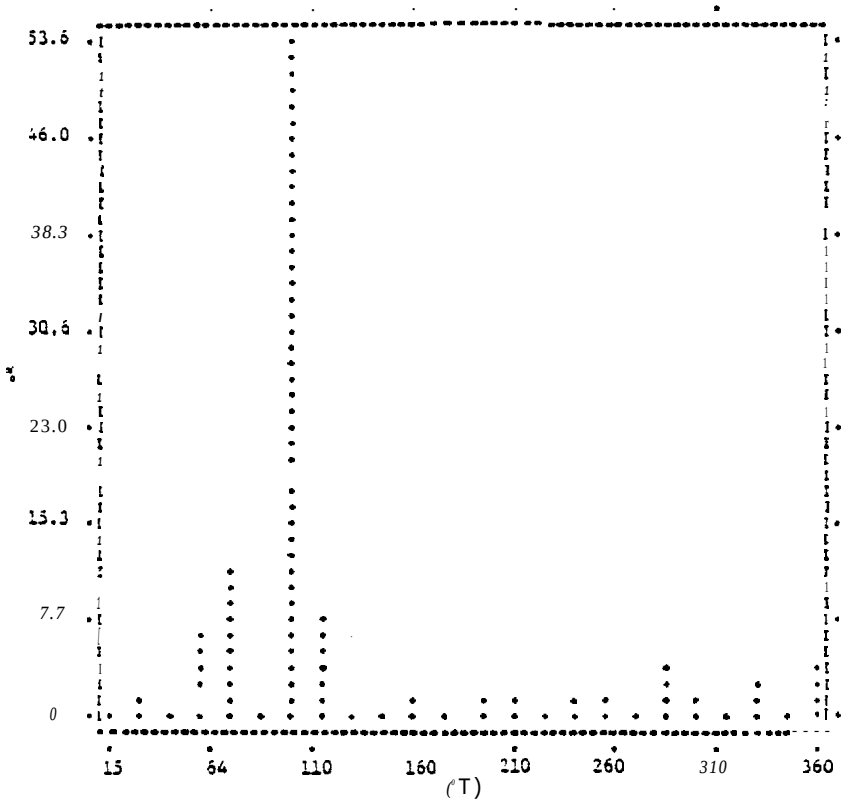

FIGURE 28: SURFACE WIND DIRECTION HISTOGRAM FOR BARTER ISLAND, ALASKA (AUGUST 1988).

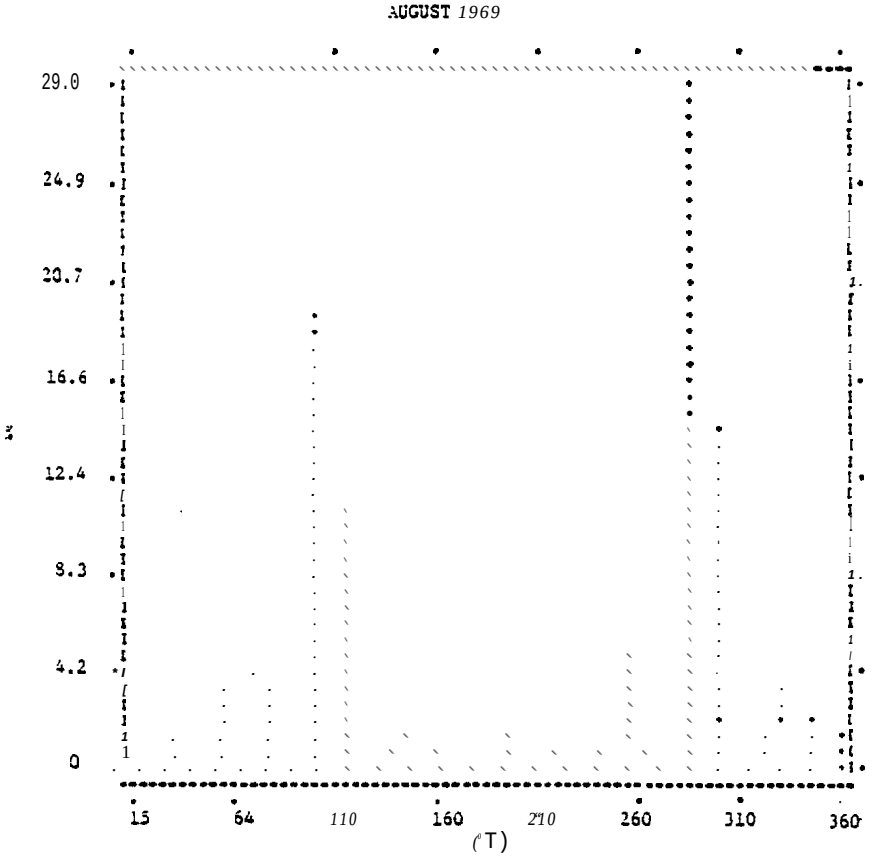

FIGURE 29: SURFACE WIND DIRECTION HISTOGRAM FOR BARTER ISLAND, ALASKA [AUGUST 1969).

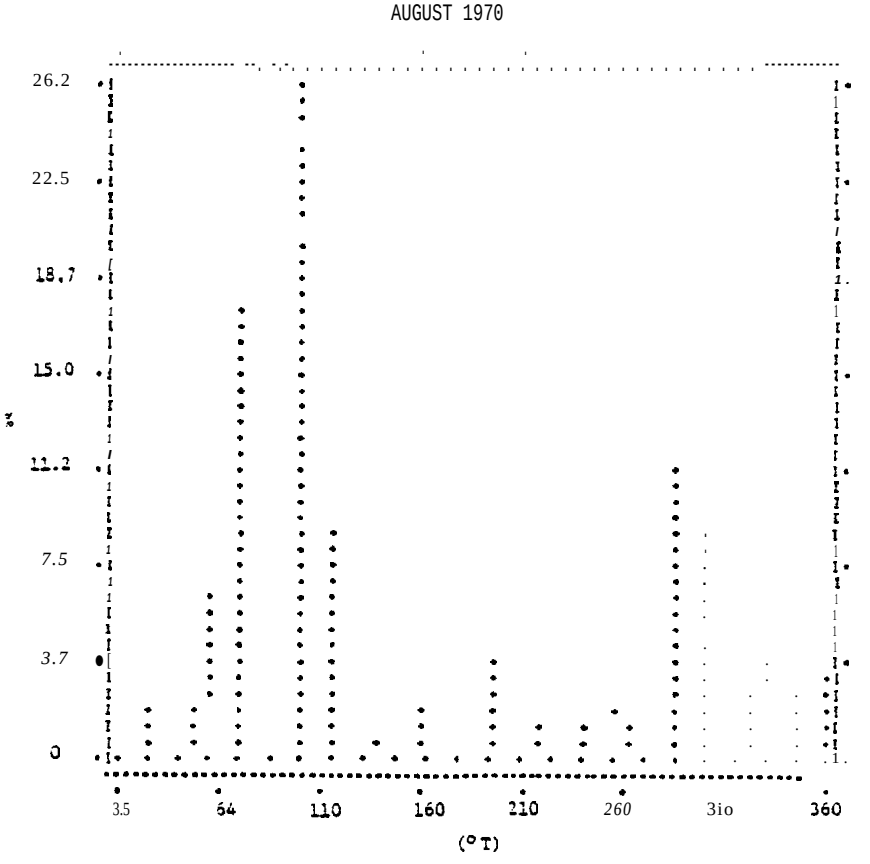

FIGURE 30: SURFACE WIND DIRECTION HISTOGRAM FOR BARTER ISLAND, ALASKA (AUGUST 1970).

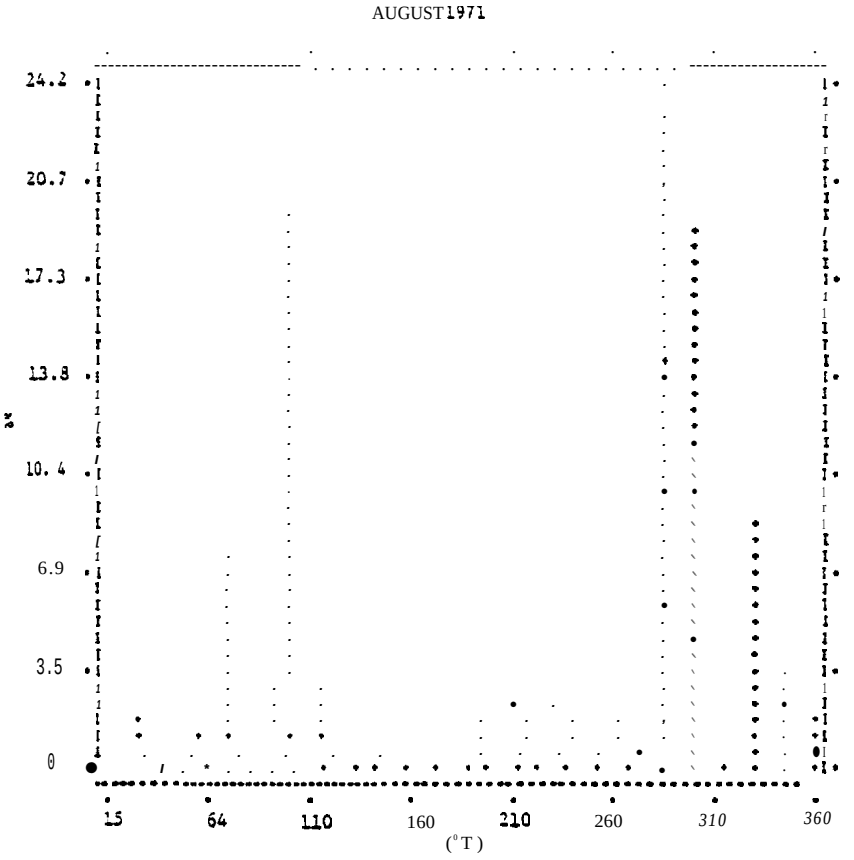

FIGURE 31: SURFACE WIND DIRECTION HISTOGRAM FOR BARTER -ISLAND, ALASKA (AUGUST 1971).

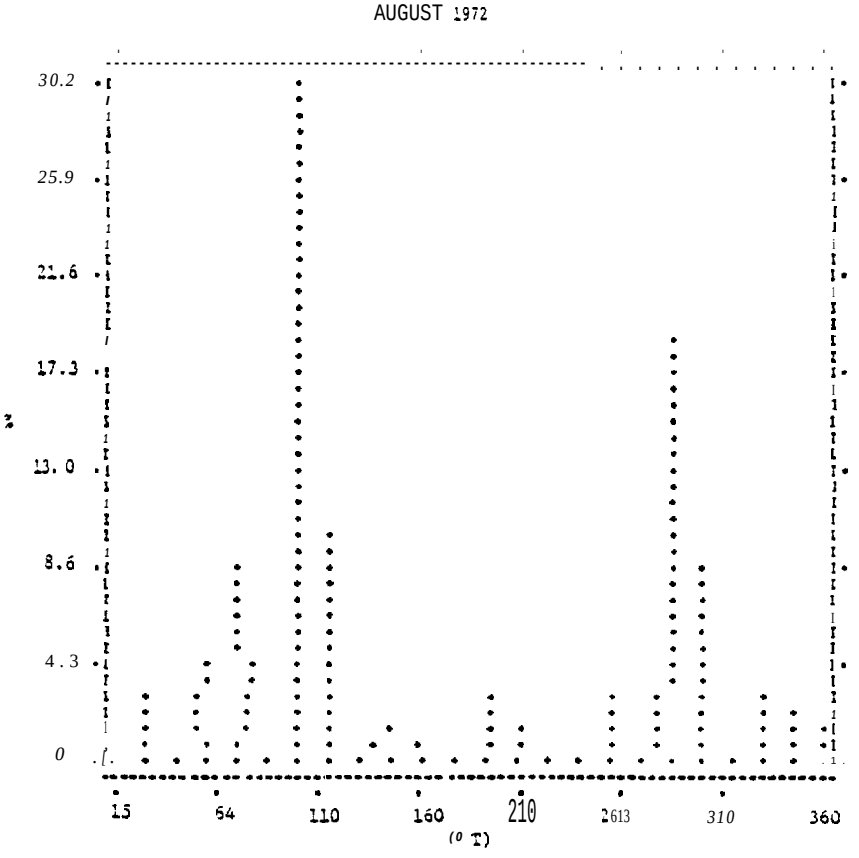

FIGURE 32: SURFACE WIND DIRECTION HISTOGRAM FOR BARTER ISLAND, ALASKA (AUGUST 1972}.

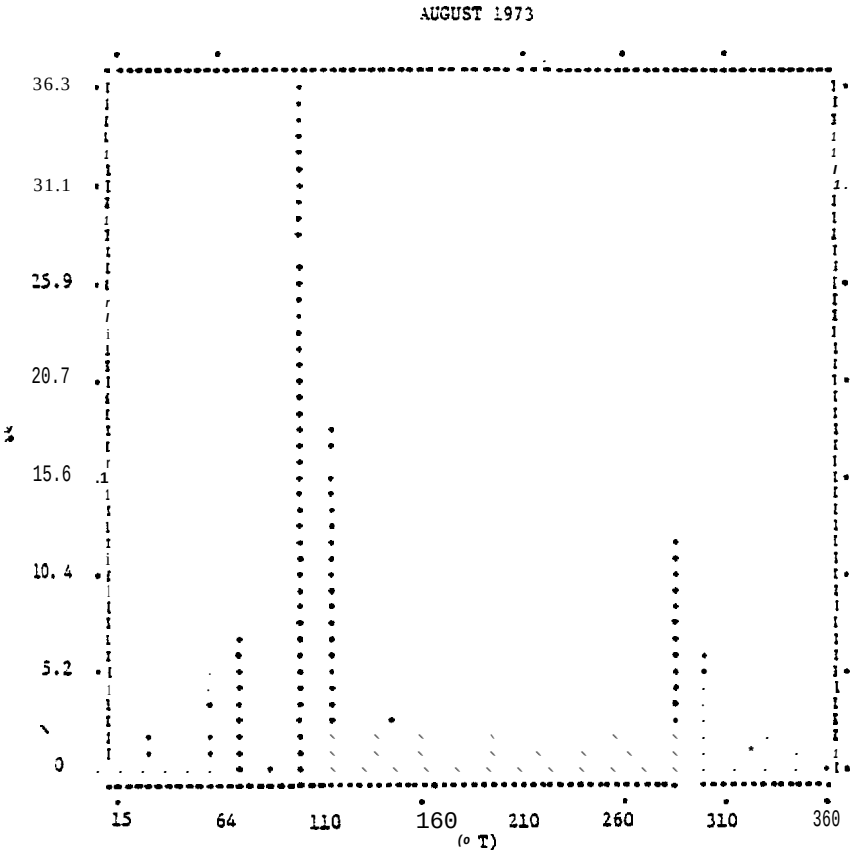

FIGURE 33: SURFACE WIND DIRECTION HISTOGRAM FOR BARTER ISLAND, ALASKA (AUGUST 1973).

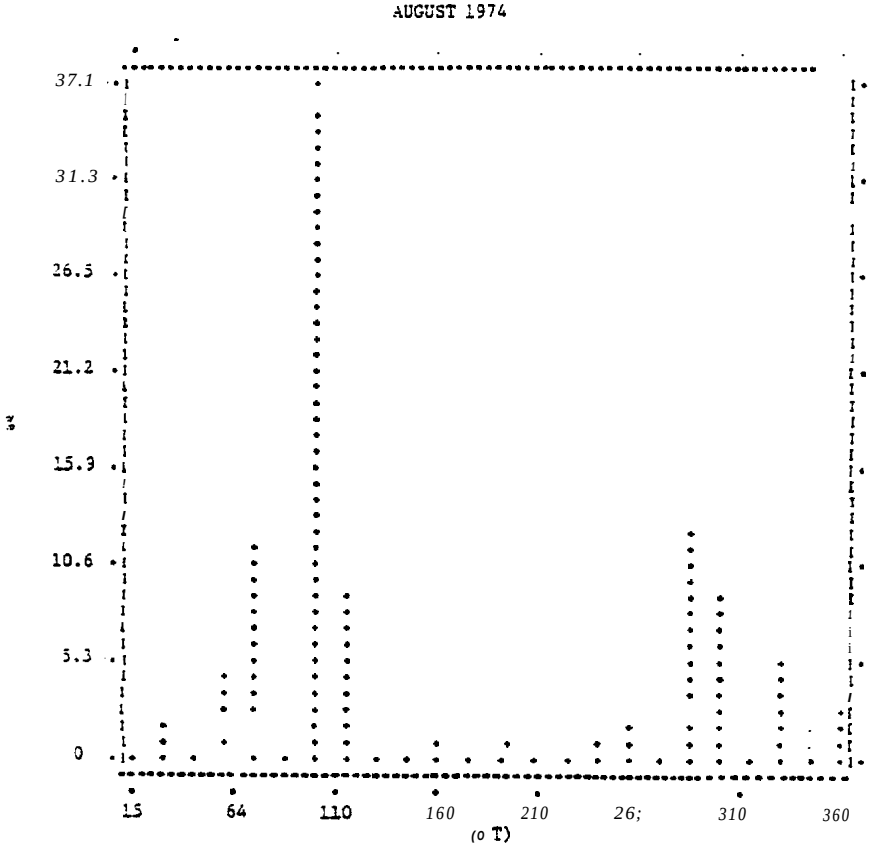

FIGURE 34: SURFACE WIND DIRECTION HISTOGRAM FOR BARTER ISLAND, ALASKA (AUGUST 1974).

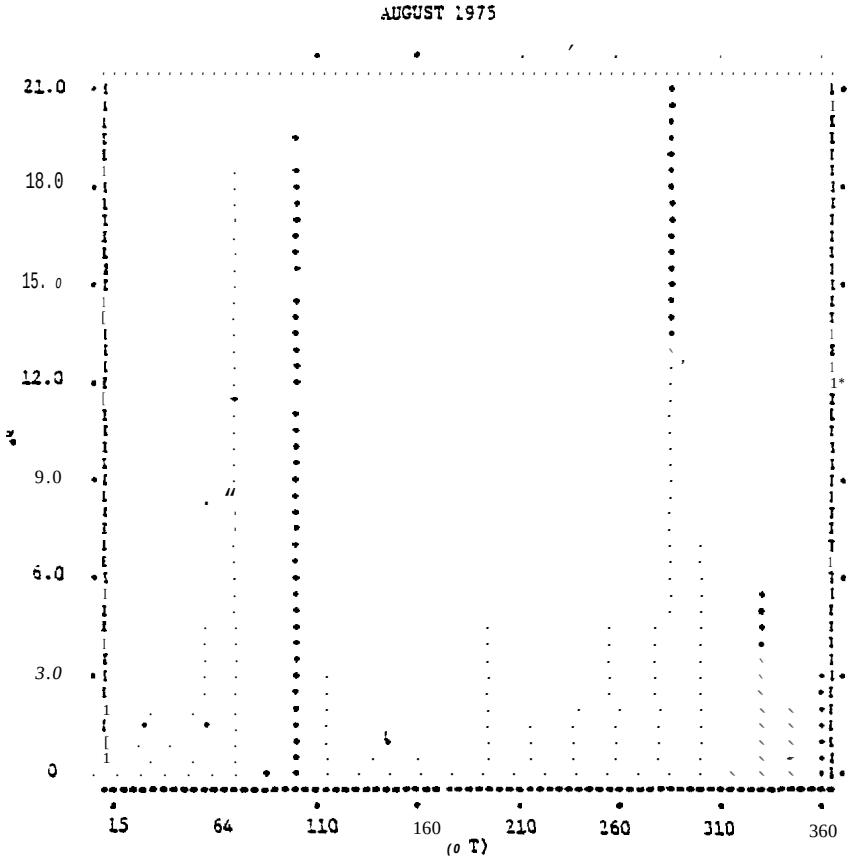

FIGURE 35: SURFACE WIND DIRECTION HISTOGRAM FOR BARTER ISLAND, ALASKA [AUGUST 1975].

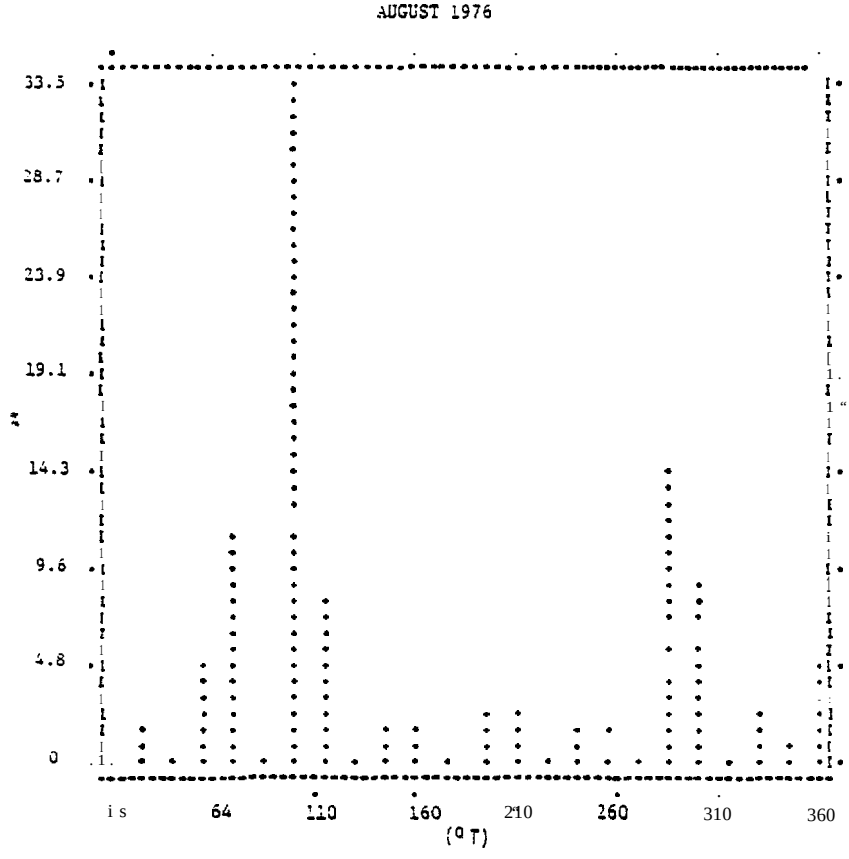

FIGURE 36: SURFACE WIND DIRECTION HISTOGRAM FOR BARTER ISLAND, ALASKA (AUGUST 1976).

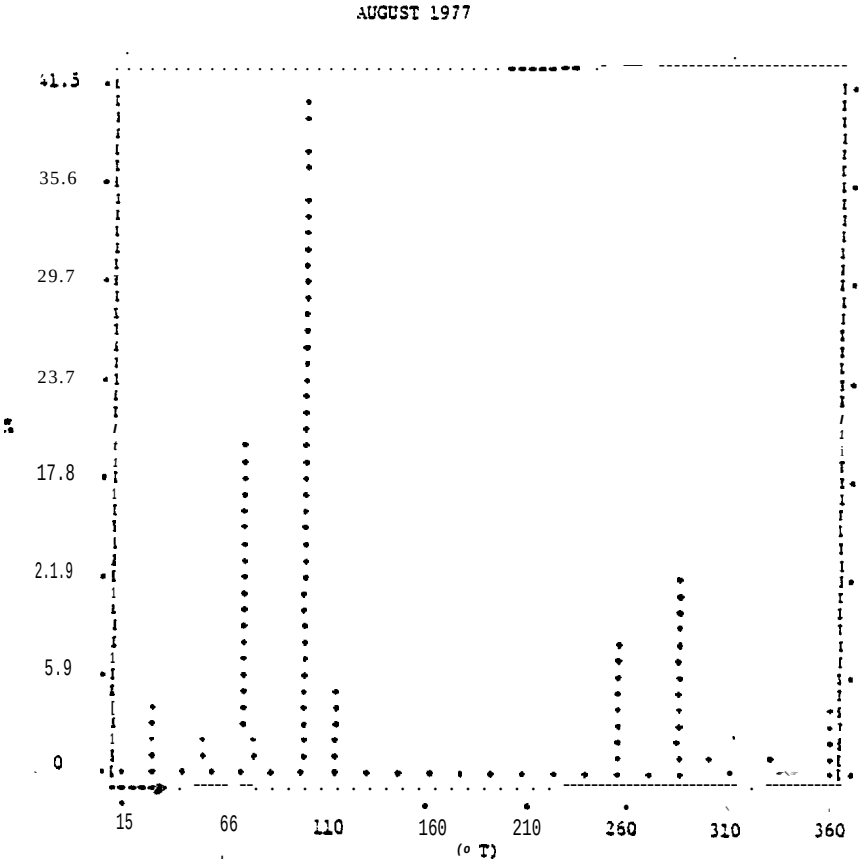

FIGURE 37: SURFACE WIND DIRECTION HISTOGRAM FOR BARTER ISLAND, ALASKA (AUGUST 1977}.

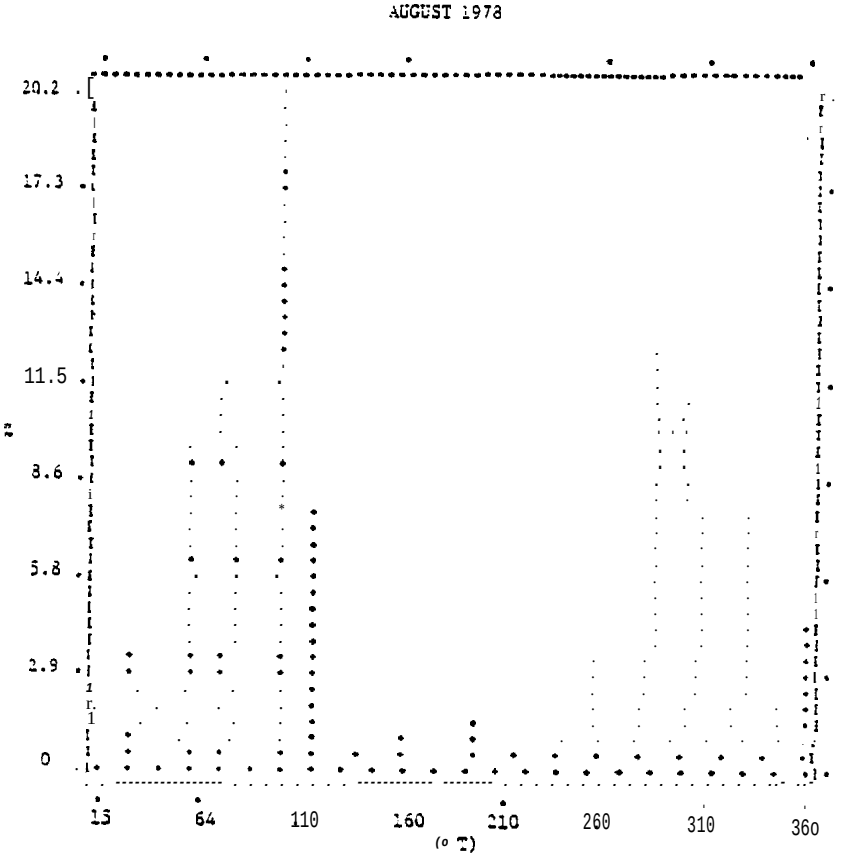

FIGURE 38: SURFACE WIND DIRECTION HISTOGRAM FOR BARTER ISLAND, ALASKA (AUGUST 1978).

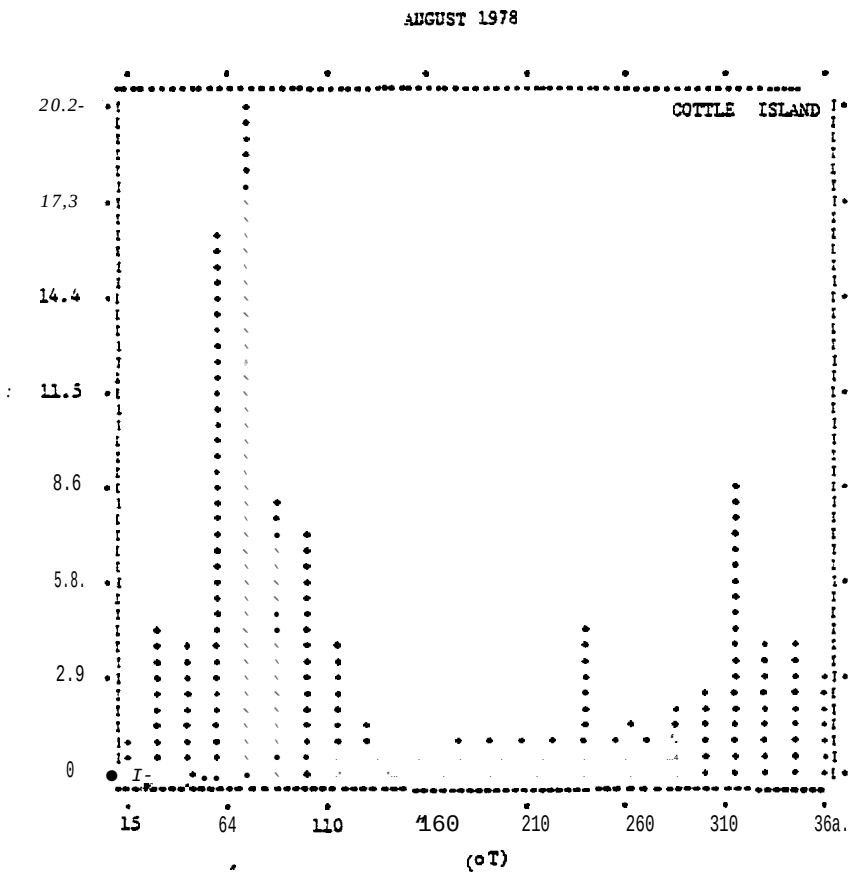

FIGURE 39: SURFACE WIND DIRECTION HISTOGRAM FOR COTTLE ISLAND ALASKA (AUGUST 1978} - TYPE I.

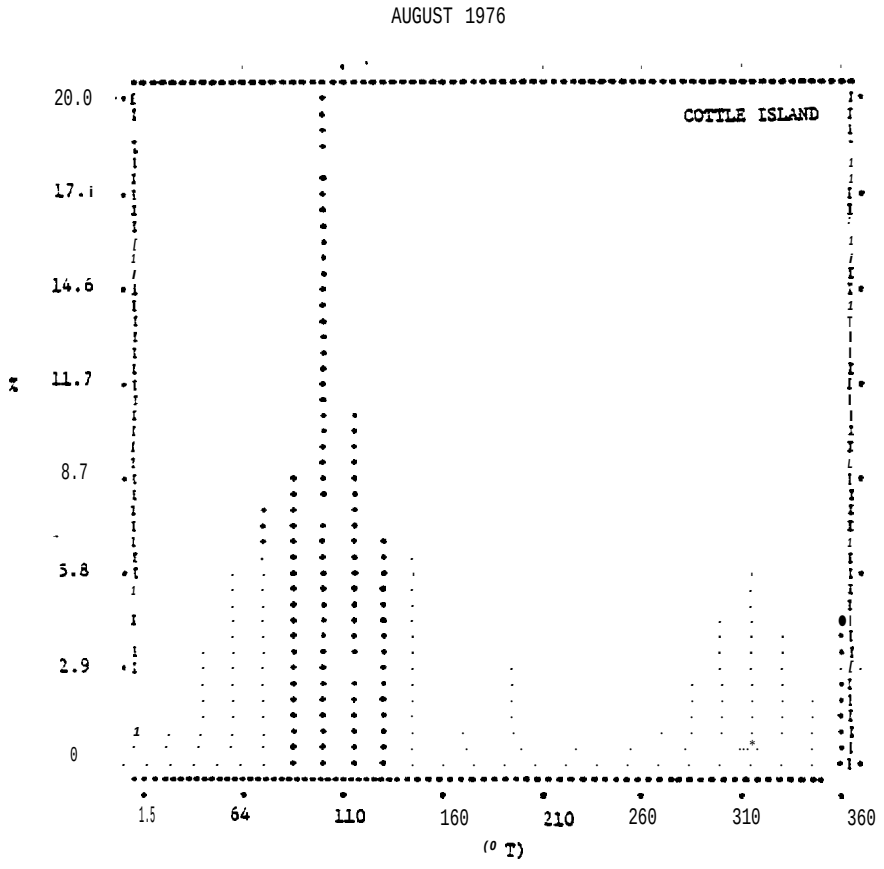

FIGURE 40: SURFACE WIND DIRECTION HISTOGRAM FOR COTTLE ISLAND ALASKA (AUGUST 1976) - TYPE i.

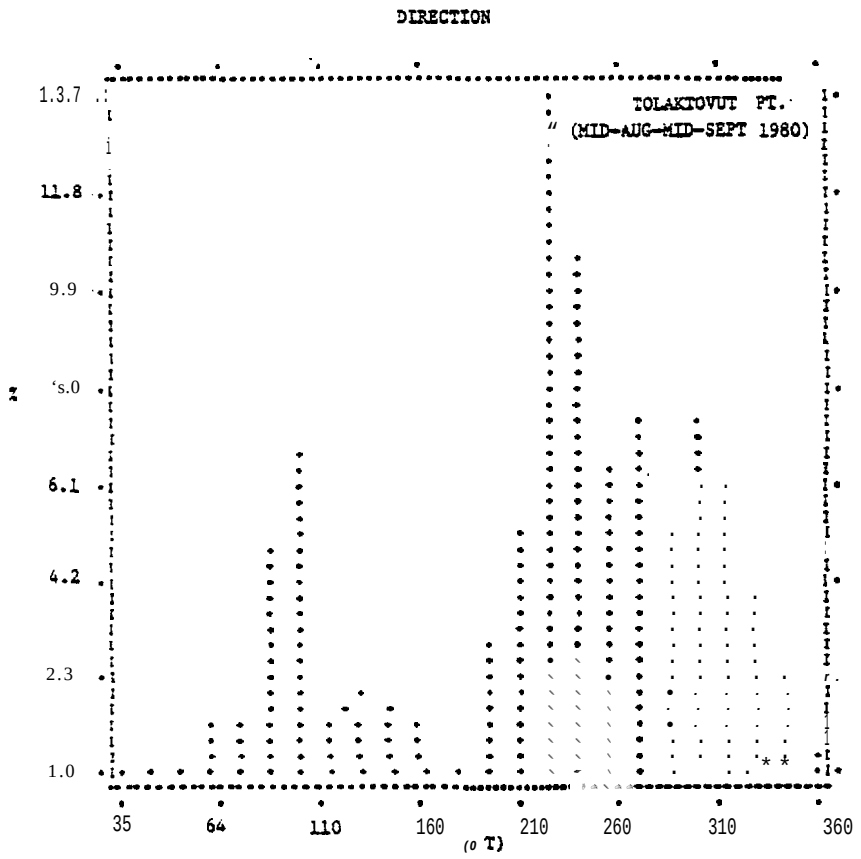

FIGURE 41: SURFACE WIND DIRECTION HISTOGRAM FOR TOLAKTOVUT POINT ALASKA (MID AUGUST TO MID SEPTEMBER 1980).

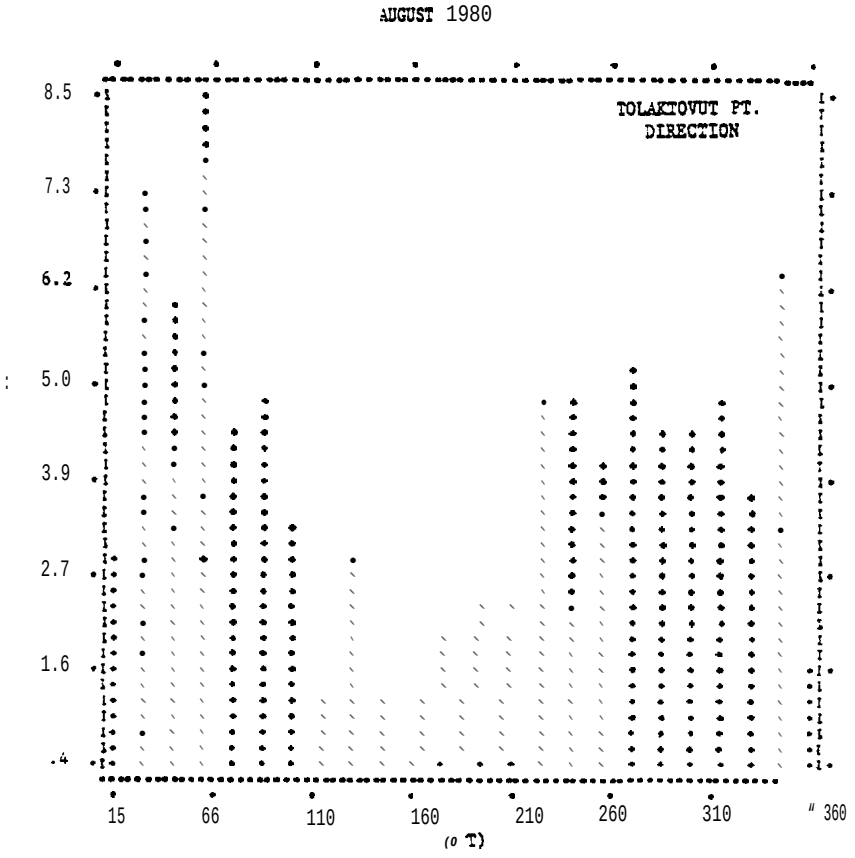

FIGURE 42: SURFACE WIND DIRECTION HISTOGRAM FOR TOLOKTOVUT POINT ALASKA (AUGUST 1980]. TYPE II.

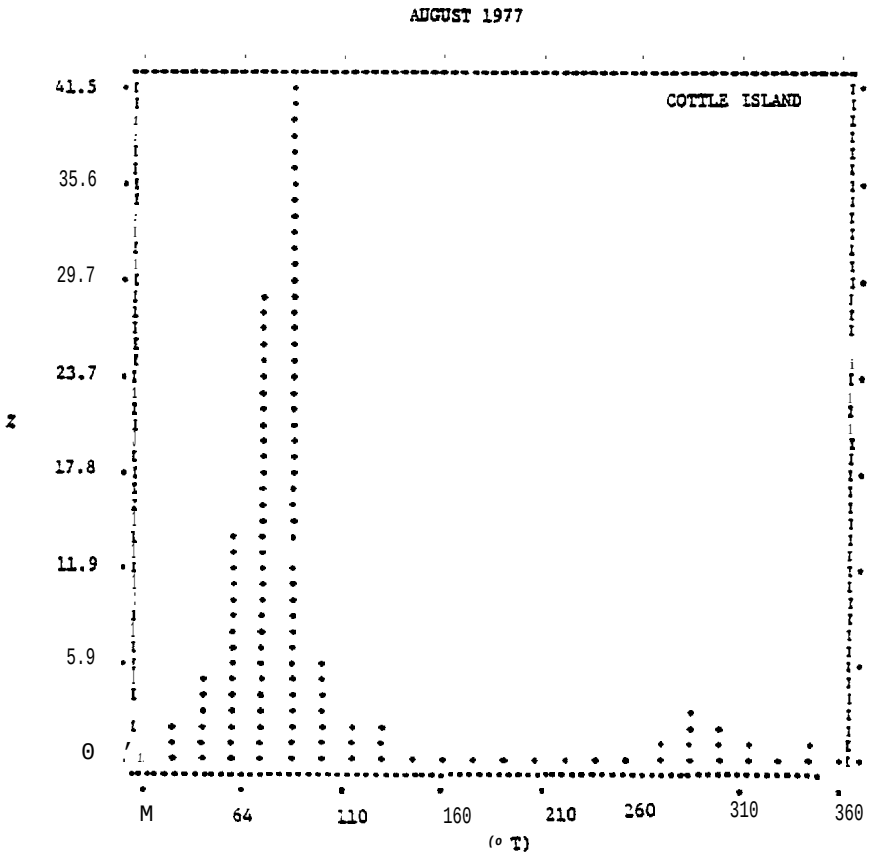

FIGURE 43: SURFACE WIND DIRECTION HISTOGRAM FOR COTTLE ISLAND ALASKA (AUGUST 1977) - TYPE III.

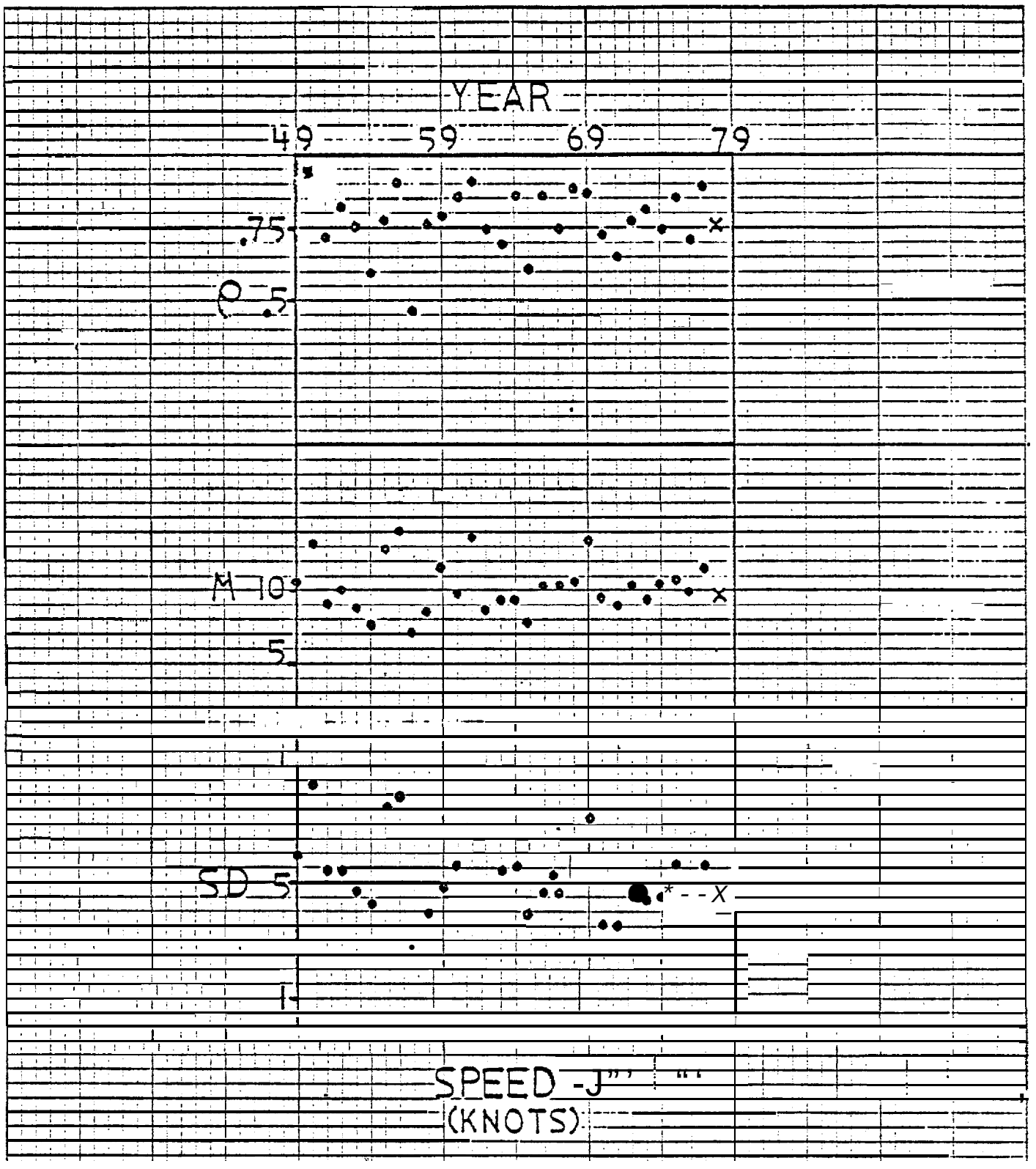

FIGURE 44: LAG–ONE AUTOCORRELATION COEFFICIENTS (P) MEAN (M), AND STANDARD DEVIATION (SD) FOR WIND SPEED DATA FROM BARTER ISLAND FOR 1 949– 1978

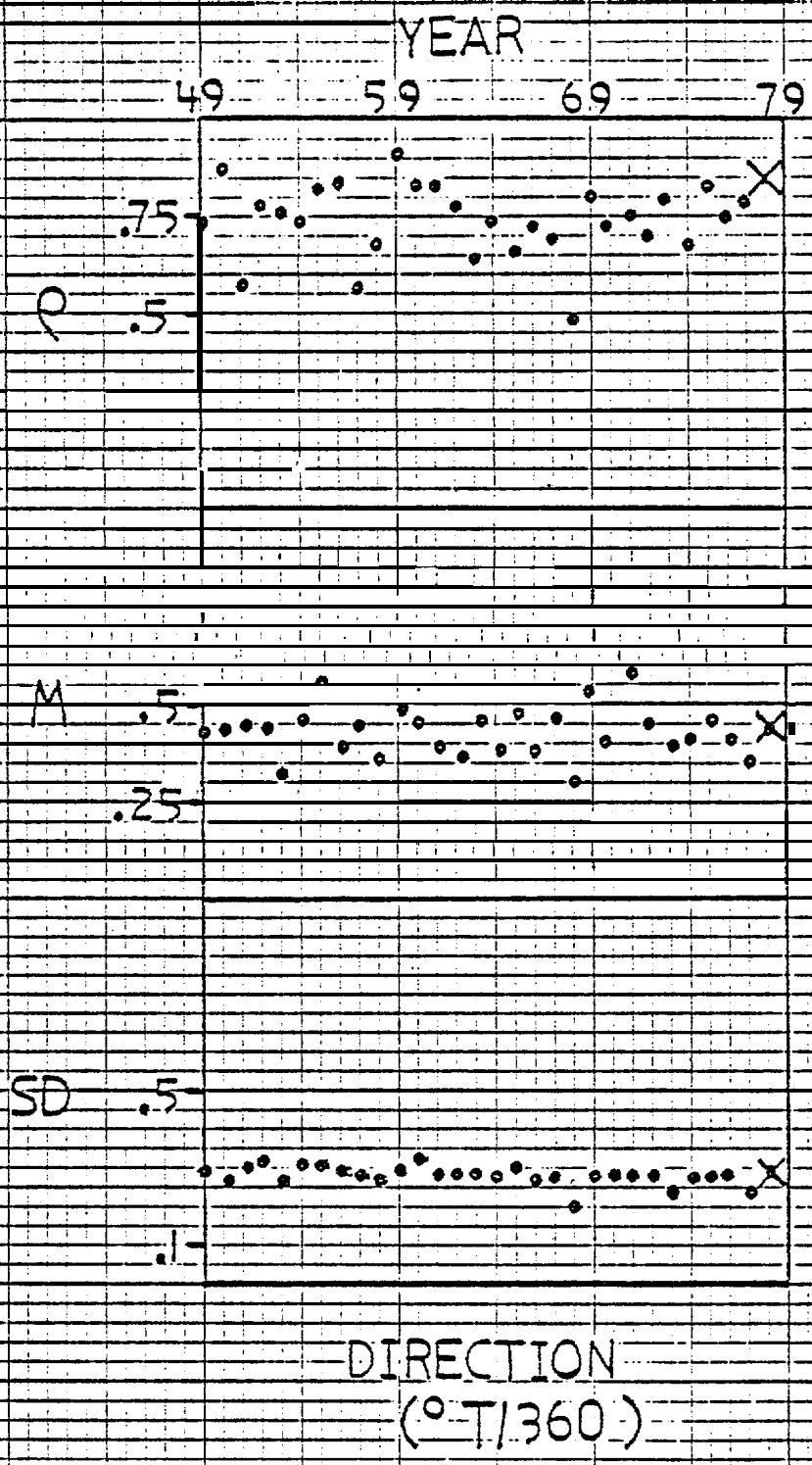

FIGURE 45: LAG–ONE AUTOCORRELATION COEFFICIENTS (P), MEAN (M), AND STANDARD DEVIATION (SD) FOR WIND DIRECTION DATA FROM BARTER ISLAND FOR 1949–1978.

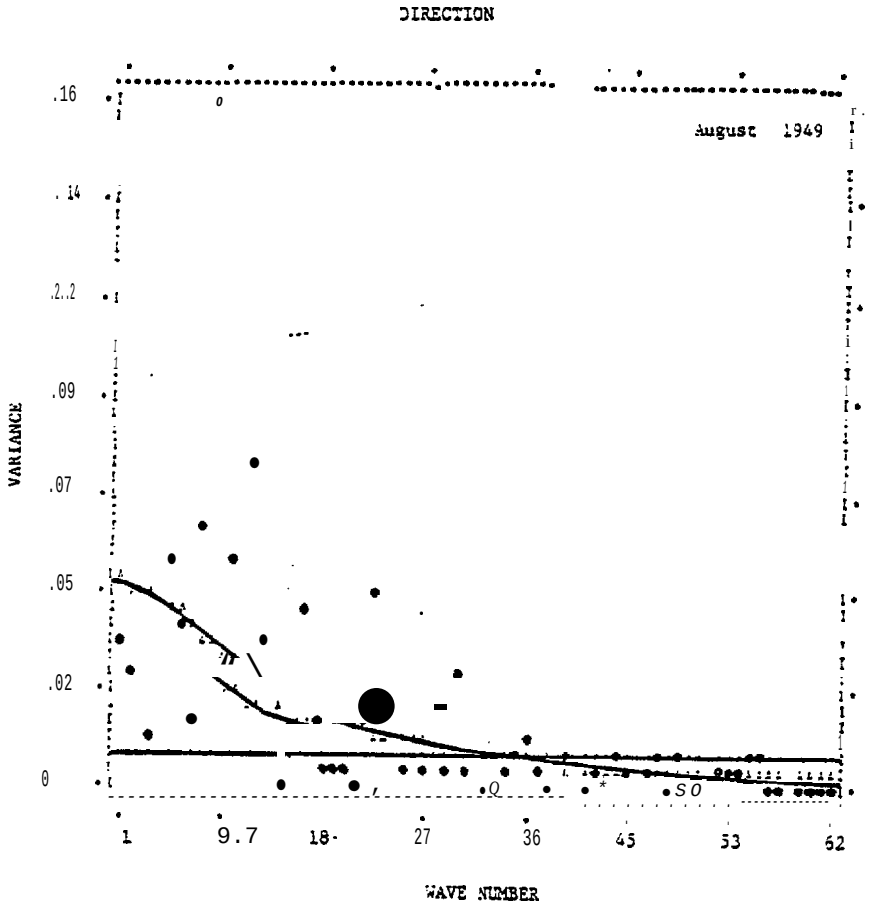

(a)

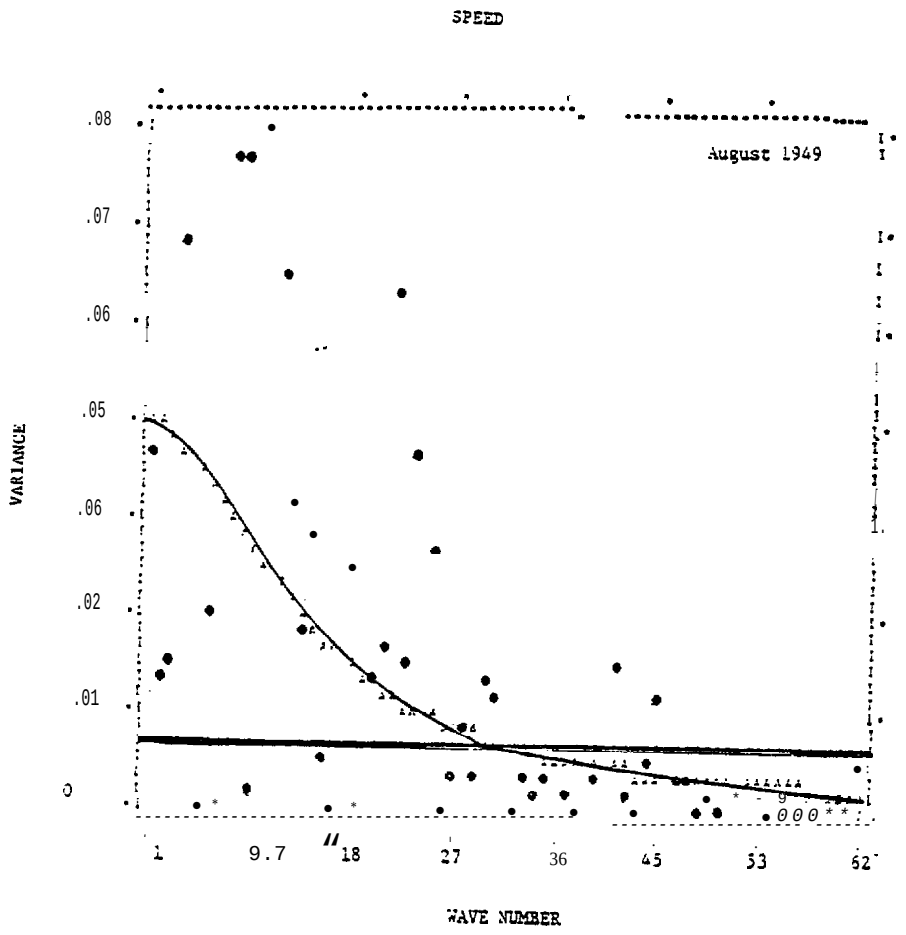

(b)

FIGURE 46: AMPLITUDE OF FOURIER COMPONENTS COMPARED TO A FIRST-ORDER MARKOV CONTINUUM (RED NOISE) AND A WHITE NOISE {RANDOM) CONTINUUM FOR DIRECTION (a) AND SPEED (b). (AUGUST 1949).

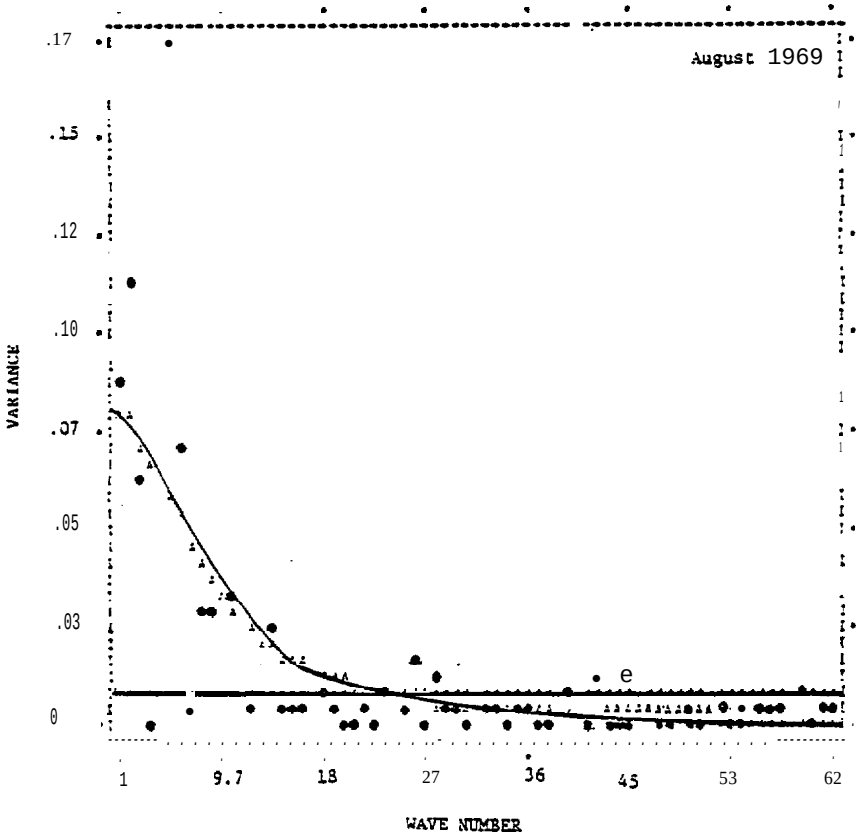

(a)

SPEED

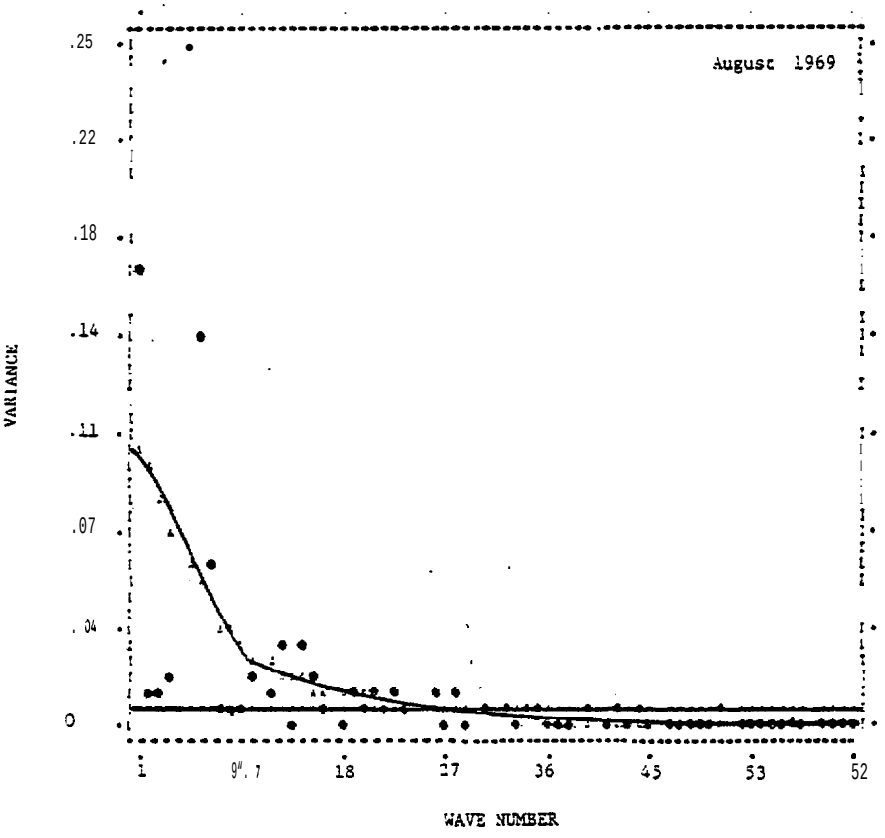

(b)

FIGURE 47: AMPLITUDE OF FOURIER COMPONENTS COMPARED TO A FIRST-ORDER MARKOV CONTINUUM {RED NOISE) AND A WHITE NOISE (RANDOM) CONTINUUM FOR DIRECTION (a) AND SPEED (b). (AUGUST 1969}.

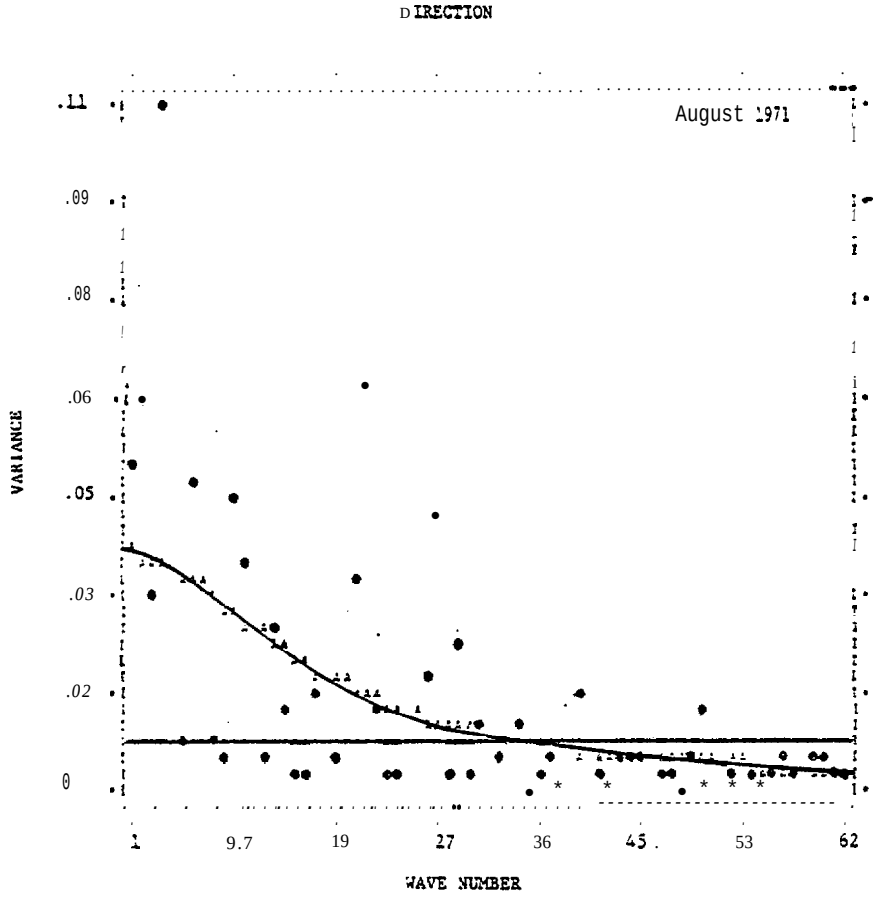

(a)

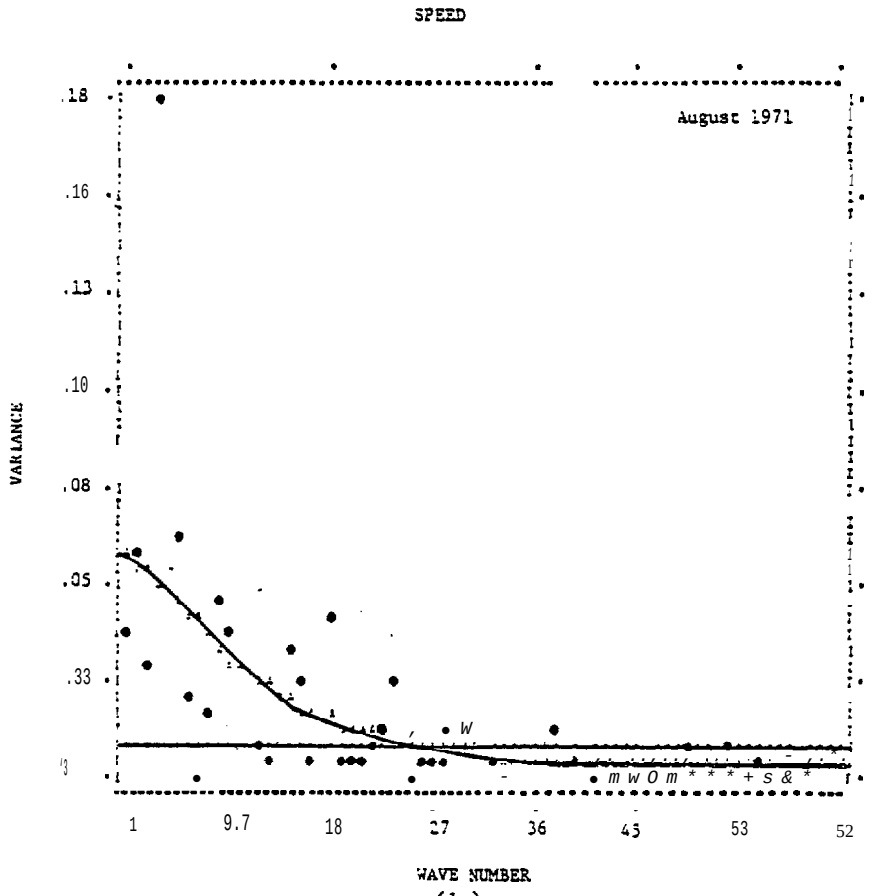

(b)

FIGURE 48: AMPLITUDE OF FOURIER COMPONENTS COMPARED TO A FIRST-ORDER MARKOV CONTINUUM (RED NOISE) AND A WHITE NOISE (RANDOM) CONTINUUM FOR DIRECTION (a) AND SPEED (b). (AUGUST 1971).

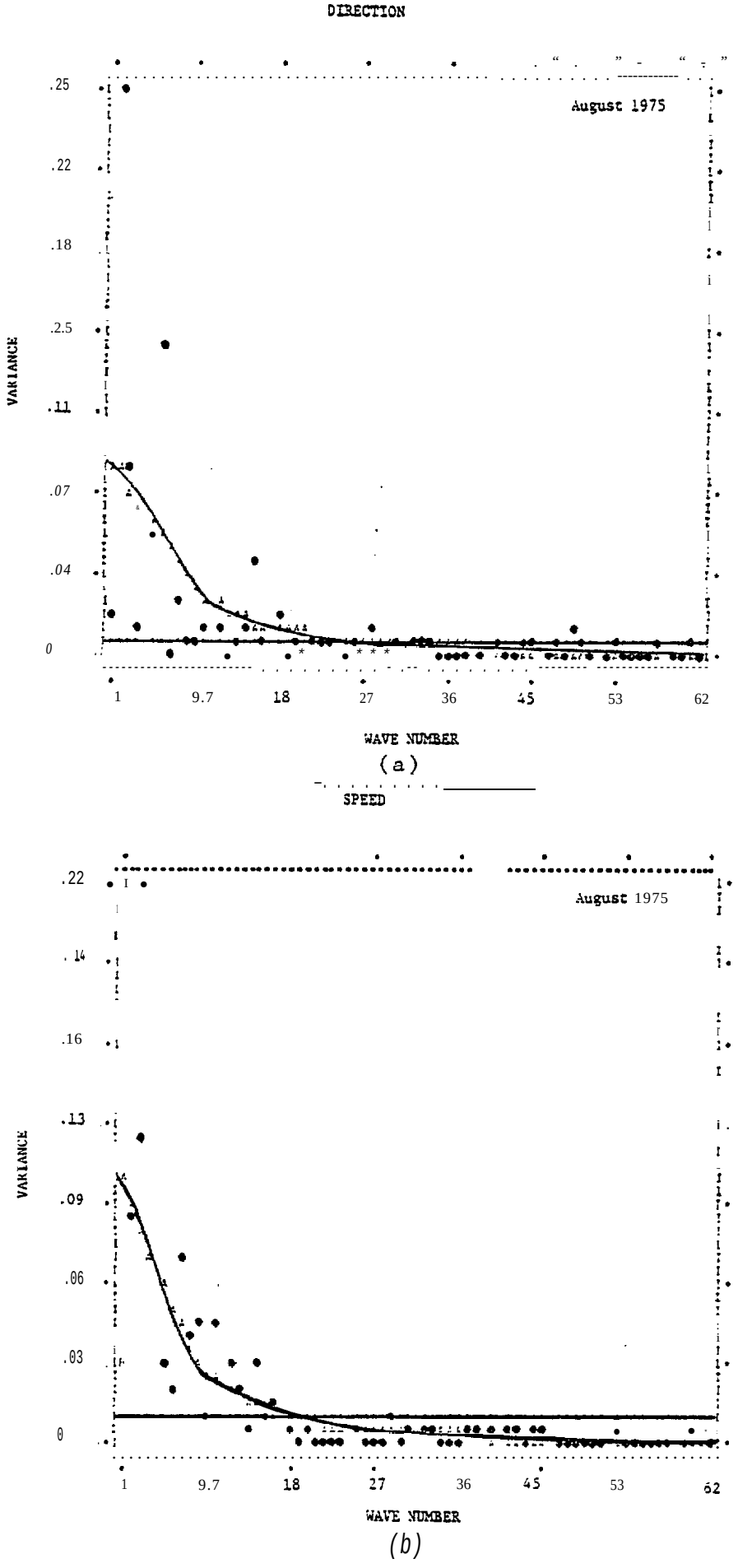

FIGURE 49: AMPLITUDE OF FOURIER COMPONENTS COMPARED TO A FIRST-ORDER MARKOV CONTINUUM (RED NOISE) AND A WHITE NOISE (RANDOM) CONTINUUM FOR DIRECTION (a) AND SPEED (b). (AUGUST 1975).

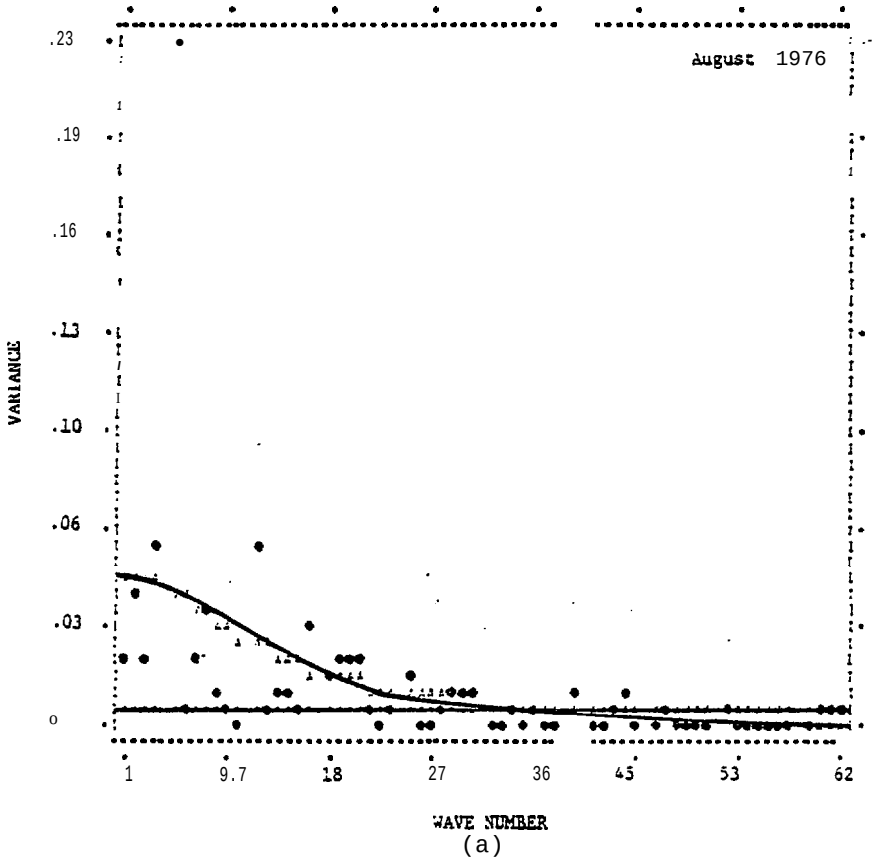

(a)

SPEED

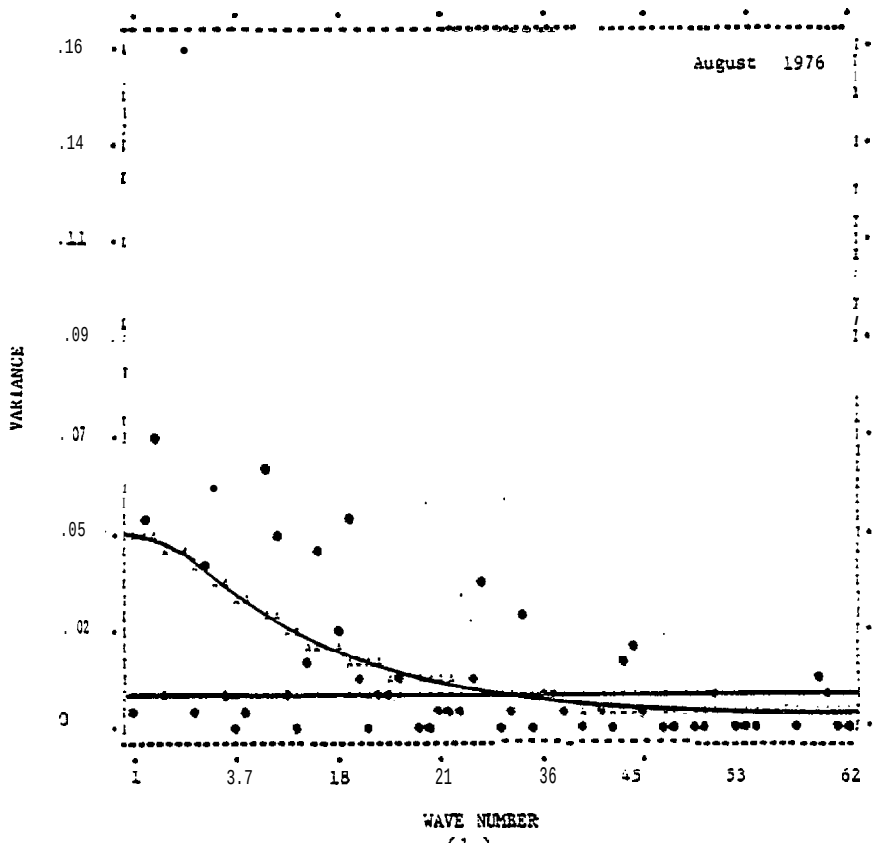

(b)

FIGURE 50: AMPLITUDE OF FOURIER COMPONENTS COMPARED TO A FIRST-ORDER MARKOV CONTINUUM {RED NOISE) AND A WHITE NOISE (RANDOM) CONTINUUM FOR DIRECTION {a) AND SPEED (b}. (AUGUST 1976).

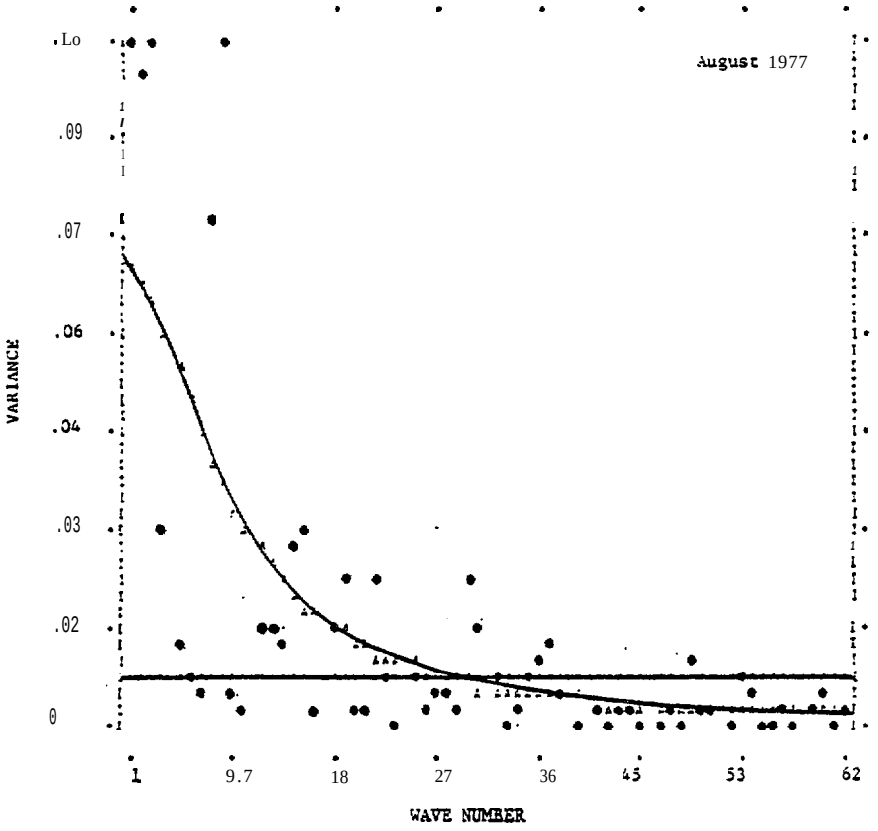

(a)

SPEED

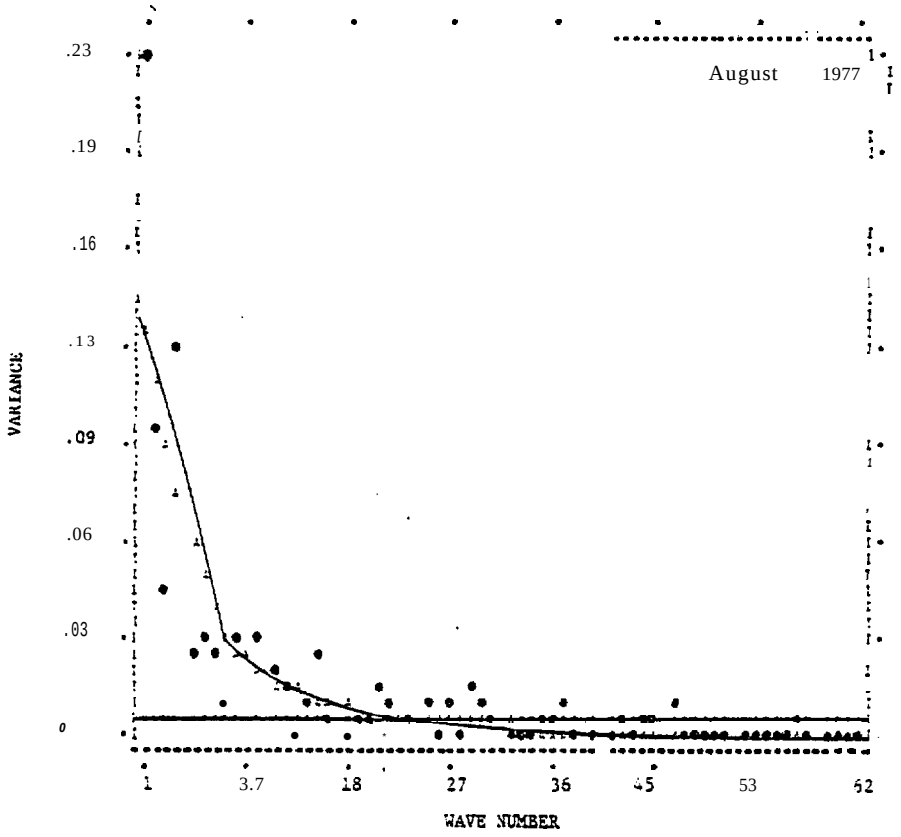

(b)

FIGURE 51: AMPLITUDE OF FOURIER COMPONENTS COMPARED TO A FIRST-ORDER MARKOV CONTINUUM (RED NOISE) AND A WHITE NOISE (RANDOM) CONTINUUM FOR DIRECTION (a) AND SPEED (b). (AUGUST 1977).

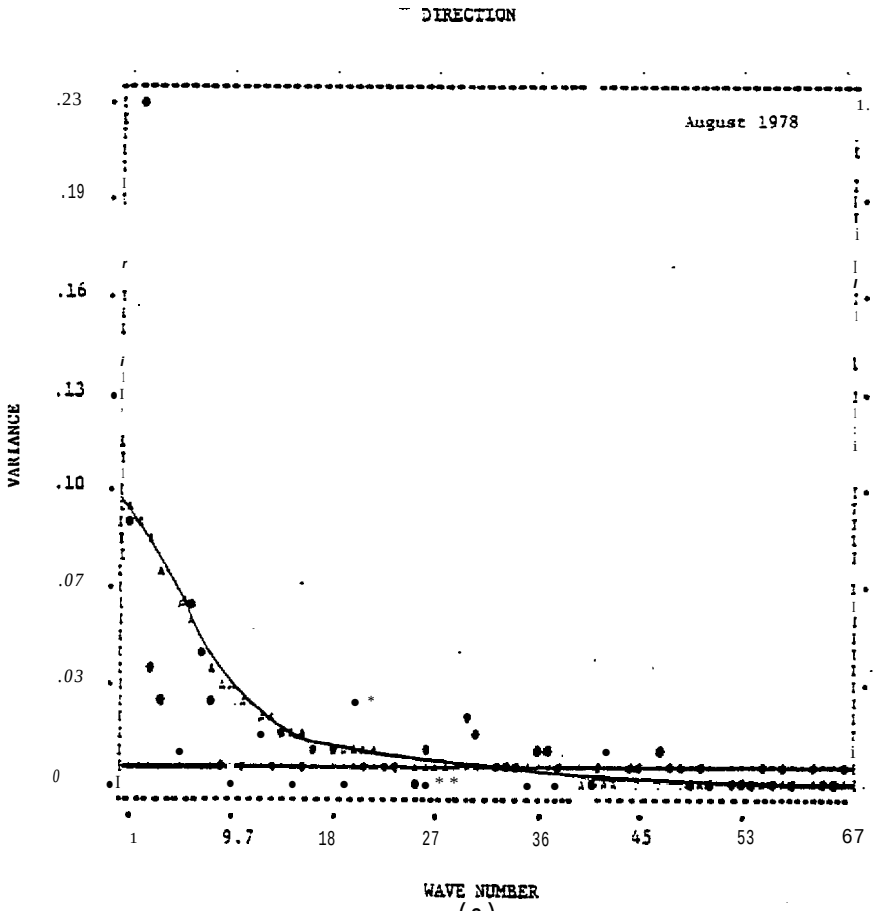

(a)

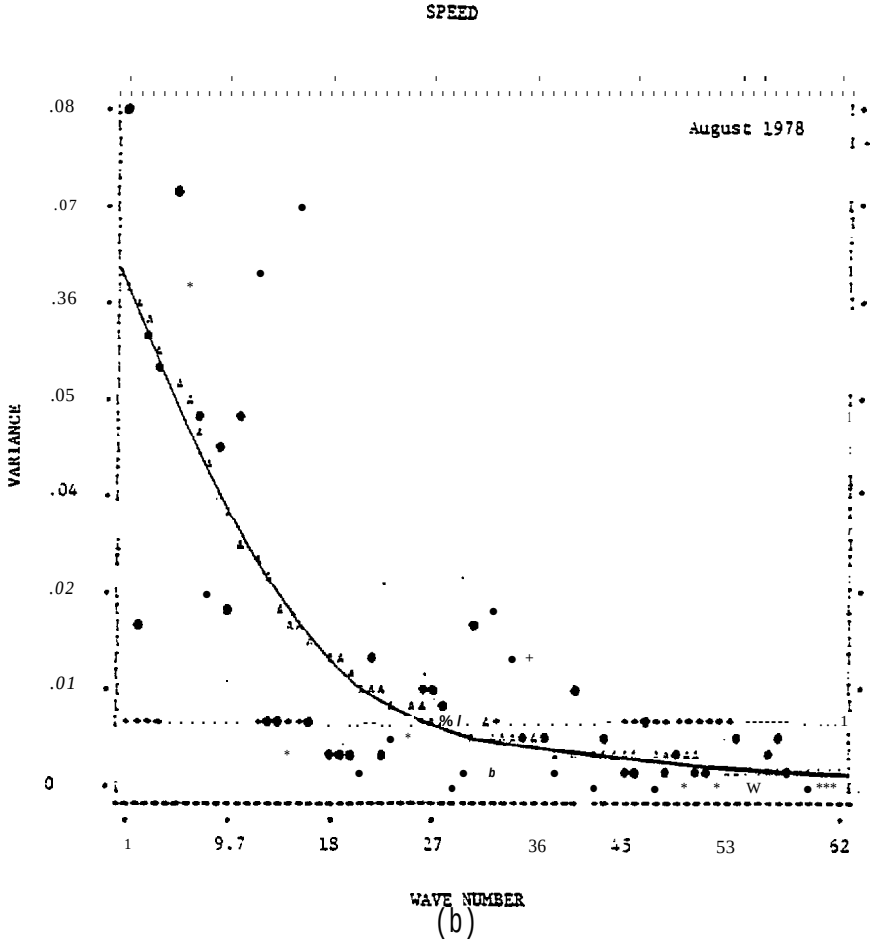

(b)

FIGURE 52: AMPLITUDE OF FOURIER COMPONENTS COMPARED TO A FIRST-ORDER MARKOV CONTINUUM (RED NOISE) AND A WHITE NOME (RANDOM) CONTINUUM FOR DIRECTION (a) AND SPEED (b). (AUGUST 1978).

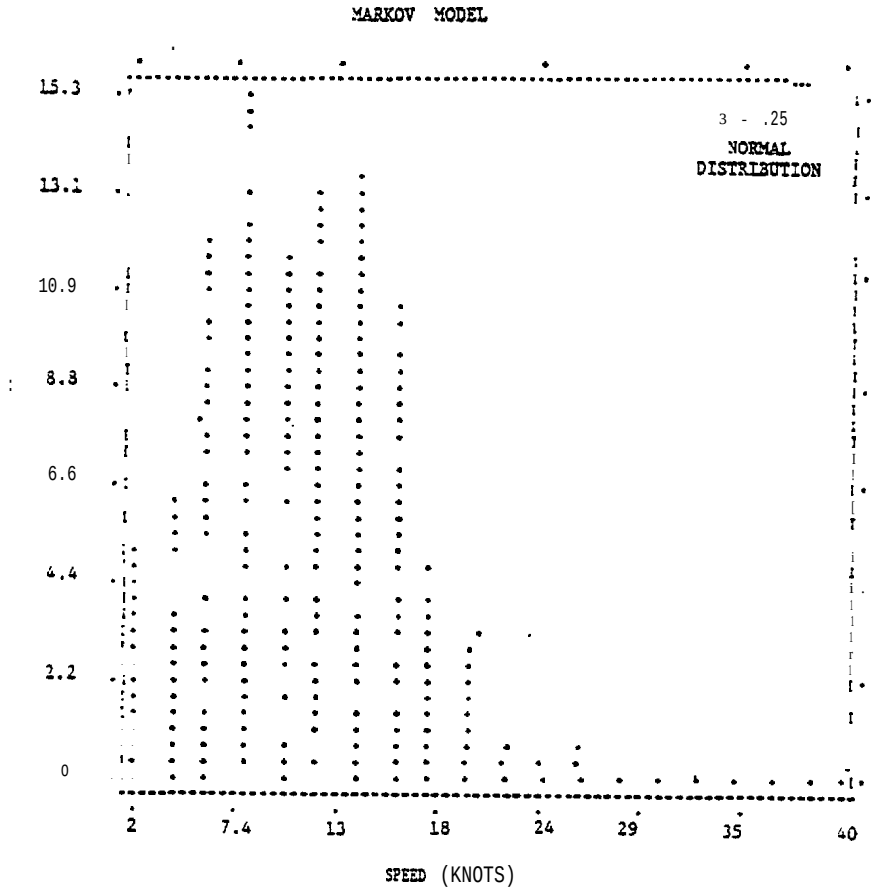

FIGURE 53: WIND SPEED HISTOGRAM GENERATED BY THE MARKOV MODEL FOR ρ =.25

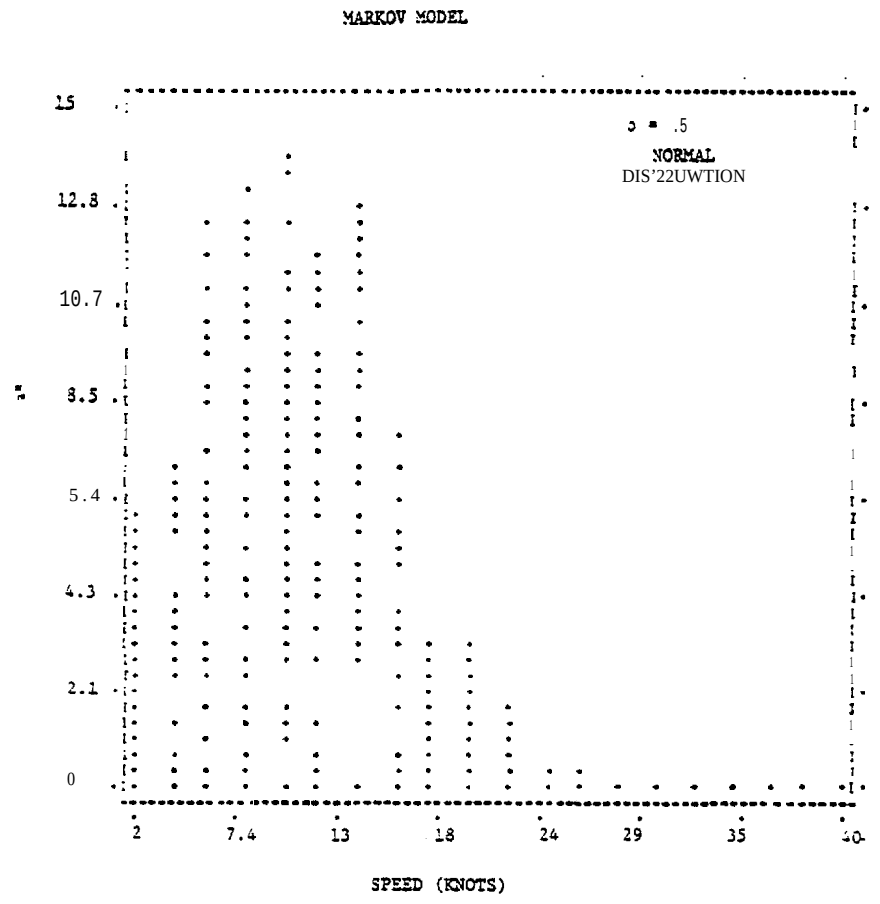

FIGURE 54: WIND SPEED HISTOGRAM GENERATED BY THE MARKOV MODEL FOR ρ = .50.

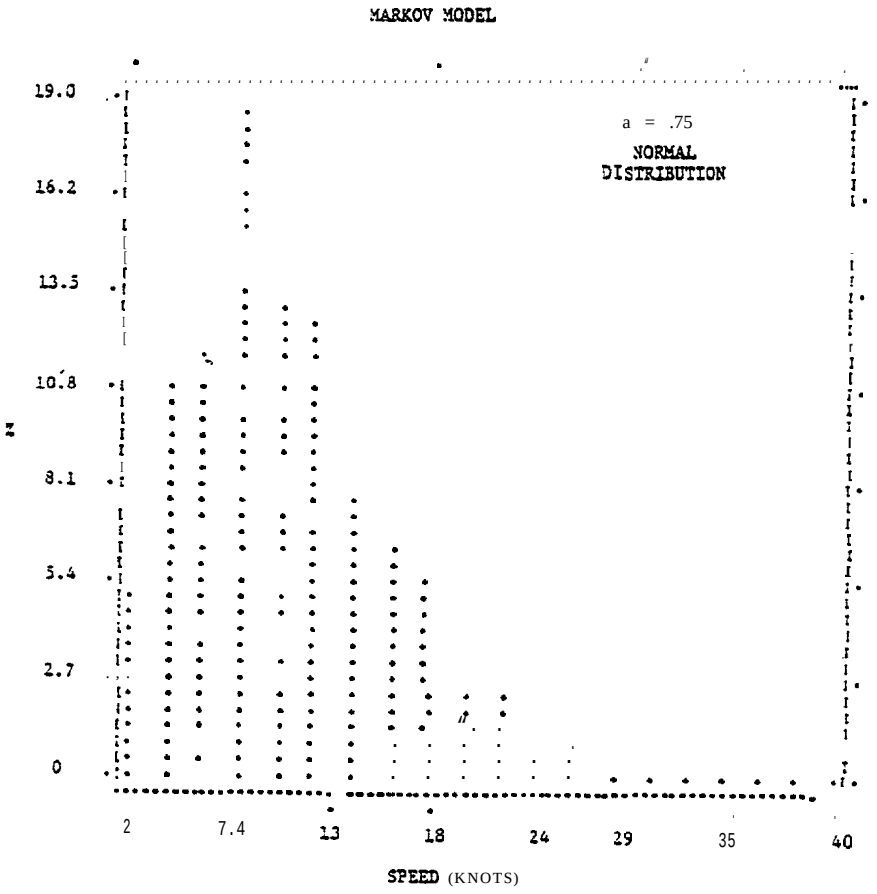

FIGURE 55: WIND SPEED HISTOGRAM GENERATED BY THE MARKOV MODEL FOR ρ = .75.

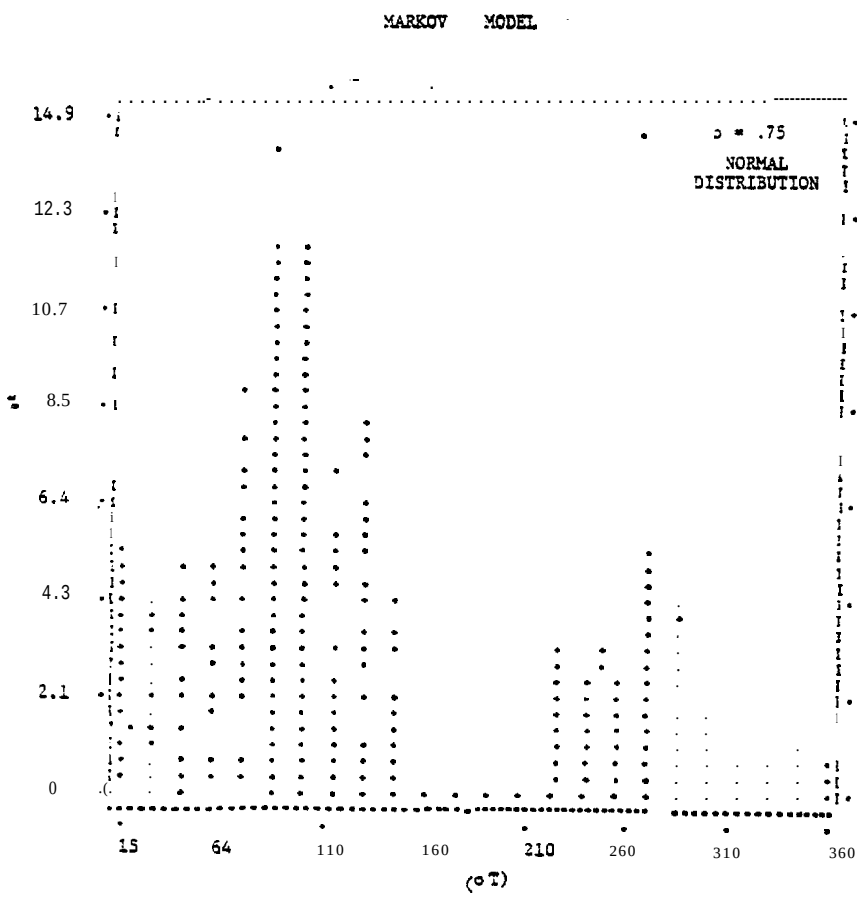

FIGURE 56: WIND DIRECTION HISTOGRAM GENERATED BY THE MARKOV MODEL TO SIMULATE ACTUAL HISTORICAL DATA. ρ = .75.

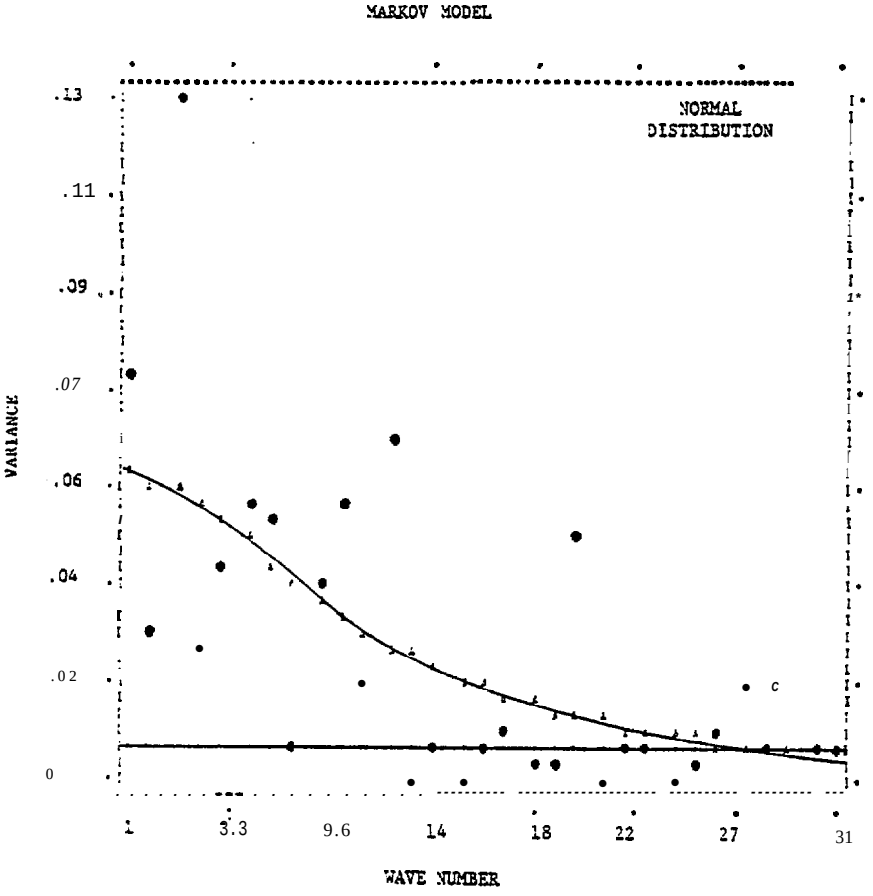

FIGURE 57: AMPLITUDE OF FOURIER COMPONENTS OF MODEL GENERATED TIME SERIES {DIRECTIONS) COMPARED TO A FIRST-ORDER MARKOV CONTINUUM (RED NOISE} AND A WHITE NOISE CONTINUUM

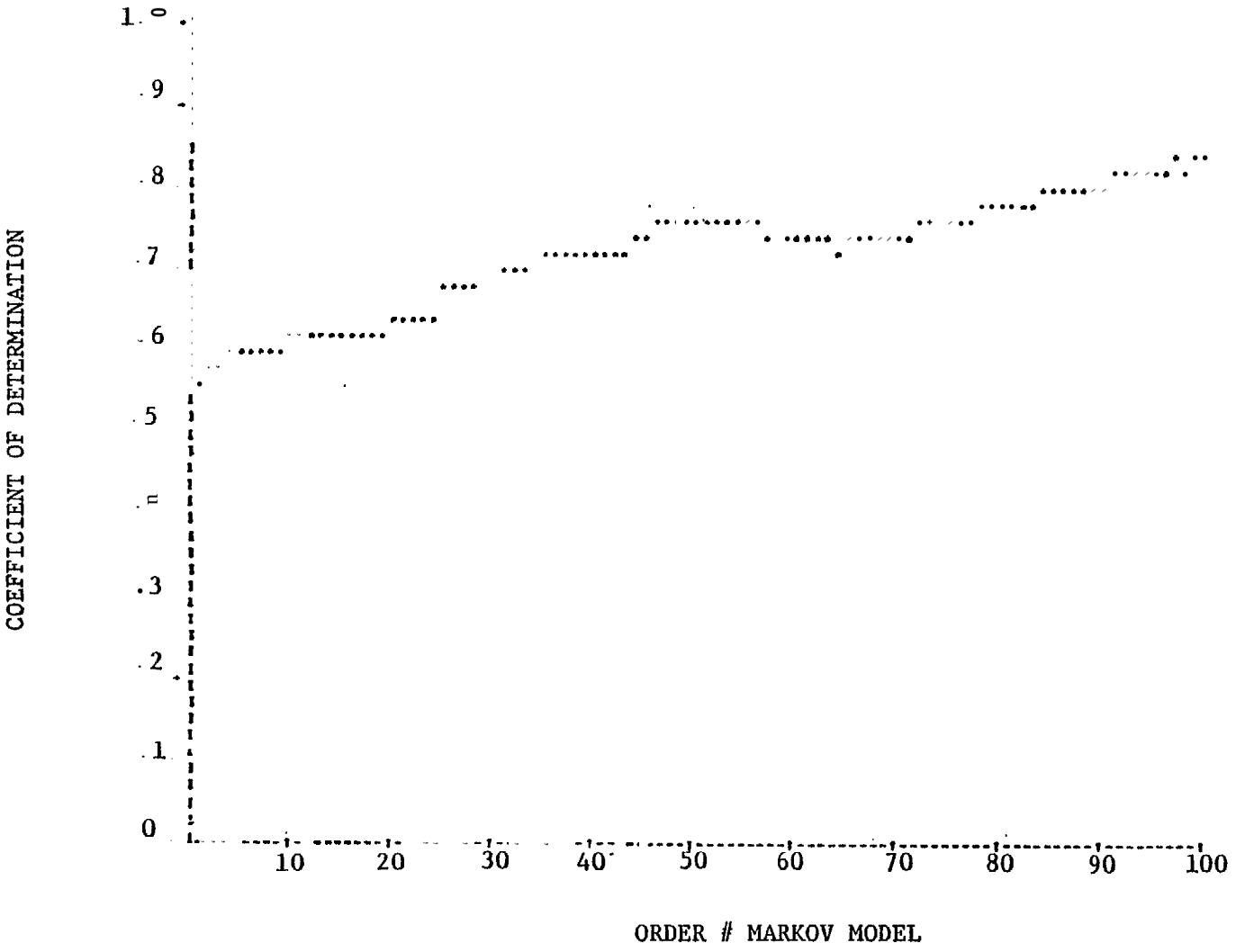

FIGURE 58: COEFFICIENT OF DETERMINATION VS. MARKOV MODEL ORDER NUMBER FOR REAL DATA FROM AUGUST 1978 (COTTLE ISLAND, TYPICAL AUGUST).

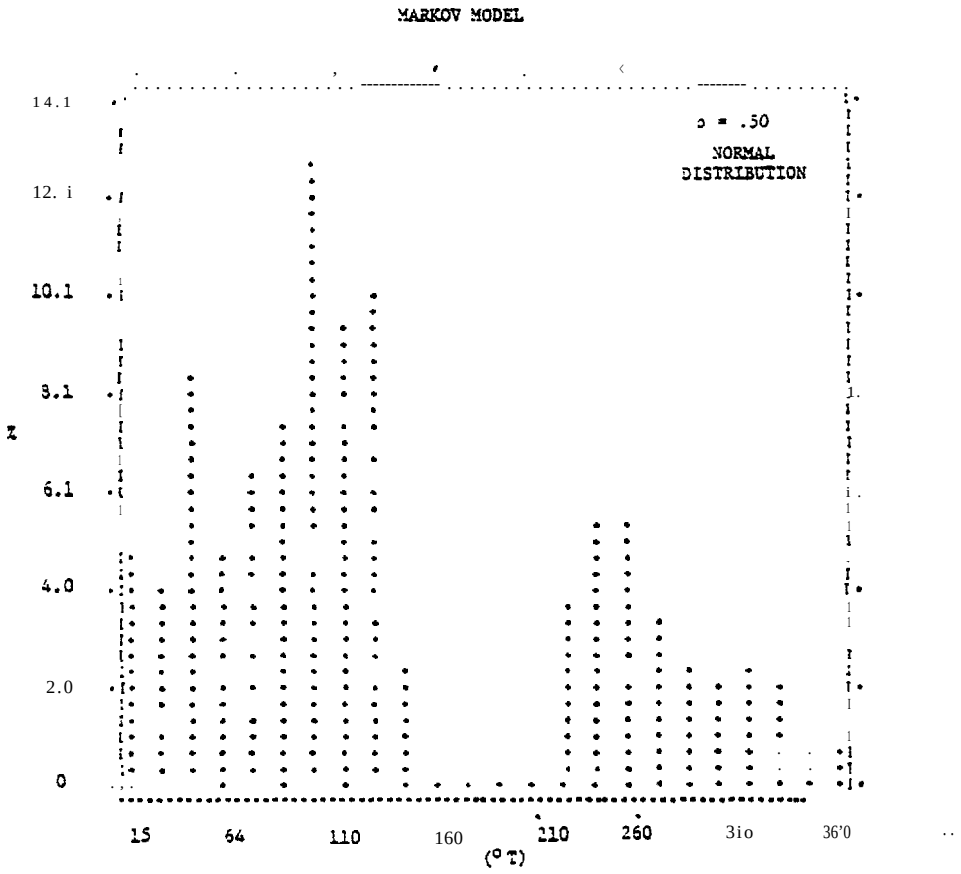

FIGURE 59: WIND DIRECTION HISTOGRAM GENERATED BY THE MARKOV MODEL FOR ρ = .5.

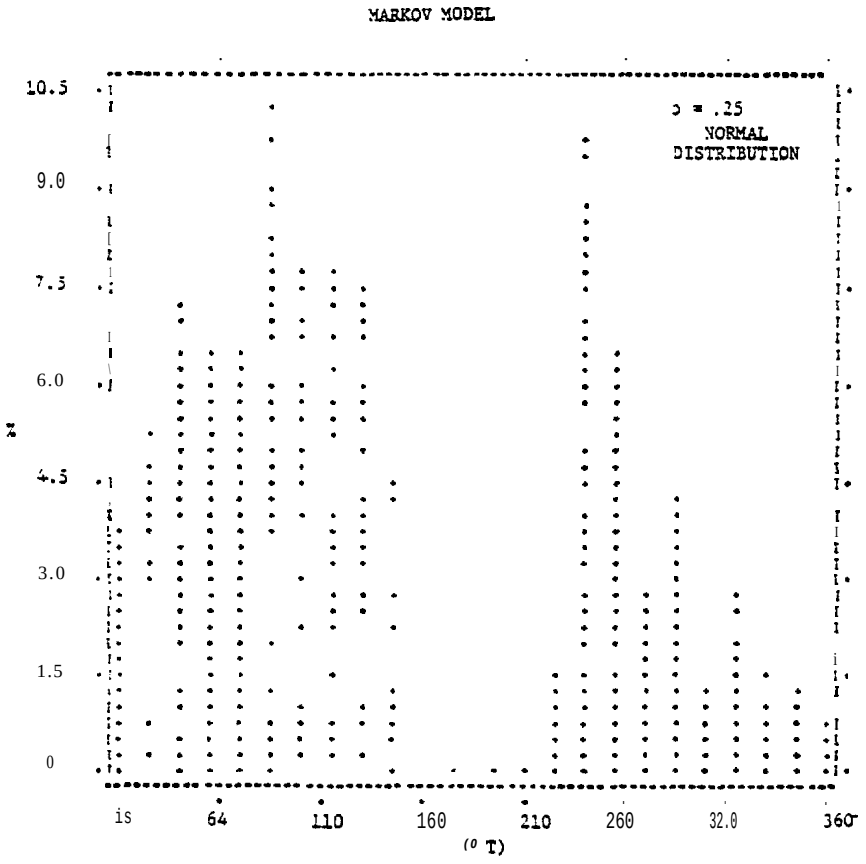

FIGURE 60: WIND DIRECTION HISTOGRAM GENERATED BY THE MARKOV MODEL FOR ρ = .25.

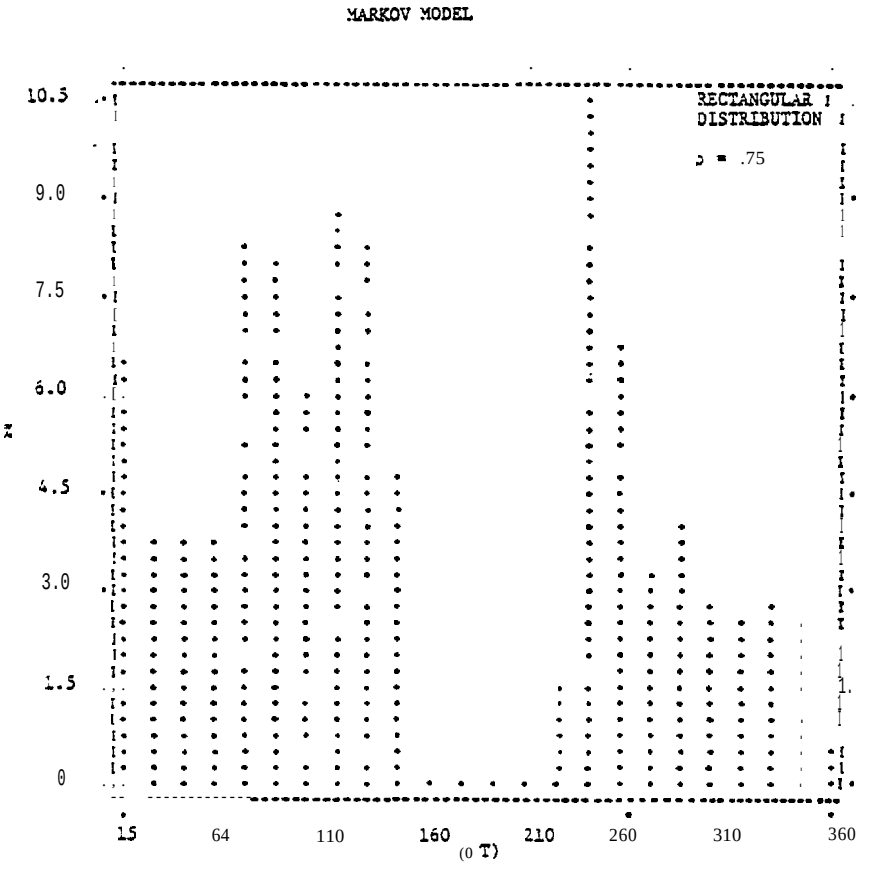

FIGURE 61: WIND DIRECTION HISTOGRAM GENERATED BY THE MARKOV MODEL FOR ρ = .75 WITH A RECTANGULAR RANDOM NUMBER DISTRIBUTION.

2.0 WAVE HINDCAST STATISTICS

2.1 INTRODUCTION

The environmental conditions characterized by the wave field in the Beaufort Sea were attempted to be determined by the wave hindcast scheme. The deep water wave height, period and direction, the breaking wave height and depth, the wave set-up and run-up, and the wave-induced current in deep water, as well as in wave breaking location, were calculated by the finite difference scheme of a Fortran code developed by Tetra Tech. The study areas include Harrison Bay, Simpson Lagoon, and Brownlow Point. Six beach profiles were selected as shown in Figure 2-1 to represent the study areas. The recorded wind speed and direction at the station of Cottle Island 1980 (negative surge), Cottle Island 1978 (typical year), and Tolaktovut Point 1977 (persistent westerly wind), were used as the wind field for the hindcast of the deep water wave field. A steady and uniform wind along a certain direction was assumed for every three-hour duration corresponding to the sampling rate (3 hourly) of the wind data used for this study. TWO fetches were simulated for the hindcast of the deep water wave. The first fetch was assumed to be infinity for a fully developed open sea condition. The second fetch starts out from the offshore location of 100 ft. contour, which was intended to simulate the condition under the effect of ice edge. As a result of this study, the

wave and its related ambient conditions were determined, which would be very useful for the assessment of the environmental impact study in the Beaufort Sea area.

2.2 THEORIES

2.2.1 Wave Generation and Propagation

Hasselmann's parametric wind-wave model (Hasselmann, K, et al. 1976) was adopted for the hindcast of the deep water wave. The fundamental concept of Hasselmann's one parameter model is based on the premise that the response of the wave field to the wind input can be described by two processes which occur at different rates: 1) the rapid adjustment of the spectrum to a universal shape and an energy level such that the input by the wind in the dominant region of the spectrum is balanced by the nonlinear transfer and possibly dissipation and, 2) the slower migration of the peak toward lower frequency due to the nonlinear energy transfer across the peak. This concept has been verified by JONSWAP'S field results (Hasselmann, K., et al. 1973) and also by Wu's laboratory results (Wu, H.Y., Hsu, and Street, 1979). The one parameter model is limited to growing seas and cannot be extended into the swell range. The governing equation for one parametric model is:

$$\frac{1}{f_o}\frac{\partial f_o}{\partial \tau} + P_o \frac{\partial f_o}{\partial \eta} = -N_o f_o^{7/3} + \frac{1}{u}\left(\frac{\partial u}{\partial \tau} + \frac{\partial u}{\partial \eta}\right)$$

where, $P_o = 0.95$

$No = 5.5 \times 10^{-4}$

$\frac{\partial}{\partial \tau} = \frac{U}{g} \frac{\partial}{\partial t}, \frac{\partial}{\partial \eta} = \frac{u}{g} \vec{V}_m \cdot \vec{\nabla}, |\vec{V}_m| = \frac{gg}{4\pi f_m}$

$f_o = Uf_m/g$, $q = 0.85$ for $\cos^2\theta$ spreading factor

u is wind speed, g is gravitational acceleration, f_m is peak wave frequency.

For a uniform wind field, the governing equation for predicting a local peak frequency can be simplified as:

$$\frac{a f_m}{\partial t} = -5.5 \times 10^{-4} \cdot \left(\frac{g}{U}\right)^{-4/3} \cdot f_m^{10/3}$$

The analytical solution of the above equation in terms of the normalized peak wave period, $\hat{T}_p$ and normalized significant wave height, $\hat{H}s$ can be expressed as follows:

For $\hat{X} < 3.5 \times 10^3$

$\hat{H}_s = 1.53 \times 10^{-3} \hat{X}^{0.5}$

$\hat{T}_p = 0.341 \hat{X}^{0.3}$

otherwise $\hat{H}_S = 0.283 \tanh (0.0125 \hat{X}^{0.42})$

$\hat{T}_p = 7.54 \tanh (0.077 X^{0.25},$

where $\hat{X} = gX/U^2$, $\hat{H}_S = gH_s/U^2$, $\hat{T}_p = gT_p/U$. The results calculated by the above equations compare quite well with the measurements. For a given set or significant wave height, Hs peak wave period, T_p and wave direction, θ, a deep water directional wave spectrum $F(\omega,\theta)$ can be approximated. When a wave spectrum propagates through the shallow water region, it

will be subject to the effects of shoaling and refraction, and the transformed spectrum can be related to the initial wave spectrum (Battjes, 1974; Collins, 1972; Longuet-Higgins, 1957), as follows:

$$F(\omega,\Theta)\ d\Theta d\omega = \frac{k}{k_o}\ \frac{(C_g)_o}{C_g}\ F_o\ (\omega,\theta_o)\ \frac{d\theta}{d\theta_o}\ d\theta_o\ \ d\omega$$

where o denotes the initial conditions and $C_g = n\omega/k$ is the group velocity. Assume the directional spectrum $F_o(\omega, \theta_o)$ can be decomposed in such a form that the energy distributed in different frequencies, $E_o(\omega)$, are weighted by a directional spreading factor $\phi(\theta_o)$, i.e.: $F_o(\omega,\theta_o) = E_o(\omega)\phi(\theta_o)$.

Under the assumption of parallel bottom contours, Snell's Law, i.e.: $\sin\theta/\sin\theta_o = k_o/k$, can be applied to relate the refracted wave angle θ_o to simplify the calculation, i.e.:

$$d\theta = \frac{k.\ \cos\theta_o\ d\theta_o}{(\ k^2 -\ \ k_o^2 \sin^2\theta_o)^{1/2}}$$

Finally, the transformed wave spectrum can be written as follows:

$$F(\omega,\theta)\ d\theta d\omega = \frac{n_o k^2 k_o \cos\ \theta_o\ \phi(\theta_o) E_o(\omega)}{n k_o^2\ [k^2 -\ k_o^2\ \sin^2\theta_o\ ]^{1/2}}\ \ d\theta_o\ d\omega$$

This transformed wave spectrum is valid prior to wave breaking. After wave breaking, a different approach for the calculation of wave height in the surf zone is applied.

2.2.2 Wave Breaking Criteria

In the ocean, as a wave exceeds certain kinematical or dynamical limits, the wave will be broken and reformed. The visible white-capping phenomena is the result of wave breaking. It has been argued (Phillips 1958, Kitaigordiskii et al. 1975, and Thornton, 1977) that in order to satisfy the kinematical or dynamical constraints of wave breaking, the wave spectrum in the high frequency range where wave breaking occurs, must have a certain universal shape exis'ting, which is known as the equilibrium range. One can employ dimensional analysis to derive a form for the equilibrium spectrum.

The equilibrium spectrum, $\psi(\omega)$ without the effect of current can be expressed as (Kitaigordiskii et al. 1975, Thornton, 1977, and Wu et al. 1980):

$$\psi(\omega) = \alpha k^{-2}(2n\omega)^{-1}$$

where a is Phillips' equilibrium constant, n is the ratio of group velocity to wave celerity, k is the wave number and ω is the angular frequency. The asymptotic forms of $\psi(\omega)$ in the deep and shallow water regions can be shown as

$$\psi_D(\omega) = \alpha g^2 \omega^{-5}$$

and

$$\psi_s(W) = \frac{\alpha}{2} g h \omega^{-3}$$

respectively. The coefficient, $\alpha/2$ needs to be verified in the shallow water region.

As a wave field propagates toward the shallow water region, the process of wave dissipation, within the equilibrium range, is not sufficient to characterize the spilling, surging, or collapsing type of breakers which occur in shallow waters. Therefore, additional shallow water wave breaking criteria are needed. As proposed by Wu et al. (1980), based on a combination of the state-of-the-art knowledge of breaking height, breaking depth, deep water wave characteristics, and beach slope, the breaking criterion can be described by

$$H < \gamma d$$

where $\gamma = H_b/d_b$ and H_b and d_b are breaking wave height and depth, respectively, which are functions of beach slope and incident wave characteristics. The breaking wave height is determined by the combination of Goda's index (Goda 1970) and LeMehaute and Koh's (1967) wave breaking condition, i.e.:

$$\gamma_b = 0.74 H_o . S^{0.11} . (H_o/L_o)^{-0.24} . (\cos\theta_o)^{0.38} . (\cos\theta_b)^{0.28}$$

and

$$\gamma_b = (0.15 + 6.4 . Ho \sqrt{\cos\theta_o}/L_o) \cdot \theta_o$$

for

$$0.002 < H_o \sqrt{\cos\theta_o}/L_o < 0.1 \quad \text{and} \quad 0.026 \leq 0.1$$

where S is the beach slope, Lo is the deep water wave length and θ_b is the wave breaking angle.

The breaking water depth d_b is the summation of the still-water breaking depth, h_b and the maximum wave set-down, η_b at the breaking location. The still-water breaking depth h_b is determined by Weggel's formula (Weggel, 1972), i.e.:

$$h_b = H_b / [b - (aH_b/gT_o^2)]$$

where

$$a = 1.36g(1 - e^{-19 \cdot S}) \quad \text{and} \quad b = 1.56/(1 + e^{-19.5 \cdot S})$$

The maximum wave set-down η_b at the wave breaking point can be estimated theoretically for a solitary wave. The theoretical form of η_b is:

$$\eta_b = -H_o^2 \sqrt{g}\ T_o \cos\theta_o / [64\pi(h_b + \eta_b)^{3/2}]$$

Finally, γ can be determined for a given set of initial wave conditions and beach slope. Then, the breaking condition can be established.

The combination of equilibrium spectrum check (which would limit the energy contained in the relatively high

frequency range of a wave spectrum), and shallow water wave breaking conditions defines *a* very good breaking criterion, predicts a better breaking location and, hence, provides a better simulation of the surf zone processes.

2.2.3 Wave Set-up

Wave set-up is defined as the rise of the mean water surface caused by the balance of the wave induced momentum flux in the surf zone. The additional momentum generated by" the waves on the water surface is termed "radiation stress" by Longuet-Higgins and Stewart (1960) . The wave set-up is dominated by the rate of decrease of radiation stress in the surf zone. Consequently, the criterion of wave breaking and the rate of decay of breaking wave height are extremely important to the wave set-up prediction.

The governing equations for the wave set-up model are the depth-integrated and time-averaged equations of motion and continuity. The problem is further simplified by the assumptions of one-dimensionality and steady state conditions, neglecting the effects of bottom friction, Coriolis force, surface wind stress, currents, and pressure gradients. Then, the governing equation at the direction normal to the coastline can be written as:

$$\frac{\partial \eta}{\partial x} = \frac{-1}{\rho g (h+\eta)} \frac{\partial S_{xx}}{\partial x}$$

where η is the mean water surface, h is the still water depth, p is the density of water, g is the gravitational acceleration, x is the direction normal to the coastline, and s_{xx} is the component of the radiation stress in the x-direction.

The radiation stress of a directional wave spectrum, $F(\omega,\theta)$ can be expressed as (Battjes, 1974):

$$s_{xx} = \rho g \int_{\omega}\int_{\Theta} [n - \frac{1}{2} + n\cos^2\theta]\ F(\omega,\Theta) \quad d\Theta d\omega$$

where Θ is the wave angle, and n is the ratio of group velocity to wave celerity, i.e., $n = 0.5\ [1+2kd/\sinh(2kd)]$. ω is the angular frequency, and $\omega^2 = gk \tanh(dk)$ for a linear wave theory. k is the wave number and $d = h+\eta$ is the total water depth. The refracted wave angle Θ can be calculated by Snell's Law for parallel bottom contours, i.e.: $\sin\Theta/\sin\Theta_o = k_o/k$, where o denotes the deep water condition or the initial condition. Once d and k are determined, n, Θ, and hence the radiation stress can be calculated by the above equation provided $F(\omega,\Theta)d\Theta\ d\omega$ was determined for *a* given water depth.

After breaking, since the breaking wave spectrum is not well understood, an empirical relationship describing the root mean square wave height, $\overline{H}$, as a function of beach slope, local water depth, d, and breaking wave height and depth is adopted. For the determination of $\overline{H}$, the functional form is:

$$\overline{H}/H_b = f(d/d_b, S)$$

Snell's Law and the dispersion relation are assumed to hold within the surf zone on a gently sloping beach. Then the radiation stress is approximated by that of a monochromatic wave represented by the root mean square wave height, mean direction, and mean period in the surf zone, i.e.:

$$S_{XX} = (n - \frac{1}{2} + n \cos^2\theta) \cdot \frac{1}{8} \rho g \overline{H}^2$$

Finally, the governing equation for the prediction of wave set-up can be solved by an explicit forward finite-difference numerical scheme.

2.2.4 Wave Run-up

Wave run-up is defined as the maximum vertical water displacement on the face of the structure above the still-water surface during the wave attack. Since no sound theoretical background assocaited with the characteristics of breaking waves has been established, the state-of-the-art calculation of wave run-up is essentially based on experimental results. Because Hunt's equation can always produce a reliable estimation of wave run-up for breaking wave cases, it was adopted for the basic analytical foundation. Hunt's equation can be described as follows:

$$\frac{R}{H} = 2.3 \cdot S \cdot (H/T)^{-1/2}$$

where T is *wave* run-up, S is beach slope, H and T are wave height and period, respectively.

2.2.5 Wave-induced Current

Since the particle motion of a finite amplitude wave cannot be closed, there must be a slight net transport of mass which is corresponding to the wave-induced current. The deep water wave-induced current, U_c can be expressed as follows: (Kinsman, B. 1964)

$$U_c = \pi^2 \delta^2 \; C \; e^{2kZ}$$

where $\delta = H/L$, H is wave height, L is wave length, C is wave speed, k is wave number and Z is the water depth. U_c at the surface of water (i.e., Z = 0) is

$$u_{co} = \pi^2 H^2 C/L^2 = \pi^2 H^2/(CT^2)$$

For a deep water wave, $C = gT/(2\pi)$ and

$$u_{co} = 2\pi^3 H^2/(gT^3)$$

where g is the gravitational acceleration and T is wave period. A rough estimate of the wave-induced current under wave breaking condition, $(U_{co})_b$ may be approximated by applying $c = 2\pi/(k_b T)$, $k_b = k\sqrt{\coth(kd)}$, and $k = 4\pi^2/(gT^2)$ in the equation of

u_{co}, which yields

$$(U_{co})_b = 2\pi^3 H^2/(gT^3) \cdot \sqrt{\mathrm{Coth}(4\pi^2 d/gT^2)}$$

where d is the water depth. Therefore the ratio of the wave-induced current between the conditions of deep water wave and breaking wave is

$$(U_{co})_b / U_{co} = \sqrt{\mathrm{Coth}(kd)} \geq 1$$

Apparently, the wave-induced current under wave breaking condition is always larger than that of under deep water wave condition.

2.3 RESULTS, DISCUSSIONS, COMPARISONS, AND CONCLUSIONS

The statistical results of the wave field in the Beaufort Sea area for the period of August of 1977 (persistent westerly wind condition), 1978 (typical year), and 1980 (negative surge) have been obtained by applying Tetra Tech's numerical models. An uniformly distributed wind field over the entire study area, which includes Harrison Bay, Simpson Lagoon, and Brownlow Point, was assumed. Thus, the deep water waves were hindcasted by the one-dimensional wave model, consequently, the shallow water waves were transformed from the deep water waves. The locally generated shallow water waves were neglected.

The probability distributions of the deep water significant wave height, Hs, peak wave" period, T_p, breaking wave height, H_b, breaking water depth, D_b, wave run-up, R, wave set-up, η, deep water wave-induced current, U_{co}, and breaking wave-induced current $(U_{co})_b$, were calculated for the selected six beach profiles. A set of probability distributions of the input wind speed, U, wind direction, θ, Hs, T_P, H_b, H_b, and percentages of U_{co}/U and $(U_{co})_b/U$ were presented in Figure 2.2 through Figure 2.9, Figure 2.10 through Figure 2.17, and Figure 2.18 through Figure 2.25 for August of the year 1977, 1978 and 1980, respectively. The probabilities indicated in the most right-hand side of the graphs represent the statistics of zero onshore waves. These have about 7%, 20% and 65% of such statistics for August of 1977, 1978, and 1980, respectively. For 1980's case, it has much higher percentage of the zero wave statistics and negative surges. These are due to the persistent offshore wind condition during August of 1980.

The mean and maximum values of Hs, T_P, H_b and D_b at two different fetches were shown in Figure 2.26 through Figure 2.28 for the years 1977, 1978 and 1980, respectively. The results corresponding to the larger fetch are generally larger compared to those of the smaller fetch. It implies that the effect of ice edge tends to reduce the values of H_s and T_P, and, hence, their corresponding values. The results for 1977 are the largest ones, as expected, due to the persistent wind conditions.

The statistics of the deep water H_s, T_p and U_{co} are almost the same for all the beach profiles because the same wind conditionswere applied. Consequently, the results of H_b, D_b, and $(U_{co})_b$ are very similar. The averaged and maximum breaker zones are located at the near shore water depths of 1.5 to 3 ft. and 3 to 11 ft., respectively. Since Harrison Bay has a broader continental shelf, therefore it has a larger breaker zone compared to those of Simpson Lagoon and Brownlow Point. The wave run-up and set-up seem to be negligible due to the gentle continental slopes and the normal deep water wave conditions. The significant finite amplitude wave-induced current seems to have the same order of magnitude as the wind-induced drift current (3 7% of the wind speed) in deep water as well as in the breaking locations. Therefore, it is strongly recommended to include the effect of wave-induced current in the estimate of the oil spill movement.

2.4 RECOMMENDATIONS

A 2-dimensional wind-wave hindcast scheme is strongly recommended for the future study. This 2-D model would have better capability to handle storm wind conditions. Therefore, better quality of the hindcast results could be expected.

The ice edge model should be incorporated with the wave prediction model for the better estimate of the fetch.

The 30 year's wind data at Cottle Island and Tolaktovut Point could be utilized for the generation of the general wave statistics, especially for the design criteria of offshore structure in the Beaufort Sea area.

The wave-induced current, long shore current and the mixing due to the breaking wave in the surf zone are particularly important for the prediction of the oil spill movement. Therefore, we strongly urge that these mechanisms be included in any future modeling effort or environmental statistical studies.

REFERENCES

Battjes, J.A., 1974, "Computation of set-up, longshore currents run-up and overtopping due to wind-generated waves," Communications on Hydraulics Department of Civil Engineering, Delft University of Technology, Report No. 74-2.

Collins, J.I., 1972, "Prediction of shallow-water spectra," J. Geoph. Res., 77, 11, 2693-2707.

Goda, Y. 1970, "A synthesis of breaker indices," Transactions of JSCE, Vol. 2, Part 2, 227-230.

Hasselmann, K., et al. 1973, "Measurements of wind-wave growth and swell decay during the Joint North Sea Wave Project," Deutches Hydrographisches Institut, Hamburg.

Hasselmann, K., 1976, "A Parametric Wave Prediction Model," J. of Phy. Oceanography. 6, 200-228.

Kitaigordiskii, S.A., V.P. Krasitskii and M.M. Zaslavskii, 1975, "On Phillips' theory of equilibrium range in the spectra of wind-generated waves," Journal of Physics Oceanography, 5, 410-420.

Le Mehaute, B. and R.C.Y. Koh, 1967, "On the breaking of waves arriving at an angle to the shore," Journal of 'Hydraulic Research, 5, No. 1.

Longuet-Higgins, M.S., 1957, "On the transformation of a continuous spectrum by refraction," Proceedings, Cambridge Phil. Sot., 53, 226-229.

Longuet-Higgins, "M.S., and R.W. Stewart, 1960, "Changes in the form of short gravity waves on long waves and tidal currents," Journal of Fluid Mechanics, 8, 565-583.

Phillips, O.M. 1958, "The equilibrium range in the spectrum of wind-generated waves," Journal of Fluid Mechanics. 4. 426-434.

Thornton, E.B., 1977, "Rederivati.on of the saturation range in the frequency spectrum of wind-generated gravity waves," J. of Physics Oceanography, Vol. 7, No. 1, 137-140.

Weggel, J.R., 1972, "Maximum breaker height," Journal of the Waterways, Harbors and Coastal Engineering Directory, WW4, 529-548.

Wu, F.H.Y., J.I. Collins and D. Divoky, 1980, "Spectral wave set-up and run-up," National Symposium on Urban Storm Water Management in Coastal Areas, Blacksburg, Virginia, May 26-28.

Wu, H.Y., E.Y. Hsu, and R.L. Street 1979, "Experimental Study of non-linear wave-wave interaction and white-cap dissipation of wind-generated waves," J. of Dynamics of Atmospheres and Oceans, 3. 55-78.

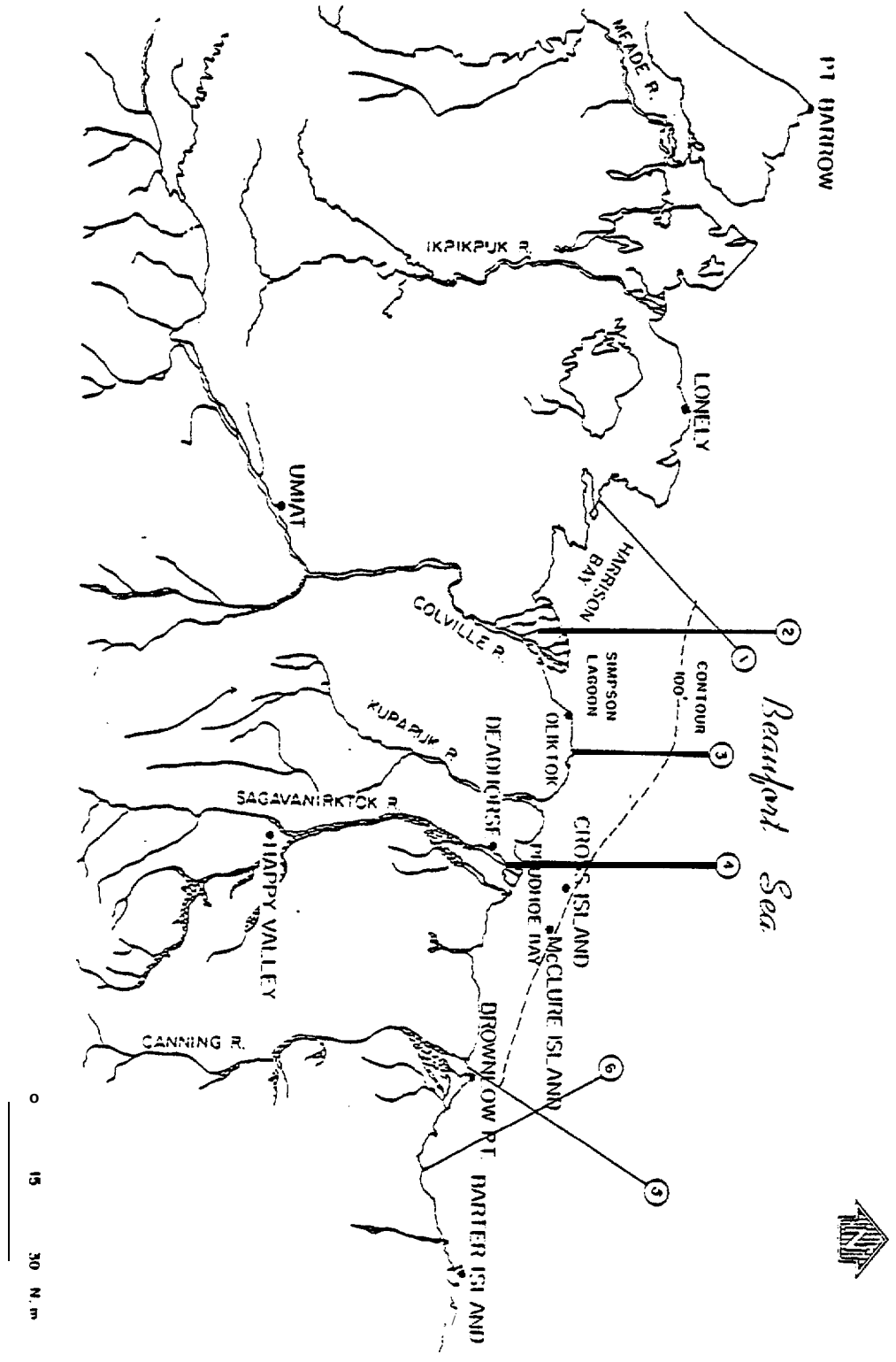

Figure 2.1 Representative Beach Profi 1 es of the study area

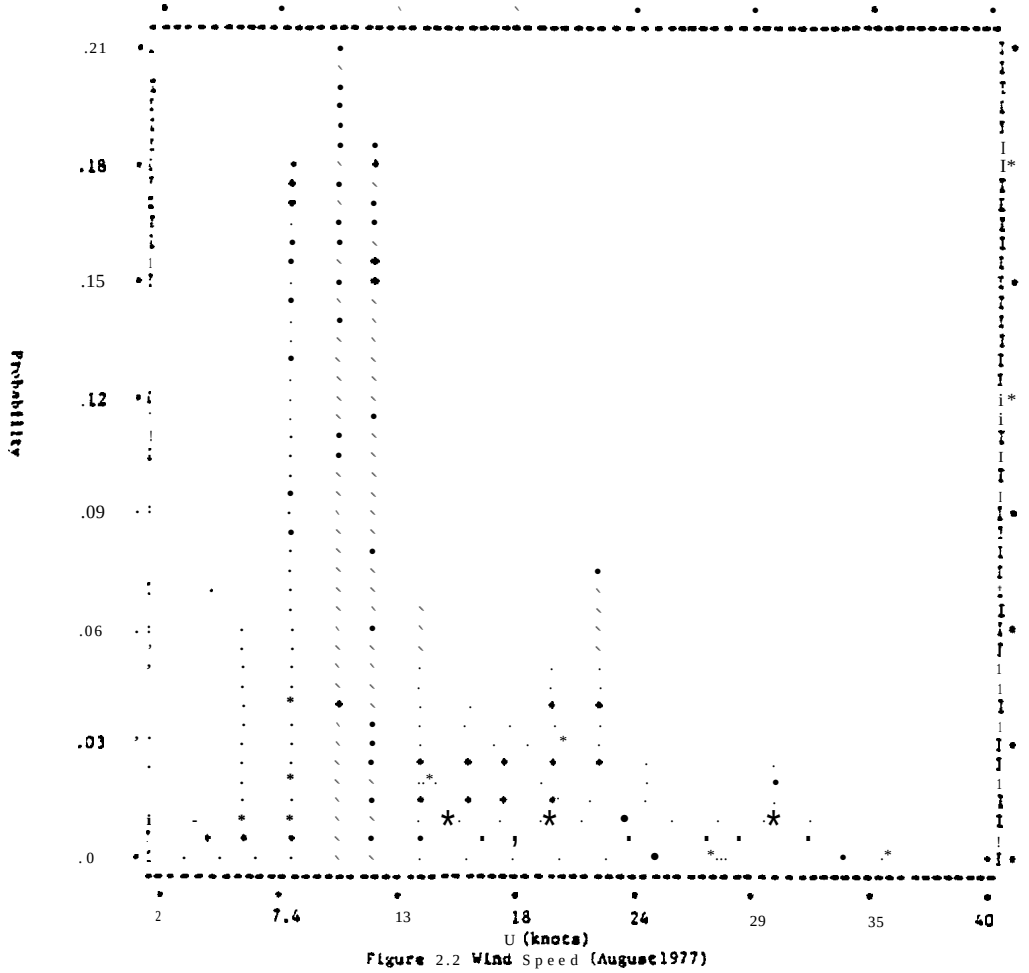

Figure 2.2 Wind Speed (August 1977)

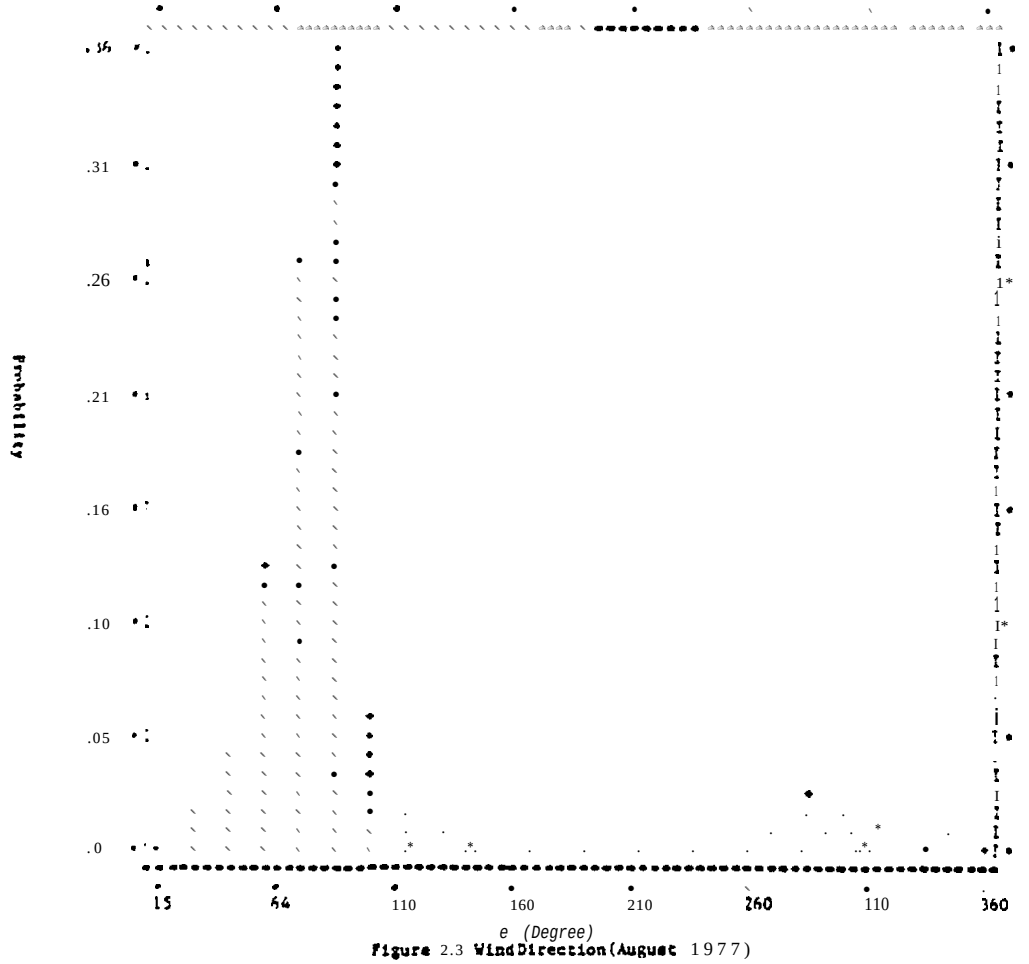

Figure 2.3 Wind Direction (August 1977)

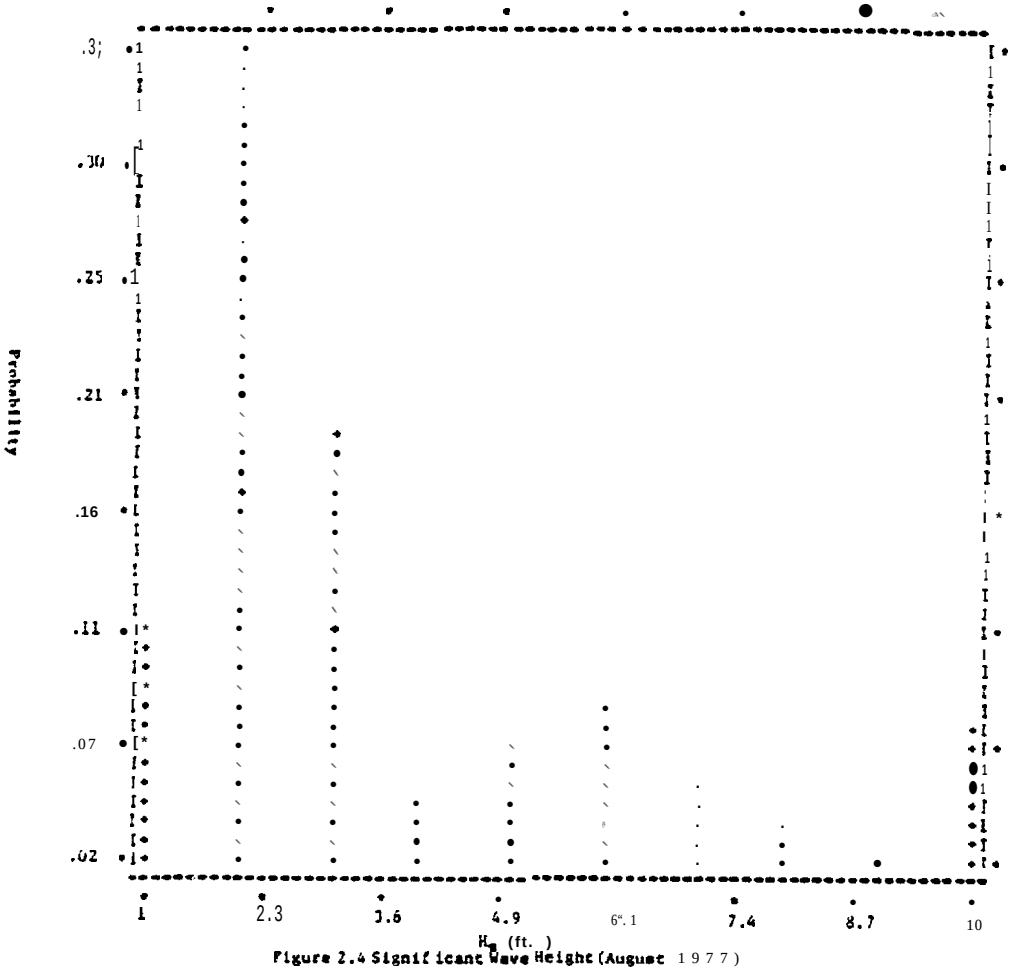

Figure 2.4 Significant Wave Height (August 1977)

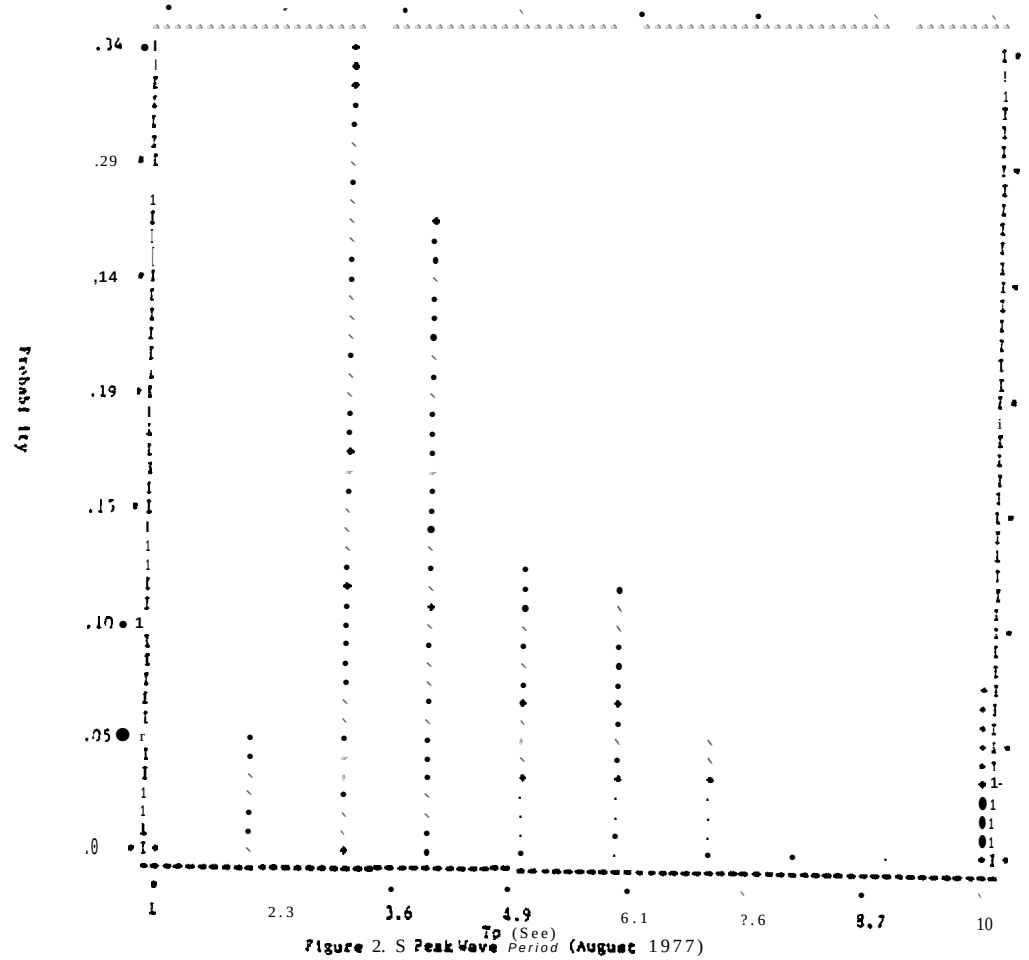

Figure 2. S Peak Wave Period (August 1977)

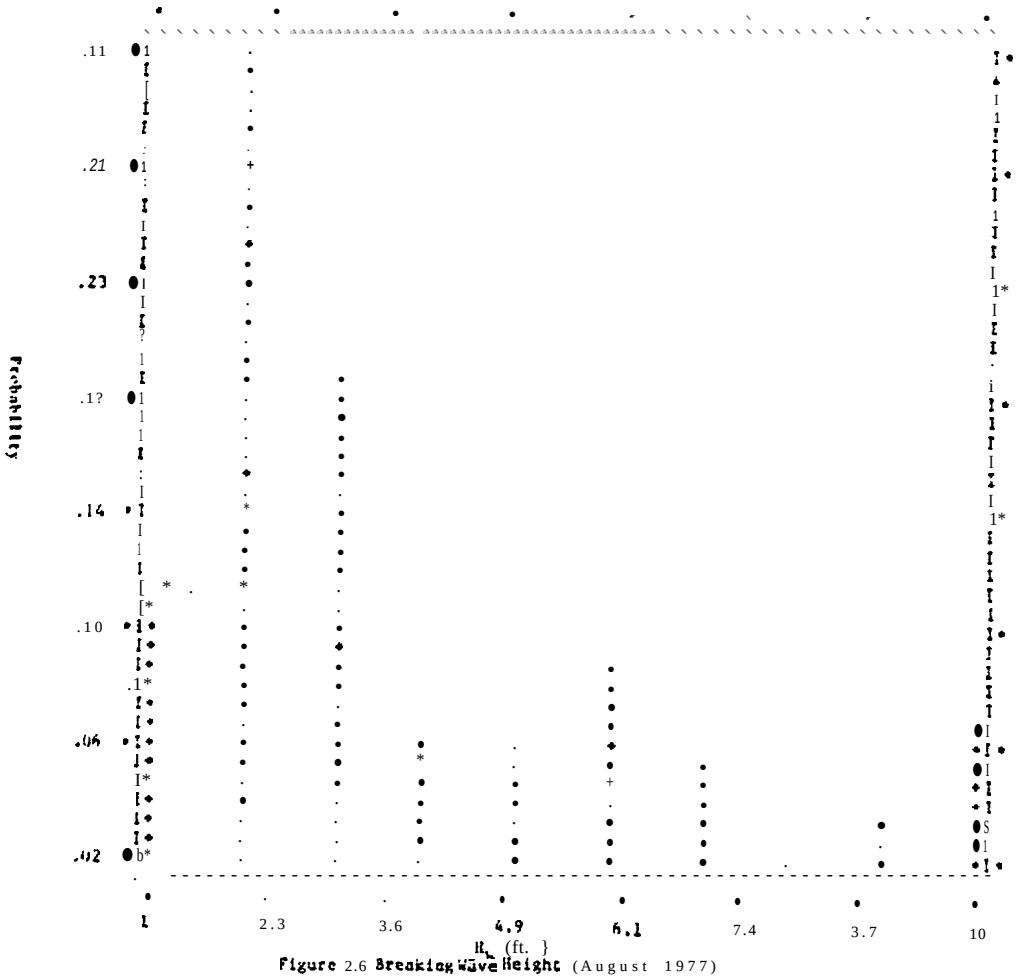

Figure 2.6 Breaking Wave Height (August 1977)

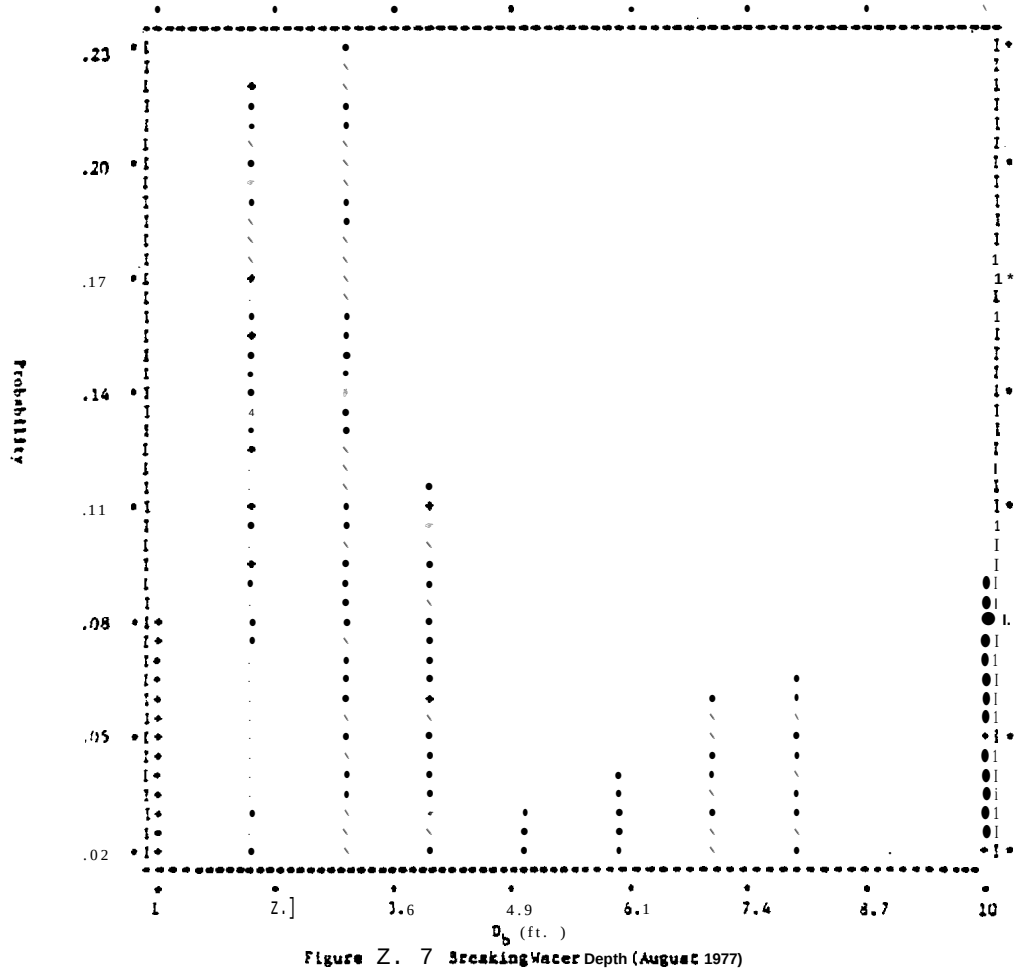

Figure Z. 7 Breaking Wacer Depth (August 1977)

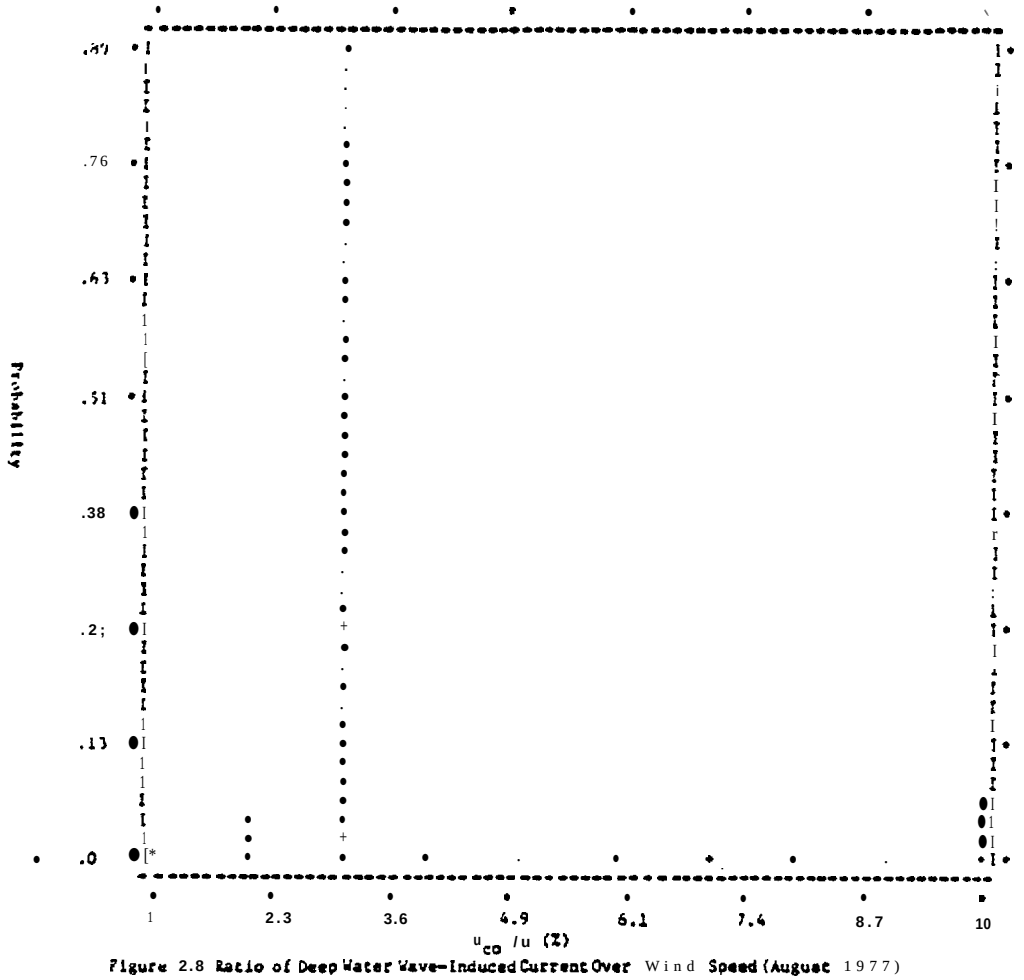

Figure 2.8 Ratio of Deep Water Wave-Induced Current Over Wind Speed (August 1977)

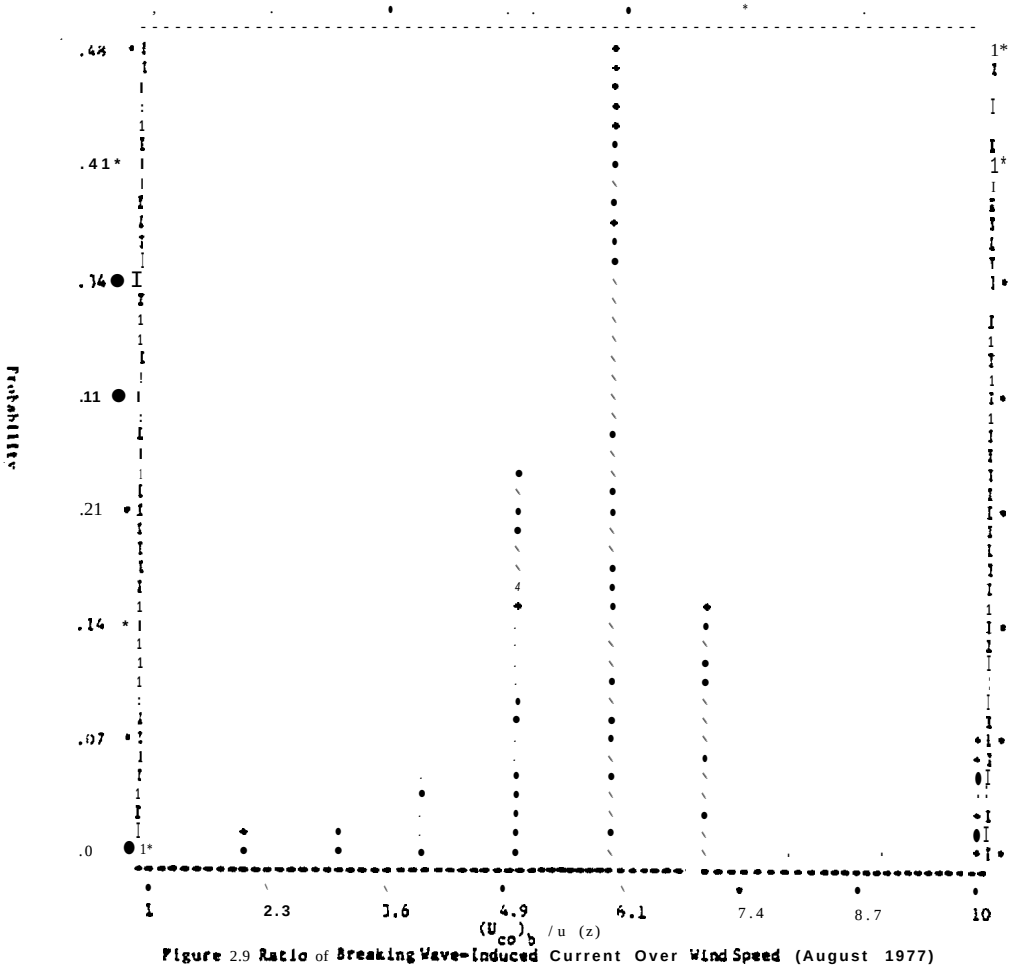

Figure 2.9 Ratio of Breaking Wave-Induced Current Over Wind Speed (August 1977)

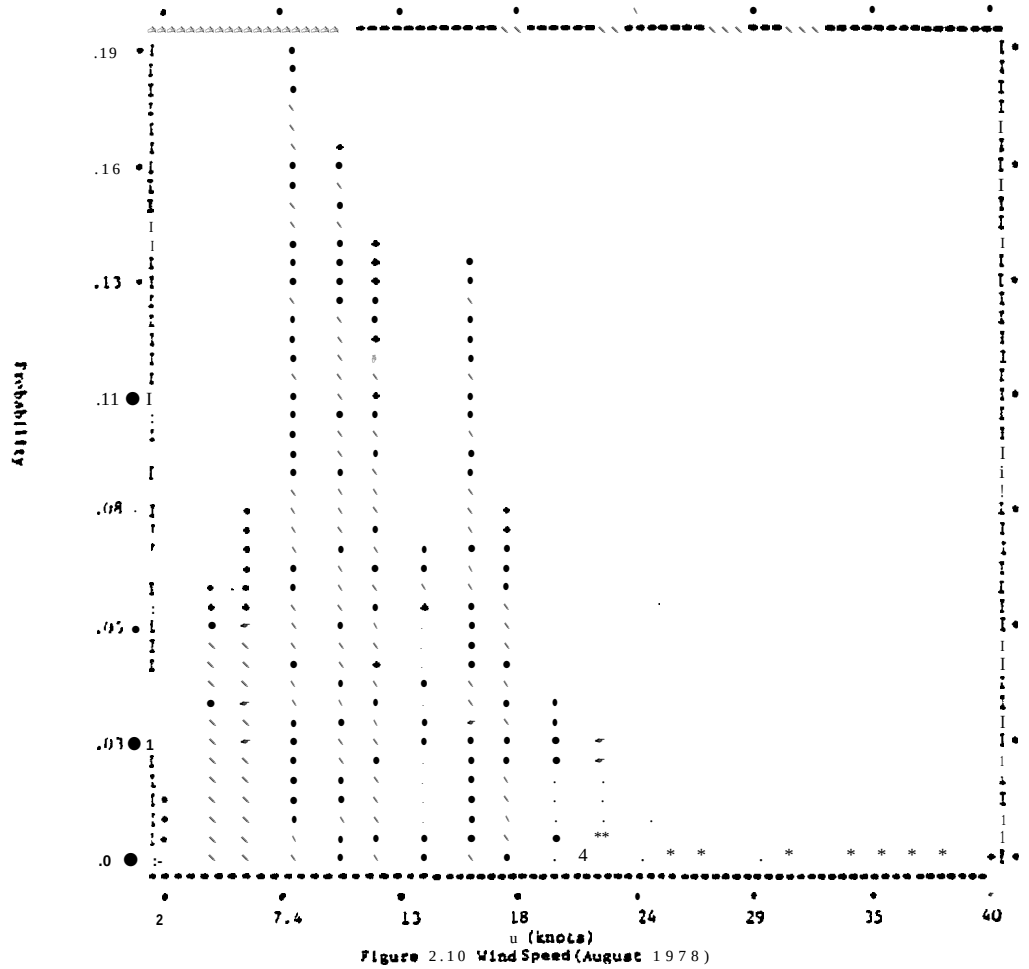

Figure 2.10 Wind Speed (August 1978)

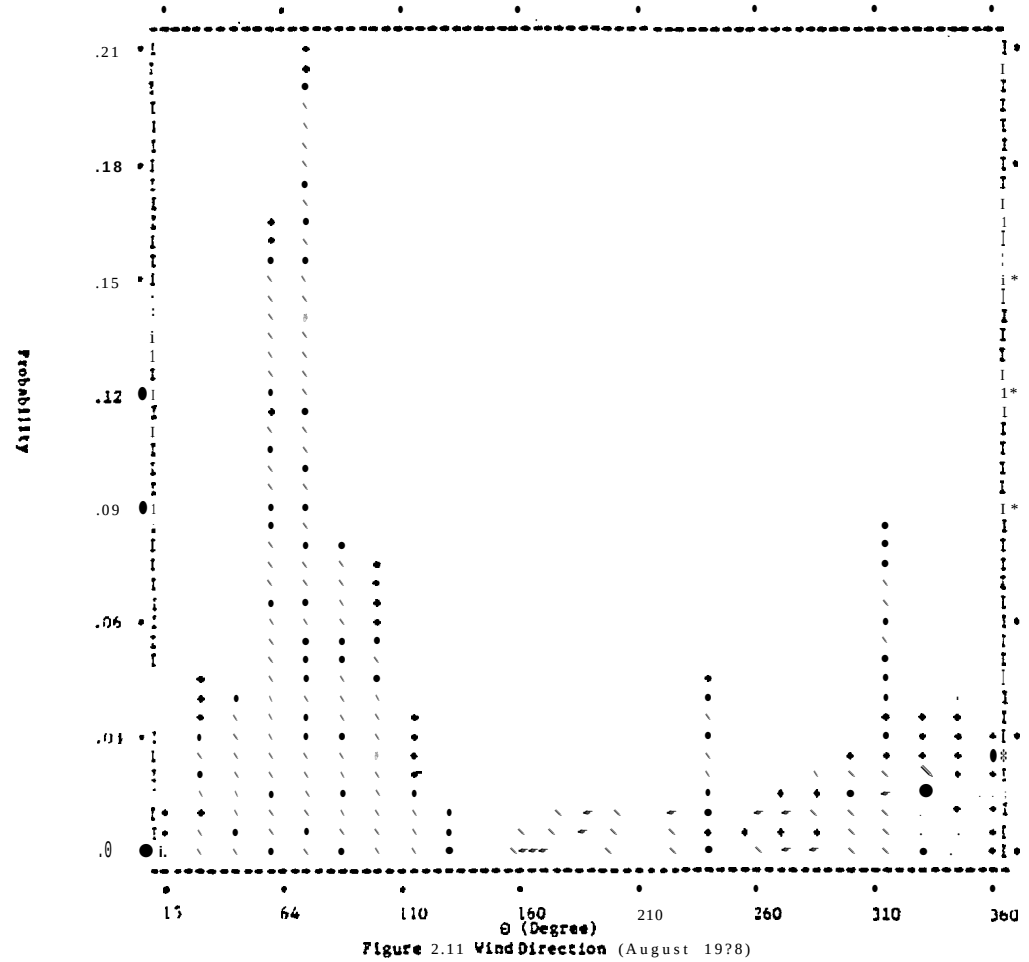

Figure 2.11 Wind Direction (August 1978)

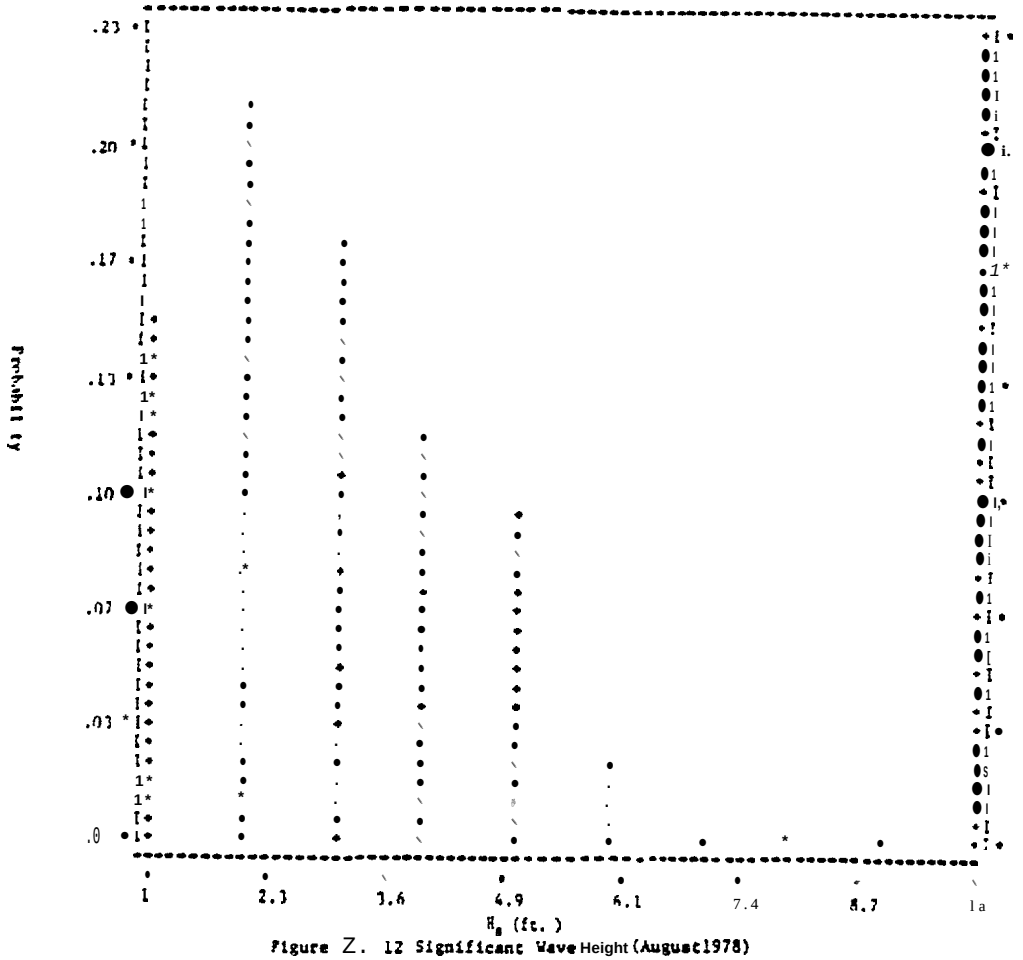

Figure Z. 12 Significant Wave Height (August 1978)

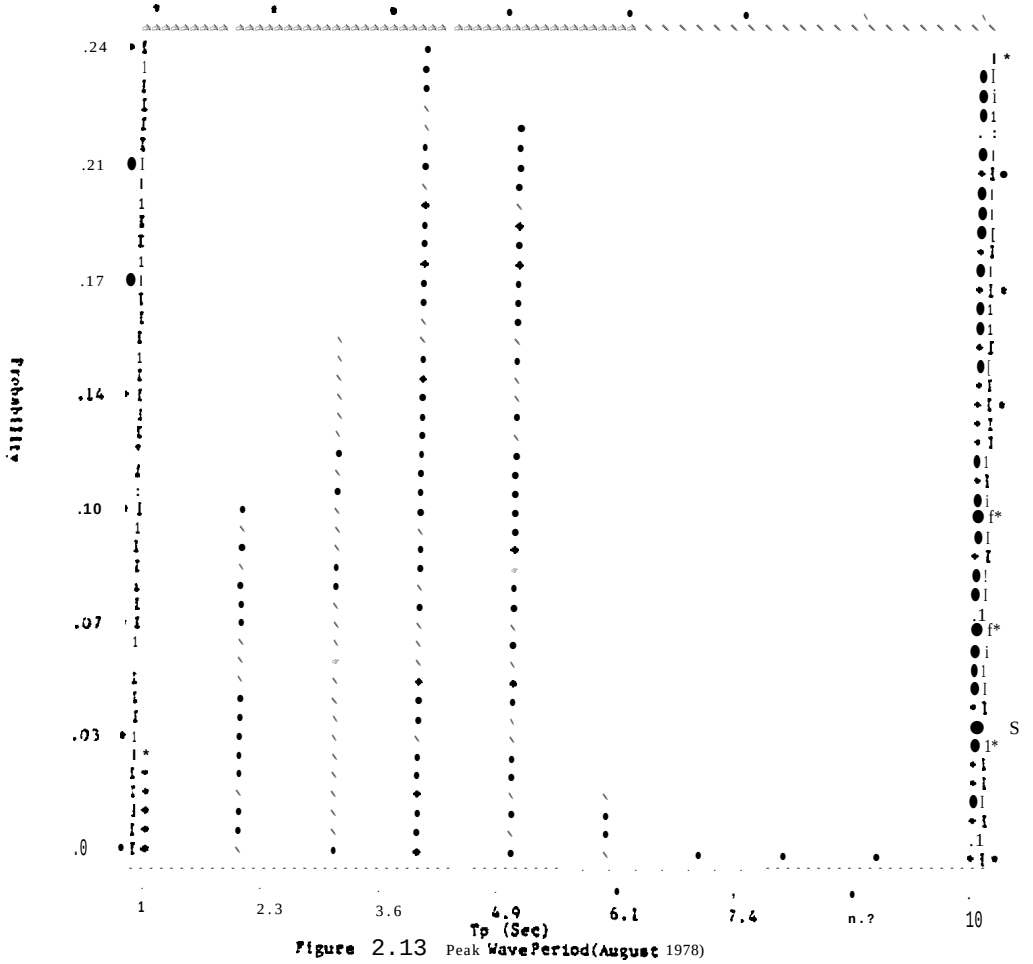

Figure 2.13 Peak Wave Period (August 1978)

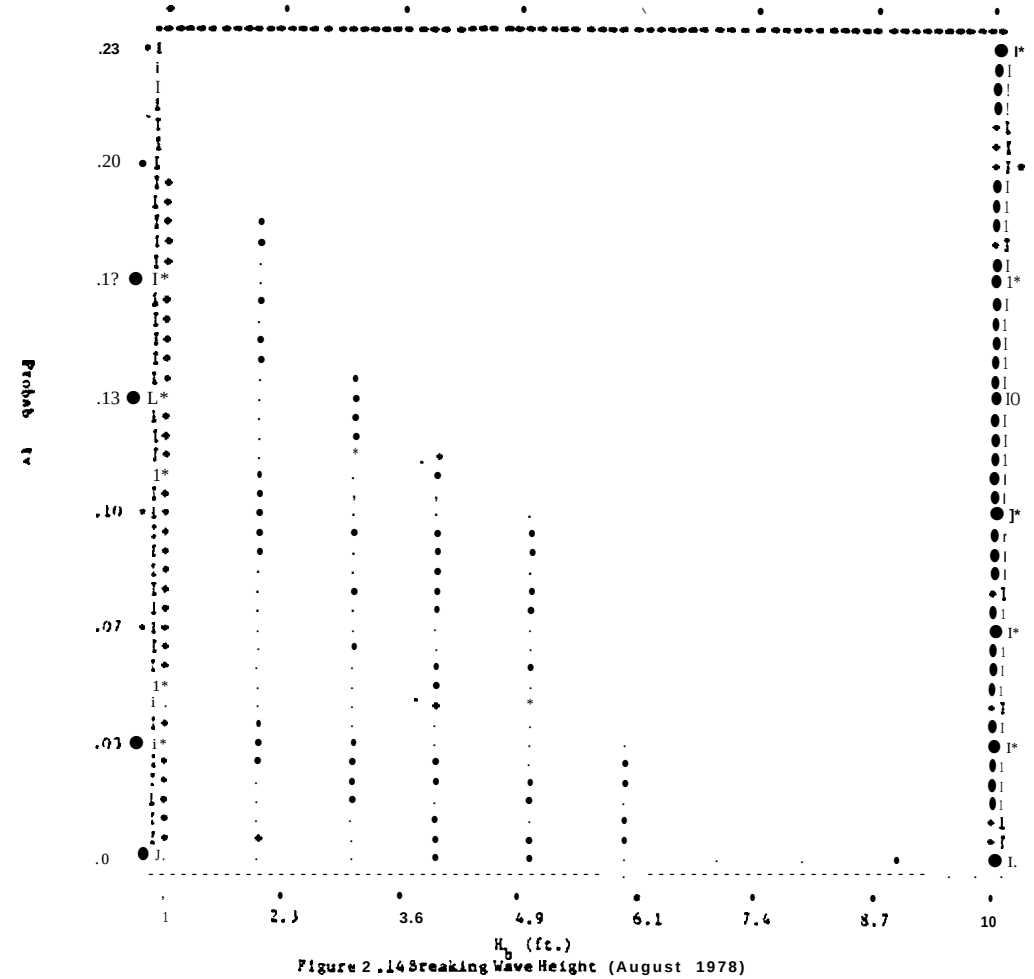

Figure 2.14 Breaking Wave Height (August 1978)

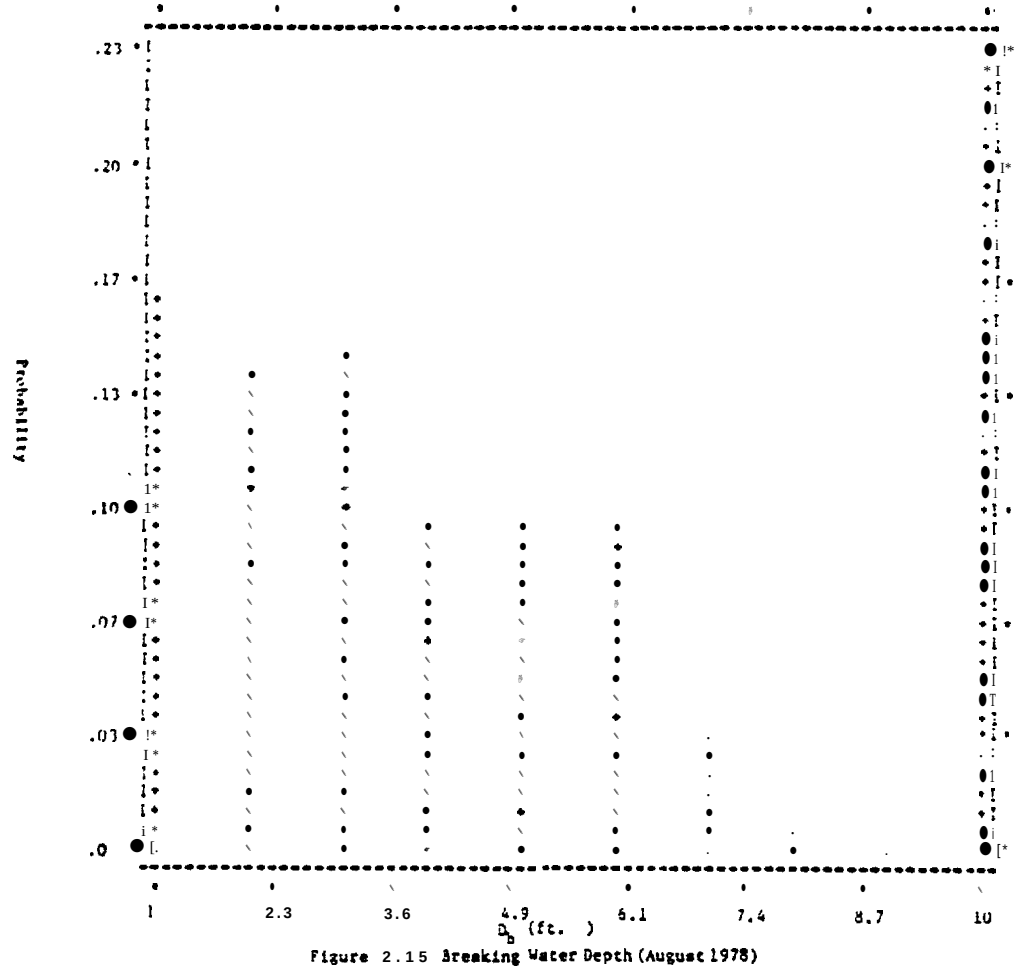

Figure 2.15 Breaking Water Depth (August 1978)

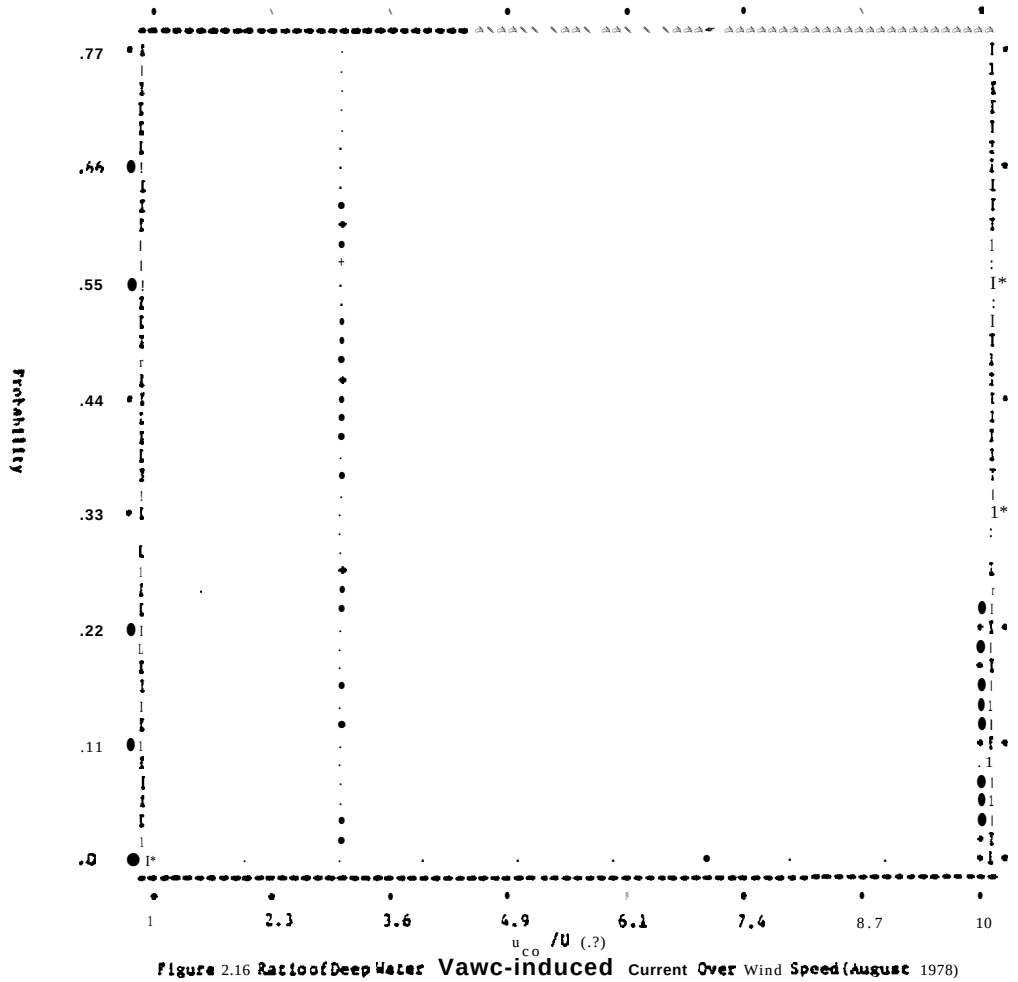

Figure 2.16 Ratio of Deep Water Vawc-induced Current Over Wind Speed (August 1978)

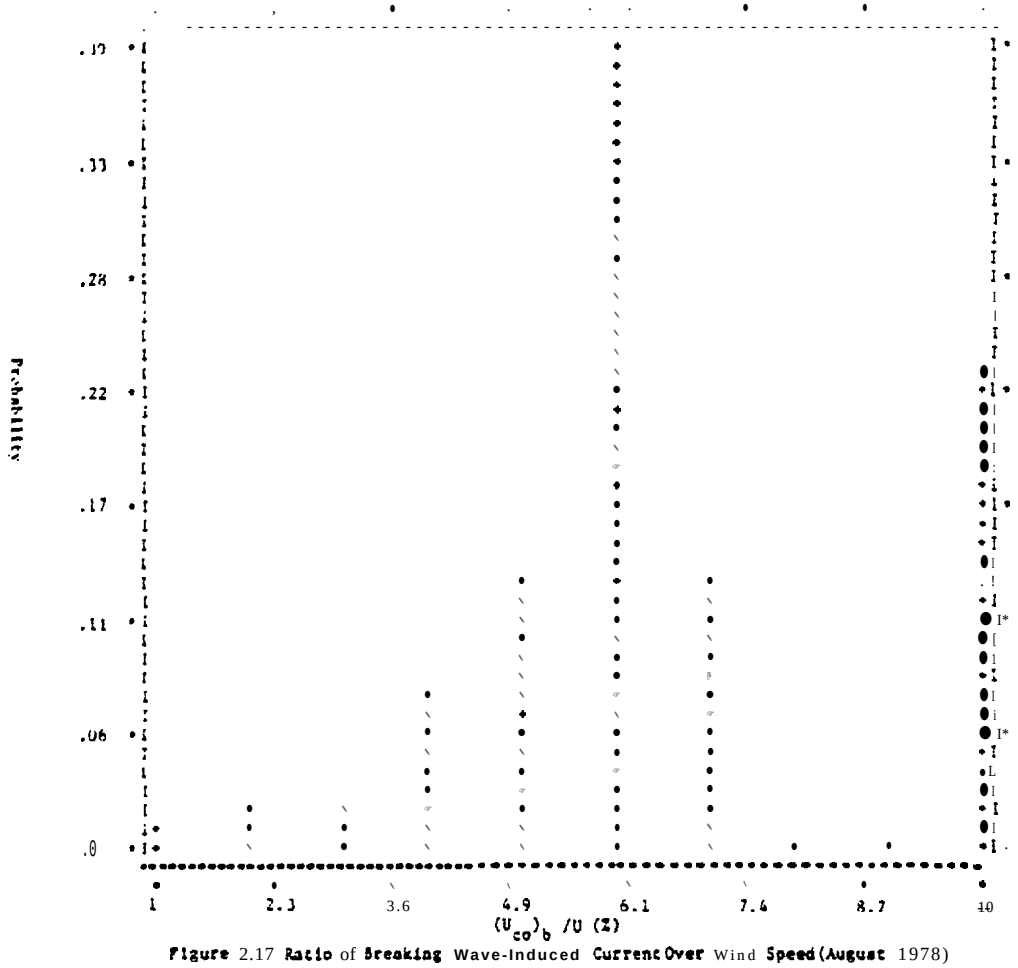

Figure 2.17 Ratio of Breaking Wave-Induced Current Over Wind Speed (August 1978)

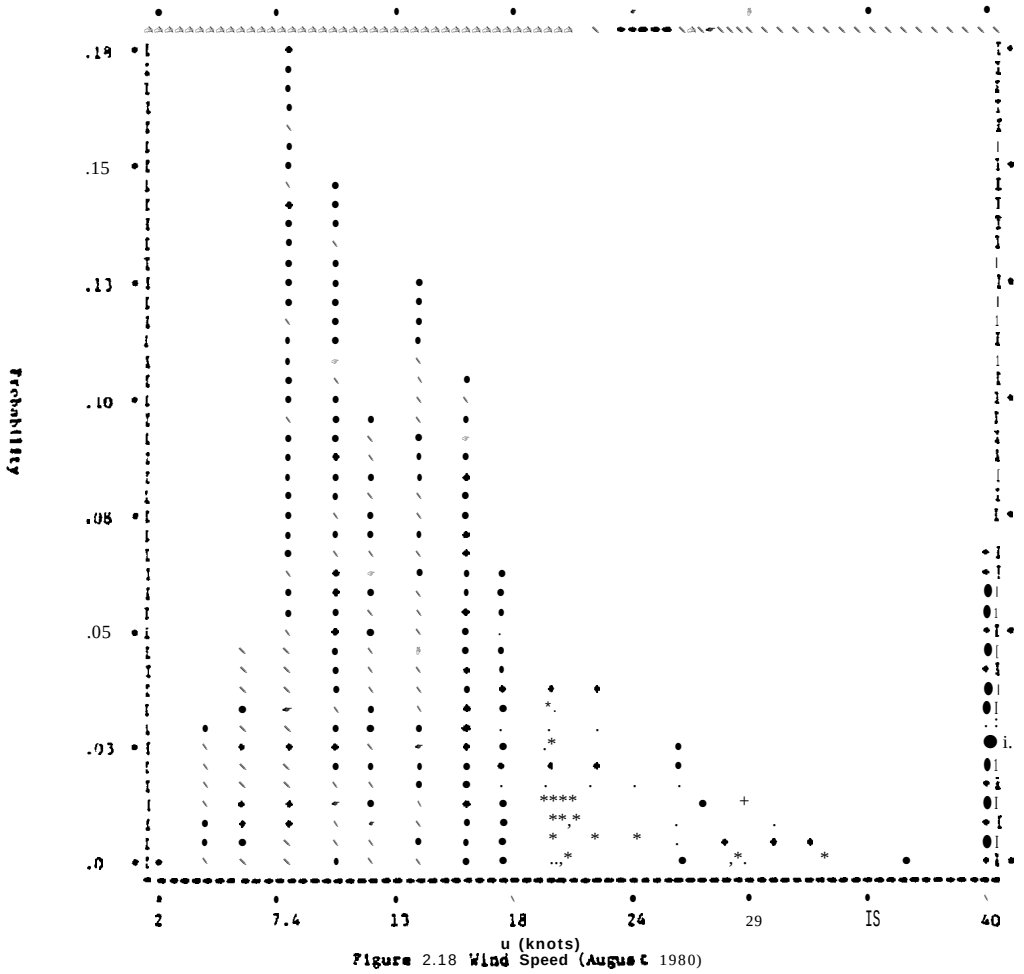

Figure 2.18 Wind Speed (August 1980)

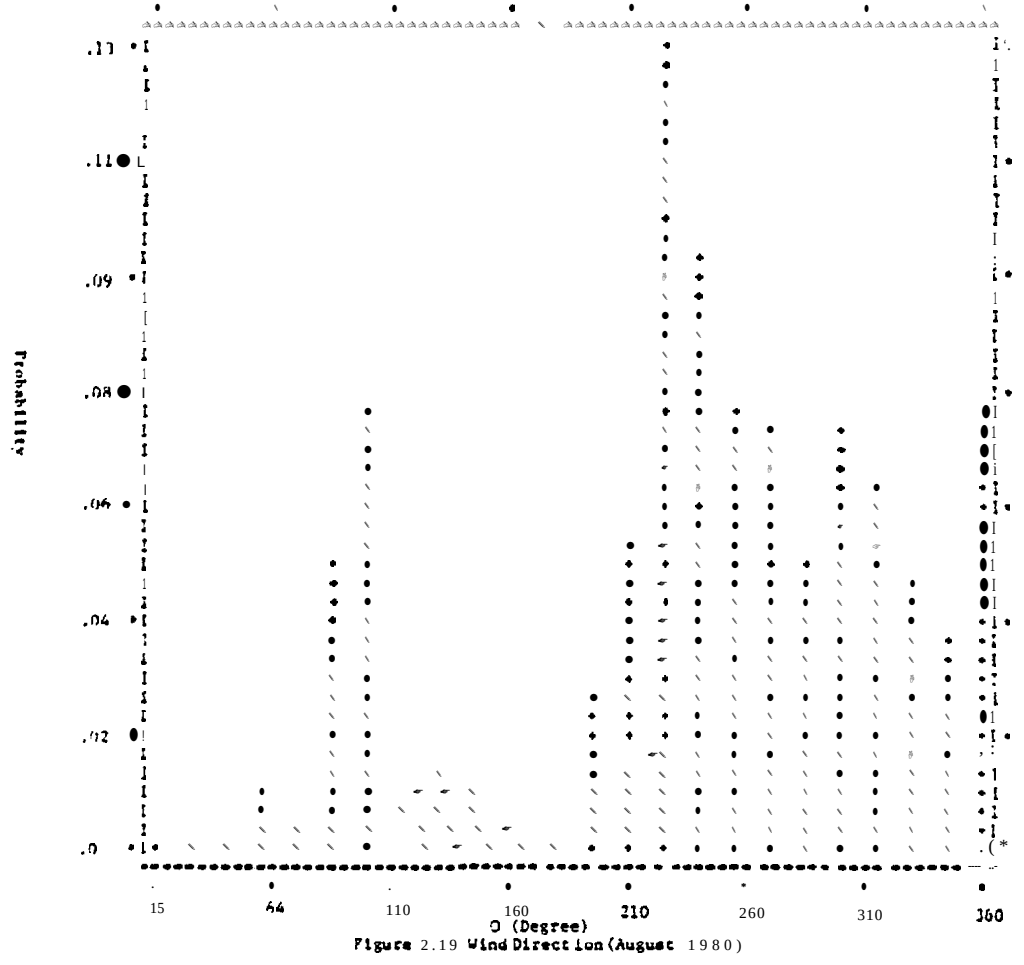

Figure 2.19 Wind Direction (August 1980)

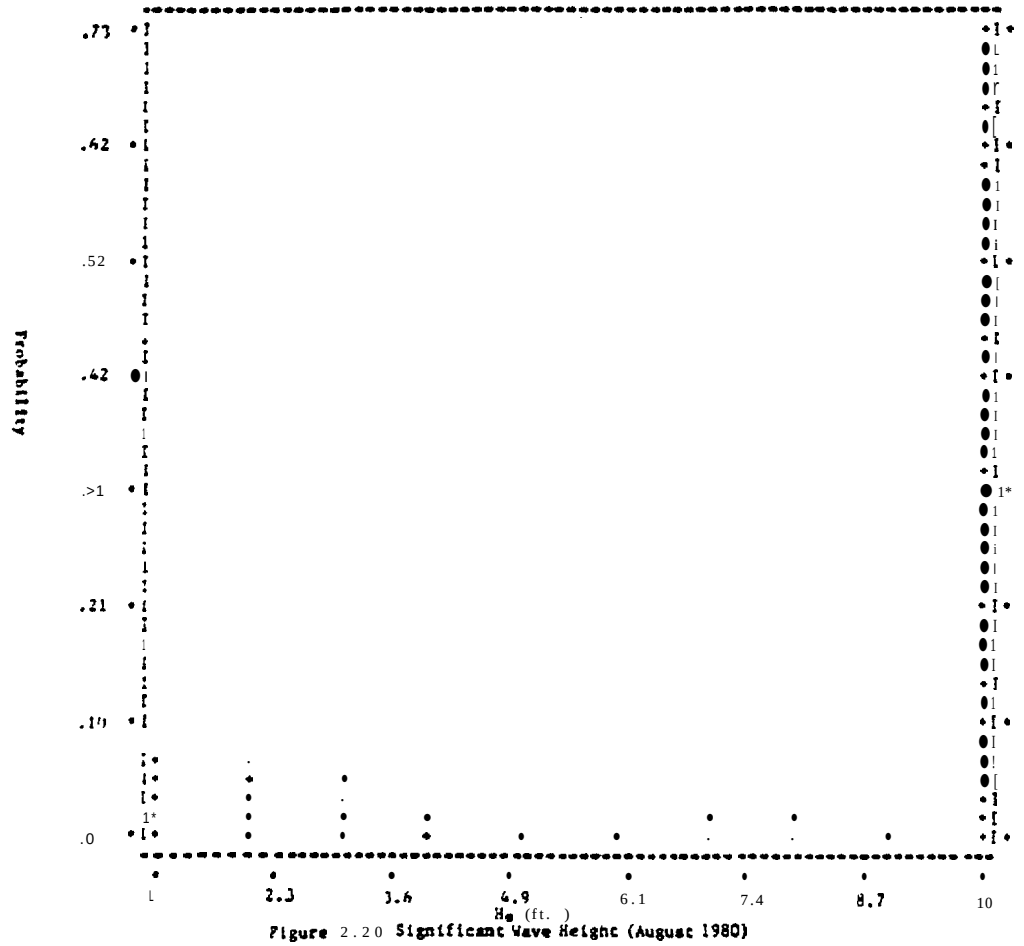

Figure 2.20 Significant Wave Height (August 1980)

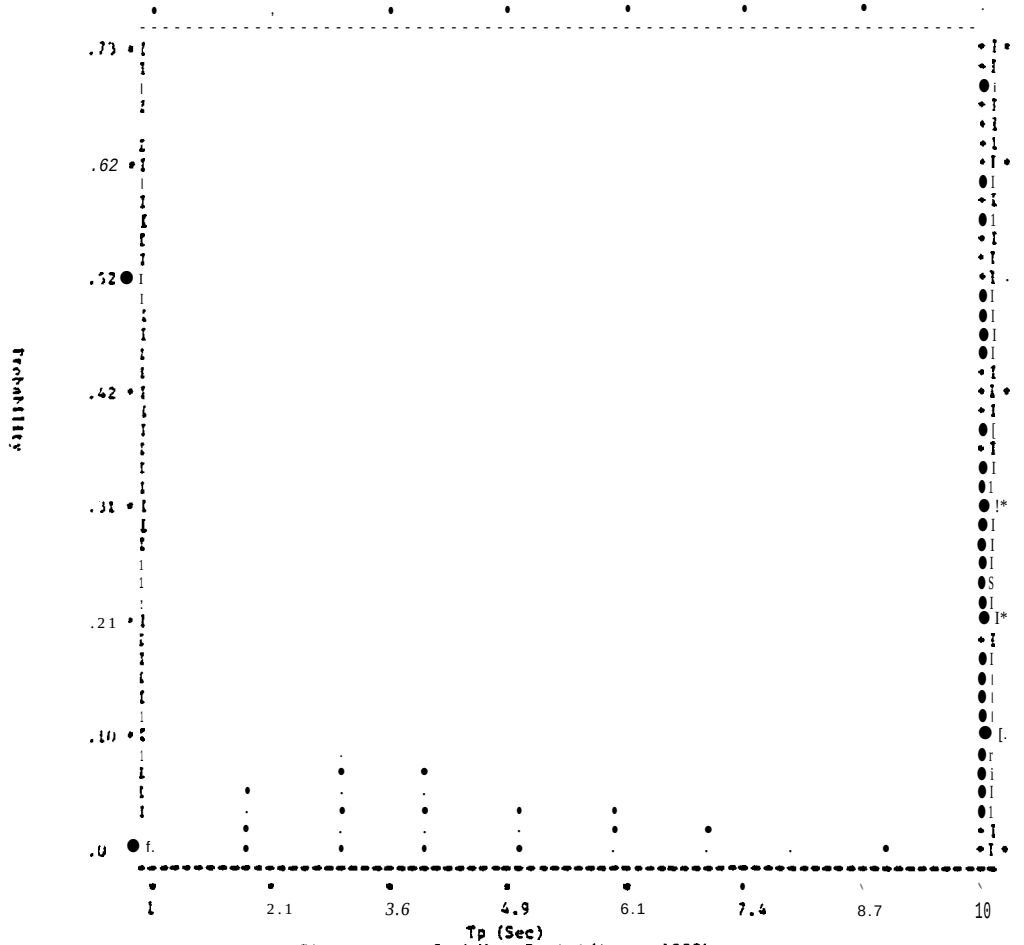

Figure 2.21 Peak Wave Period (August 1980)

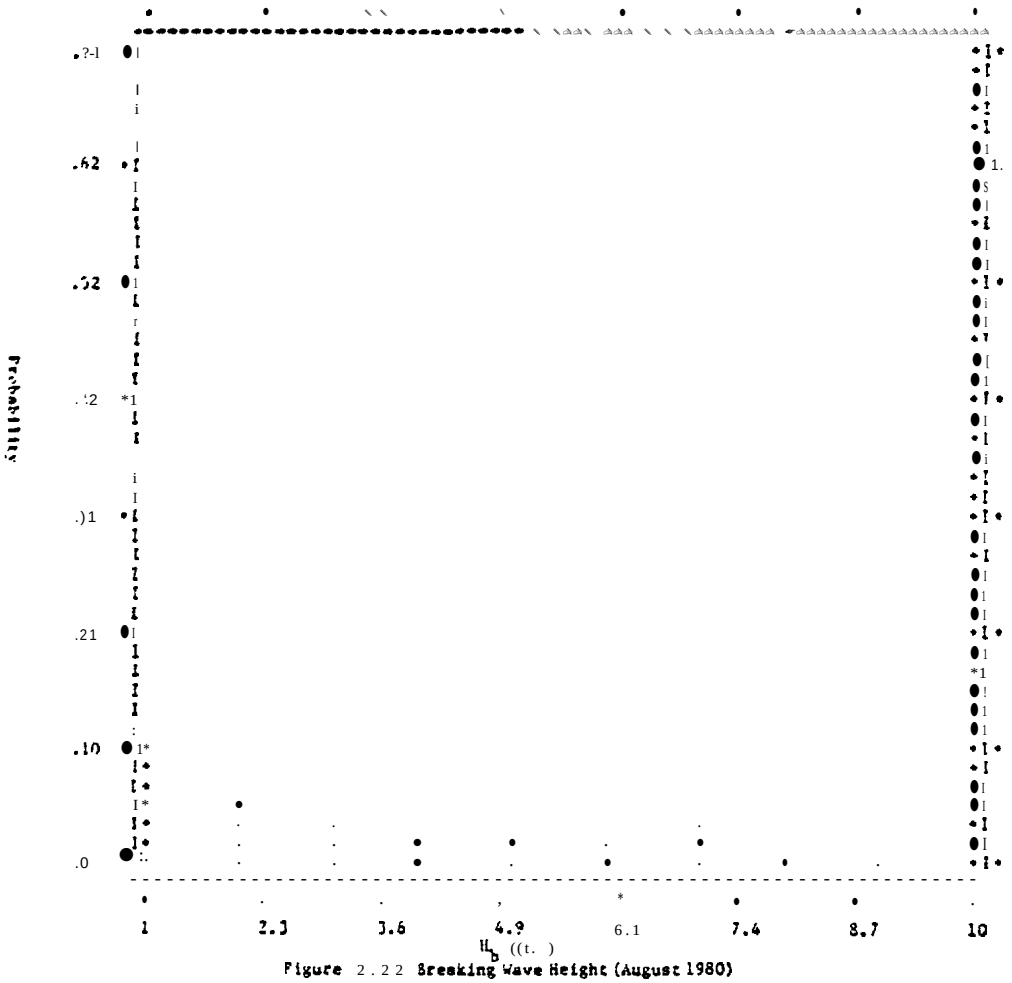

Figure 2.22 Breaking Wave Height (August 1980)

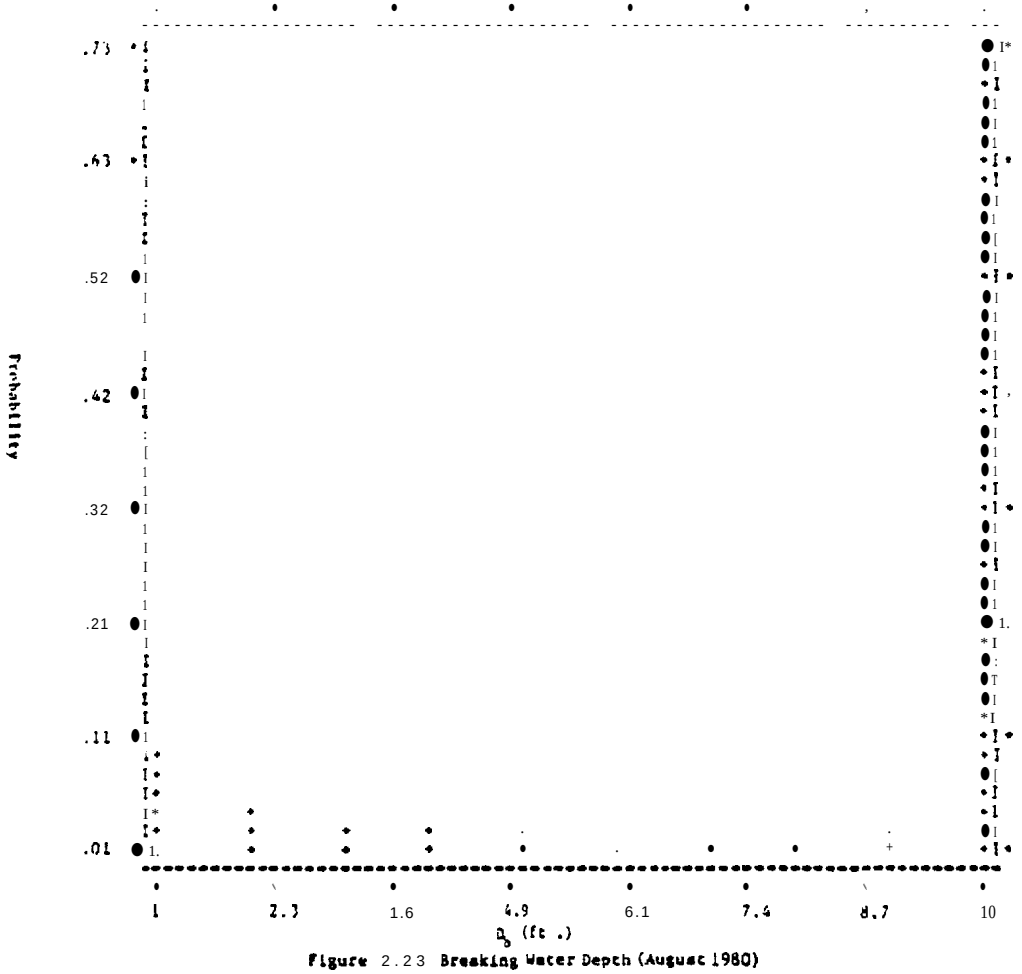

Figure 2.23 Breaking Water Depth (August 1980)

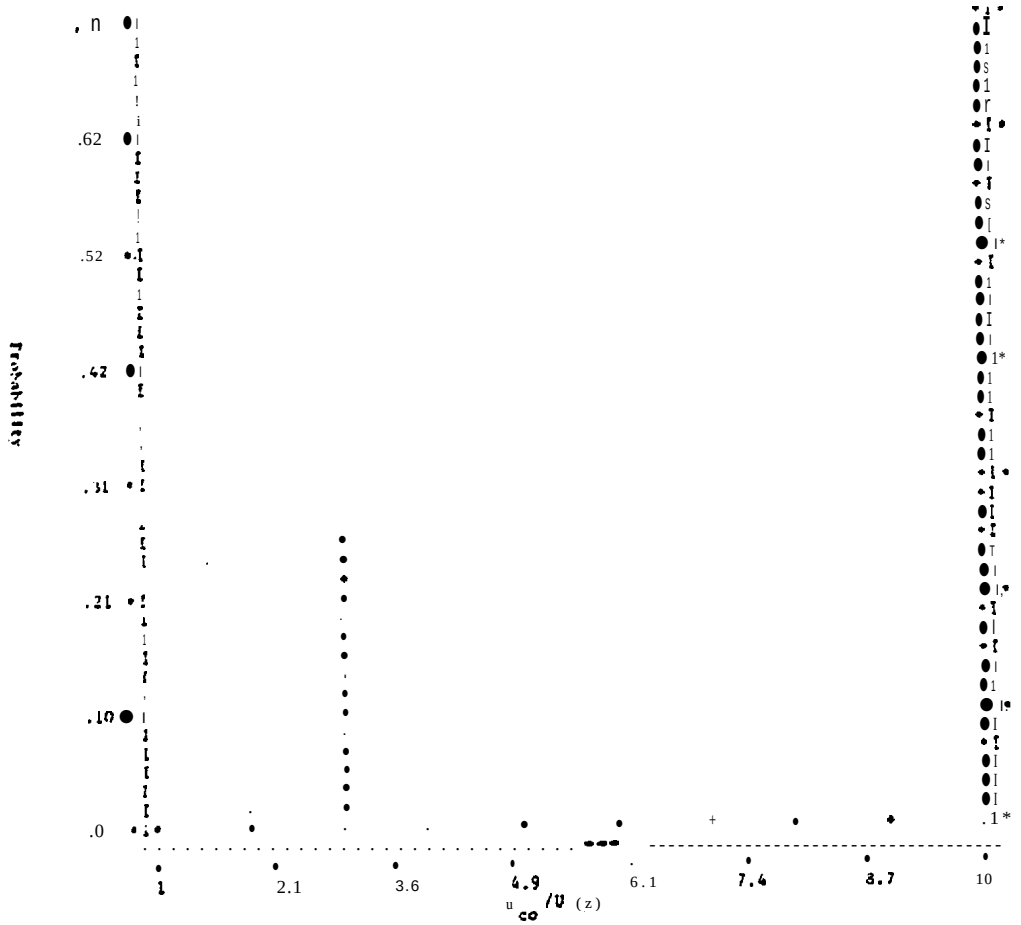

Figure 2. 24 Ratio of Deep Water Wave-Induced Current Over Wind Speed (August 1980)

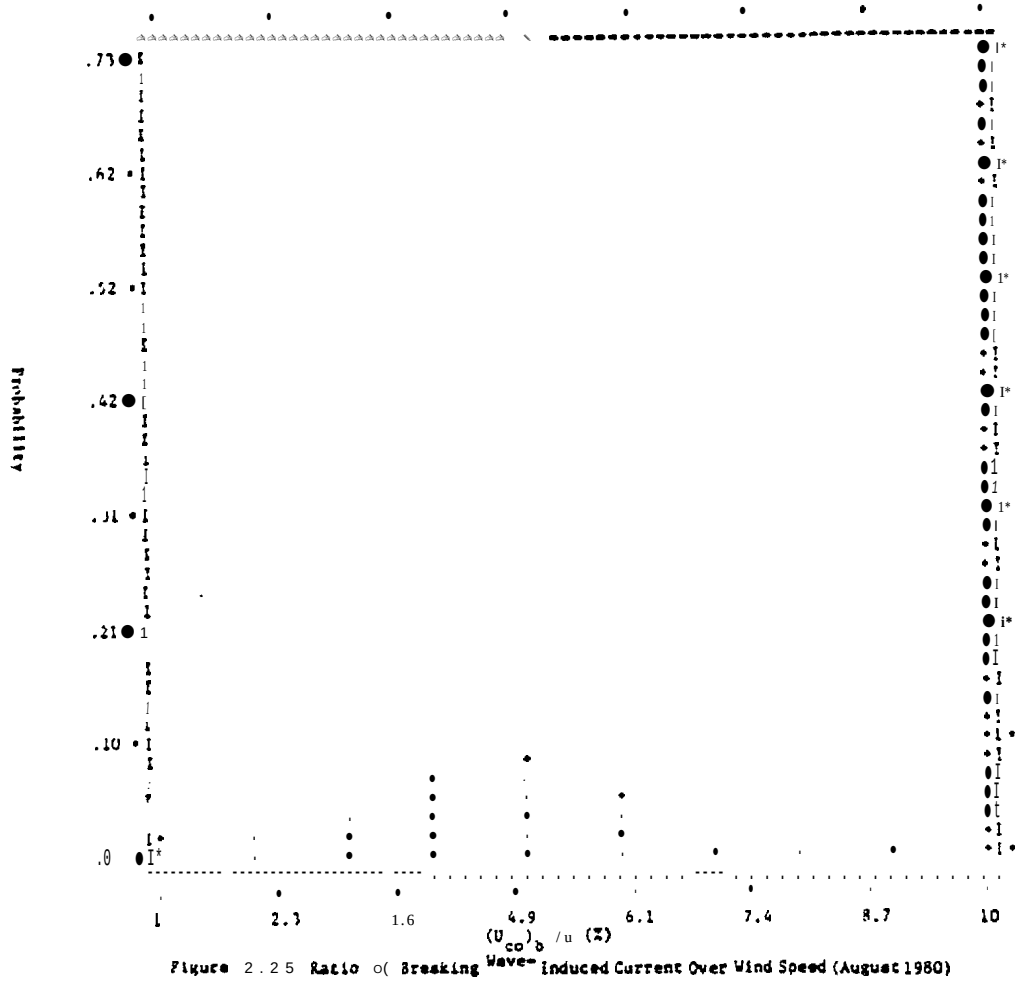

Figure 2.25 Ratio o(Breaking Wave-Induced Current Over Wind Speed (August 1980)

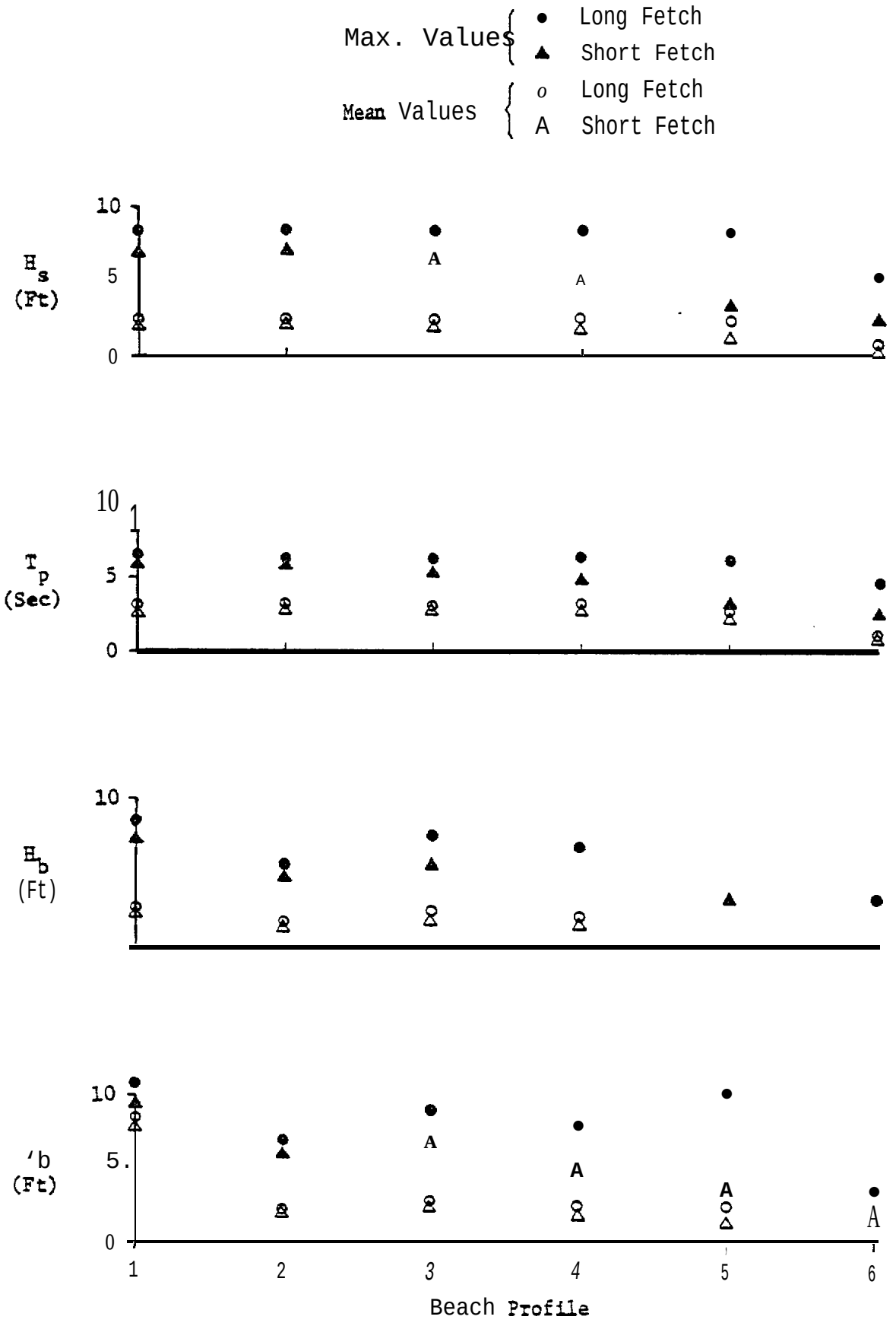

Figure 2.26 Maximum and Mean Values of 1977, August

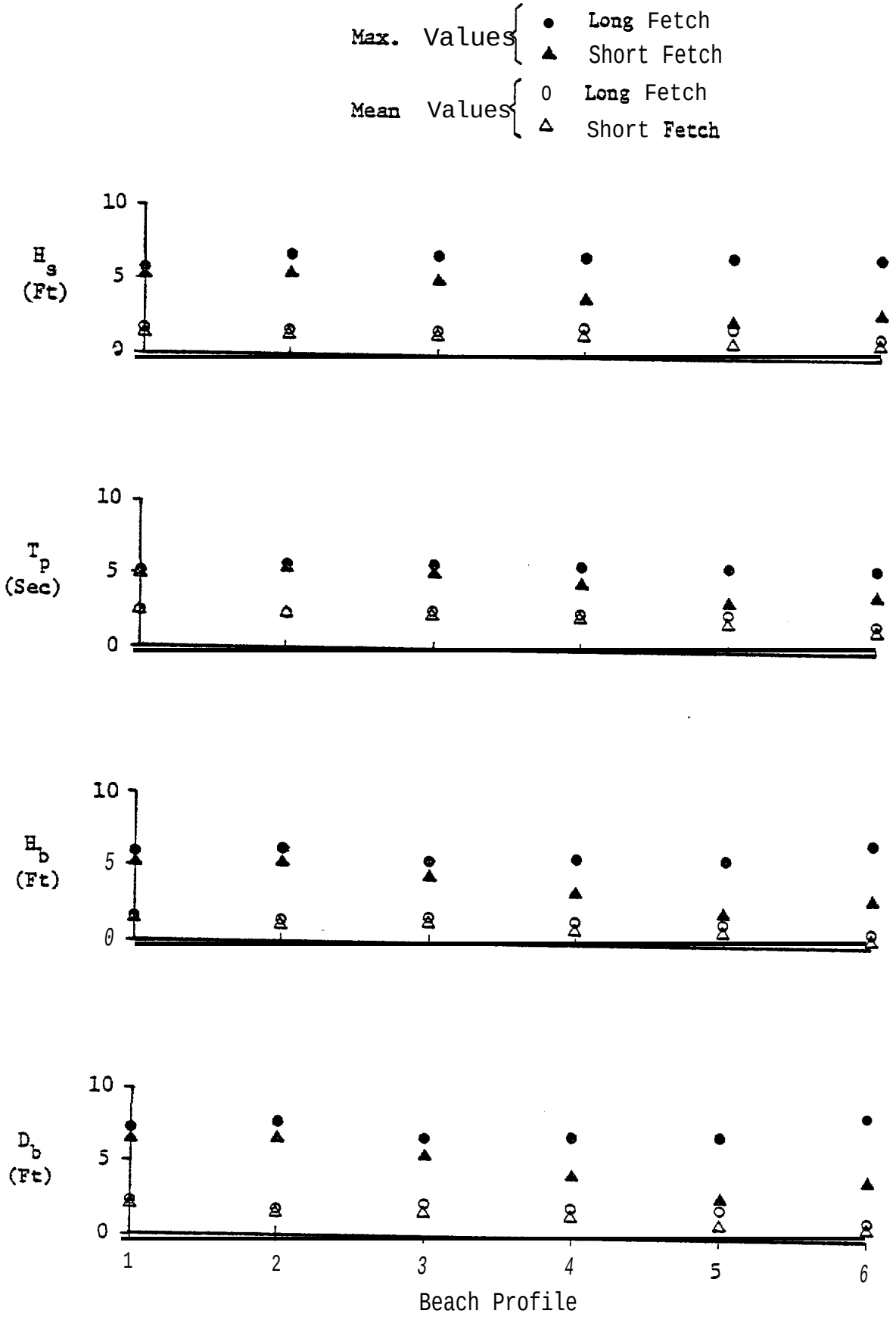

Figure 2.27 Maximum and Mesa Values of 1978, *August*

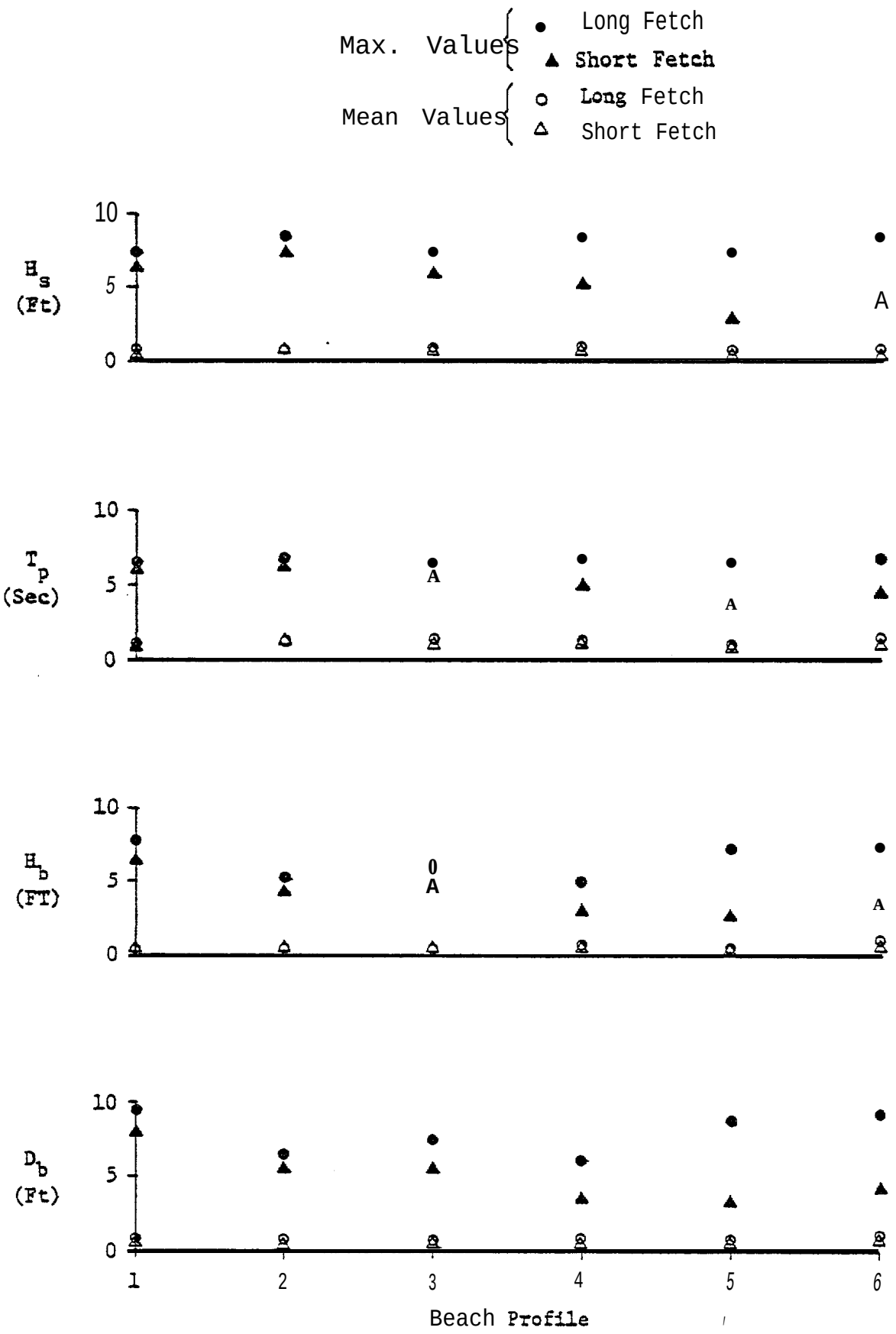

Figure 2.28 Maximum and Mean Values of 1980; August